Universidad de Málaga

Escuela Técnica Superior de Ingeniería de Telecomunicación

Programa de Doctorado en Ingeniería de Telecomunicación

TESIS DOCTORAL POR COMPENDIO DE PUBLICACIONES

Spectral Shaping Techniques for OFDM Signals

Autor:
Javier Giménez de la Cuesta

Directores:
José Antonio Cortés Arrabal
Luis Díez del Río

Año 2025

AUTOR: Javier Giménez de la Cuesta

http://orcid.org/0000-0001-9637-4717

EDITA: Publicaciones y Divulgación Científica. Universidad de Málaga

DECLARACIÓN DE AUTORÍA Y ORIGINALIDAD DE LA TESIS PRESENTADA PARA OBTENER EL TÍTULO DE DOCTOR

D./Dña JAVIER GIMÉNEZ DE LA CUESTA
Estudiante del programa de doctorado EN INGENIERÍA DE TELECOMUNICACIÓN de la Universidad de Málaga, autor/a de la tesis, presentada para la obtención del título de doctor por la Universidad de Málaga, titulada: SPECTRAL SHAPING TECHNIQUES FOR OFDM SIGNALS

Realizada bajo la tutorización de LUIS DÍEZ DEL RÍO y dirección de LUIS DÍEZ DEL RÍO Y JOSÉ ANTONIO CORTÉS ARRABAL (si tuviera varios directores deberá hacer constar el nombre de todos)

DECLARO QUE:

La tesis presentada es una obra original que no infringe los derechos de propiedad intelectual ni los derechos de propiedad industrial u otros, conforme al ordenamiento jurídico vigente (Real Decreto Legislativo 1/1996, de 12 de abril, por el que se aprueba el texto refundido de la Ley de Propiedad Intelectual, regularizando, aclarando y armonizando las disposiciones legales vigentes sobre la materia), modificado por la Ley 2/2019, de 1 de marzo.

Igualmente asumo, ante a la Universidad de Málaga y ante cualquier otra instancia, la responsabilidad que pudiera derivarse en caso de plagio de contenidos en la tesis presentada, conforme al ordenamiento jurídico vigente.

En Málaga, a 6 de OCTUBRE de 2025

Fdo.: JAVIER GIMÉNEZ DE LA CUESTA Doctorando/a	Fdo.: LUIS DÍEZ DEL RÍO Tutor/a
Fdo.: LUIS DÍEZ DEL RÍO Director/es de tesis	JOSÉ ANTONIO CORTÉS ARRABAL

UNIVERSIDAD DE MÁLAGA

Ingeniería de Comunicaciones

AUTORIZACIÓN PARA LA LECTURA DE LA TESIS DOCTORAL POR COMPENDIO DE PUBLICACIONES.

Por la presente, Dr. D. Luis Díez del Río y Dr. D. José Antonio Cortés Arrabal, profesores doctores del Departamento de Ingeniería de Comunicaciones de la Universidad de Málaga, certifican que el doctorando Javier Giménez de la Cuesta ha realizado en el Departamento de Ingeniería de Comunicaciones de la Universidad de Málaga, bajo su dirección, el trabajo de investigación correspondiente a su TESIS DOCTORAL POR COMPENDIO DE PUBLICACIONES titulada:

"Spectral Shaping Techniques for OFDM Signals"

Los resultados expuestos han dado lugar a las siguientes publicaciones en revistas y congresos:

1. J. Giménez, J.A. Cortés, F. Javier Cañete, E. Martos-Naya and L. Díez, "Low-complexity Spectral Shaping Method for OFDM Signals with Dynamic Transmission Band Location," in *IEEE International Symposium on Power Line Communications and its Applications* (Presented in the *Recent Results* session), Oct. 2021

2. J. Giménez, J.A. Cortés and L. Díez, "Low-Complexity Spectral Shaping Method for OFDM Signals with Dynamically Adaptive Emission Mask," in *IEEE Transactions on Communications*, vol. 71, no. 4, pp. 2351-2363, April 2023.

3. J. Giménez, J.A. Cortés and L. Díez, "A Low-Complexity Spectral Shaping Method for OFDM Signals with Dynamically Defined Emission Mask: Optimization Procedure,", *14th Workshop for Power Line Communications,* Sept. 2023

4. J. Giménez, J.A. Cortés, F. Javier Cañete, E. Martos-Naya and L. Díez, "A Modified Pulse and Design Framework to Halve the Complexity of OFDM Spectral Shaping Techniques," in *IEEE Communications Letters*, vol. 28, no. pp. 2146-2150, Sept. 2024.

5. J. Giménez, J.A. Cortés, E. Martos-Naya and L. Díez, "Spectral Shaping Method for OFDM Combining Time-Shifted Active Interference Cancellation and Adaptive Symbol Transition," in *IEEE Open Journal of the Communications Society,* vol. 6, pp. 4476-4490, 2025

Respecto a estas publicaciones, la tesis por compendio realiza una introducción más completa de las técnicas de conformación espectral habitualmente utilizadas en señales OFDM, profundiza más en las estrategias que combinan los métodos AIC y AST, y contribuye a ampliar estas últimas con las propuestas hechas en la tesis.

Por todo ello, consideran que esta Tesis por COMPENDIO DE PUBLICACIONES es apta para su presentación al Tribunal que ha de juzgarla. Y para que conste a efectos de lo establecido, AUTORIZAN la presentación de esta Tesis en la Universidad de Málaga. Igualmente, certifican que las publicaciones que avalan la tesis no han sido empleadas en trabajos anteriores a la misma.

En Málaga, a 6 de octubre del 2025

Fdo.: Dr. D. Luis Díez del Río

Fdo.: Dr. D. José Antonio Cortés Arrabal

A mis padres y mis hermanos,
porque si he llegado aquí, ha sido gracias a ellos

Agradecimientos

En primer lugar, me gustaría dar las gracias a mis directores de tesis, Luis y José Antonio. Por ofrecerme la oportunidad de realizar la tesis bajo su supervisión, y por los más de seis años de trabajo que han dedicado a ser mis mentores. Les agradezco su total disposición a resolverme cualquier duda o preocupación, ya sea en la investigación, la docencia, o en el ámbito personal. Me han sabido transmitir el rigor y la perseverancia que requiere la carrera académica, y me siento muy afortunado de haberlos tenido como directores de tesis. Me gustaría extender este agradecimiento a Francis, quien, sin ser mi director, también ha sido un apoyo y guía durante los años de tesis, en lo profesional y lo personal. También a Eduardo, por su dedicación a este proyecto de tesis, aportando conocimientos y nuevos puntos de vista que han sido clave en la consecución de las publicaciones.

Quiero agradecer al profesor Lutz Lampe la oportunidad de realizar una estancia de investigación en Vancouver bajo su supervisión. En ese período pude, además de trabajar, conocer lugares increíbles y hacer grandes amigos allí.

Merecen una mención especial en estos agradecimientos mis amigos Ana, Pablo, Miguel, Pedro y Hao, con quienes ya desde los años de grado he compartido faenas, risas, celebraciones y algún viaje. En ellos he encontrado un fundamental apoyo en estos años de tesis, pues nadie mejor que ellos han sabido escuchar y entender los altibajos propios del doctorado. Espero haberos sabido corresponder el apoyo que he sentido por vuestra parte. Quiero dar también las gracias a mis compañeros de laboratorio (1.3.5 y 1.3.6.), por los ratos que hemos compartido en estos años, y por su energía y compañerismo. También a los compañeros del laboratorio 1.3.2., por los muchos almuerzos que hemos compartido.

Por último, pero no menos importante, me quiero centrar en quienes más apoyo me han dado fuera de la Escuela. A mis padres, Mamen y Alberto, que nunca han dudado de mí y que, junto a mis hermanos, Carmen Mª, Alberto y Juan, me han dado todo el amor y el apoyo que pudiera necesitar para llegar hasta aquí. A mis amigos, por haber creído en mí, haber permanecido a mi lado y haberme aportado su cariño incondicional. A Roberto, quien desde el principio de esta aventura me ha escuchado con mis preocupaciones y dudas, y me ha acompañado en todo momento, dándome todo su amor y apoyo.

Contents

List of Figures

List of Tables

Abstract

Orthogonal frequency division multiplexing (OFDM) is a widespread modulation, but suffers from low spectral confinement. A plethora of strategies have been proposed to mitigate this effect. In particular, pulse shaping, adaptive symbol transition (AST), active interference cancellation (AIC) and spectral precoding techniques are addressed in this thesis. Also, a combination of several of these methods is used as foundation for the contributions of this thesis, due to their computational simplicity and effectiveness in reducing the out-of-band emissions (OOBE) of OFDM signals.

As first contribution, a strategy has been proposed to reduce the computational complexity of the aforementioned spectral shaping strategies. It requires modifying the waveform conventionally used in OFDM so that it has Hermitian symmetry. This adjustment is enough for many AIC, AST and spectral precoding techniques to benefit from nearly halving their optimization and implementation costs. Moreover, a design framework is set so that future proposals can benefit from the same reduction.

In second place, a framework is devised to reduce the computational cost of recomputing the solutions to the spectral shaping problem in systems where the power emission constraints can change dynamically with time. Most state-of-the-art spectral shaping techniques are forced to solve an optimization problem each time the power spectral density (PSD) constraints change. As an alternative, we propose a strategy in which a set of precomputed solutions is seamlessly adapted to these changes by applying some simple transformations that can be performed online within the system. This framework is based on AIC and AST techniques, due to their ability to be applied transparently to the receiver.

Finally, a spectral shaping method that enhances the number of degrees of freedom available for the reduction of the OOBE in OFDM signals is proposed. It is also based on the AIC and AST techniques, and consists in incorporating time-advanced and time-delayed versions of these terms such that they overlap with preceding and succeeding OFDM symbols. The additional degrees of freedom can be used to mitigate the data rate penalty associated to AIC techniques. Alternatively, they can be used to further reduce the OOBE.

Resumen

La modulación OFDM (Orthogonal Frequency Division Multiplexing) se emplea en un amplio abanico de sistemas. Sin embargo, tiene como inconveniente su bajo confinamiento espectral. En la literatura se pueden encontrar numerosas estrategias de conformación espectral. En particular, en esta tesis nos centramos en la conformación de pulsos, técnicas AST (Adaptive Symbol Transition), técnicas AIC (Active Interference Cancellation) y en el precoding espectral. Una combinación de estos métodos se utiliza como base para el desarrollo de las contribuciones de esta tesis, dado el bajo coste computacional y la efectividad de estas técnicas a la hora de reducir las emisiones fuera de banda de las señales OFDM.

La primera de las contribuciones de esta tesis es un esquema de diseño que permite reducir el coste computacional de las estrategias mencionadas. Propone usar un pulso con simetría Hermítica que sustituye al usado convencionalmente. Con este cambio, se consigue reducir el coste de muchas implementaciones de técnicas AIC, AST y de precoding espectral en hasta un 50%, tanto en los costes de optimización como los de implementación. Además, se propone un esquema de diseño con un problema de optimización modelo. Si cualquiera de los mencionados métodos usa el pulso propuesto y resuelve un problema que se ajuste al mencionado modelo contará con los mismos beneficios.

La segunda contribución es una estrategia para reducir el coste de recalcular las soluciones al problema de conformación espectral en sistemas en los que los requisitos de emisión fuera de banda cambian de forma dinámica. Muchos métodos de conformación espectral de la literatura necesitan resolver un problema de optimización cada vez que la máscara que impone los límites de densidad espectral de potencia (DEP) cambia. Nosotros proponemos una estrategia que consiste en obtener las nuevas soluciones a partir de un conjunto de soluciones precalculadas, adaptándolas online (en el dispositivo) mediante un conjunto de transformaciones sencillas. Esta estrategia se basa en las técnicas AIC y AST, ya que pueden aplicarse de forma transparente al receptor.

La última contribución es una innovación de las técnicas de conformación espectral AIC y AST. Consiste en extender su influencia a símbolos anteriores y posteriores, lo cual se consigue utilizando versiones desplazadas de los términos que convencionalmente se usan. Estos términos se desplaza un número entero de periodos de símbolo, solapándose con los

símbolos OFDM anteriores y posteriores. Los grados de libertad adicionales que se consiguen con estos nuevos términos se pueden emplear para mitigar la reducción en el régimen binario que provoca el uso de las técnicas AIC. Si esto no fuera necesario, se pueden emplear para reducir más aún las emisiones fuera de banda de la señal OFDM.

List of Acronyms

3GPP	**T**hird **G**eneration **P**artnership **P**roject
4G	**F**ourth **G**eneration
5G	**F**ifth **G**eneration
ACLR	**A**djacent **C**hannel **L**eakage **R**atio
AIC	**A**ctive **I**nterference **C**ancellation
AST	**A**daptive **S**ymbol **T**ransition
BER	**B**it **E**rror **R**ate
BW	**B**and**W**idth
CC	**C**ancellation **C**arriers
CCDF	**C**omplementary **C**umulative **D**istribution **F**unction
CFO	**C**arrier **F**requency **O**ffset
CP	**C**yclic **P**refix
CR	**C**ognitive **R**adio
DFT	**D**iscrete **F**ourier **T**ransform
DSL	**D**igital **S**ubscriber **L**ine
EMC	**E**lectro**M**agnetic **C**ompatibility
EU	**E**uropean **U**nion
EVM	**E**rror **V**ector **M**agnitude
FEQ	**F**requency **EQ**ualizer
FIR	**F**inite **I**mpulse **R**esponse
ICI	**I**nter**C**arrier **I**nterference
IDFT	**I**nverse **D**iscrete **F**ourier **T**ransform
IIR	**I**nfinite **I**mpulse **R**esponse
ISI	**I**nter**S**ymbol **I**nterference

LS	**L**east **S**quares
LTE	**L**ong-**T**erm **E**volution
MIMO	**M**ultiple-**I**nput **M**ultiple-**O**utput
NR	**N**ew **R**adio
OFDM	**O**rthogonal **F**requency **D**ivision **M**ultiplexing
OOBE	**O**ut-**O**f-**B**and **E**mission
PAM	**P**ulse **A**mplitude **M**odulation
PAPR	**P**eak-to-**A**verage **P**ower **R**atio
PLC	**P**ower **L**ine **C**ommunications
PRB	**P**hysical **R**esource **B**lock
PSD	**P**ower **S**pectral **D**ensity
RB	**R**esource **B**lock
RC	**R**aised **C**osine
RHS	**R**ight **H**and **S**ide
SCS	**S**ub**C**arrier **S**pacing
SFO	**S**ampling **F**requency **O**ffset
SIR	**S**ignal to **I**nterference **R**atio
SVD	**S**ingular **V**alue **D**ecomposition
w.r.t.	**W**ith **R**espect **T**o
WOLA-OFDM	**W**eighted **O**ver**L**ap and **A**dd **OFDM**

Chapter 1

Introduction

Many wireless and wired communication systems choose orthogonal frequency division multiplexing (OFDM) over other modulation schemes due to its multiple advantages, such as its robustness, the simplicity of the transceiver, its ability to perform spectrum aggregation, and the straightforward implementation of multiple-input multiple-output (MIMO) techniques [1]. However, it is well known that conventional OFDM signals exhibit poor spectral confinement due to the use of rectangularly-shaped pulses, which produce a spectrum with high sidelobes that decay slowly in frequency, leaking into neighbouring subbands. To avoid the latter, many of these systems devote wide regions of the spectrum to work as guard bands. This results in large inefficiencies, as many data carriers are nullified instead of conveying data. This effect is present in wireless mobile communication systems, such as long-term evolution (LTE) and fifth generation (5G) new radio (NR). In these technologies, guard bands can take up to 10% of the channel bandwidth. Since spectral resources are becoming increasingly scarce, these inefficiencies need to be addressed [2].

The poor spectral confinement of OFDM signals is particularly adverse for cognitive radio (CR) systems [3]. The CR paradigm is suitable for scenarios in which a so-called primary system is allocated a portion of the spectrum, but makes a partial use of it. The latter condition allows secondary systems to dynamically access the unused frequency regions when the primary system is not actively transmitting. Since the goal of this strategy is to exploit these unused subbands to its maximum, the size of the guard bands should be reduced to the minimum. Note that despite its name, CR is used also in wired systems: in power line communications (PLC) it is used to prevent its radiated emissions from interfering with other wired services, such as digital subscriber line (DSL), and wireless systems as well, like aeronautical mobile services, that might coexist in the same area [4] [5] [6].

To overcome the aforesaid issues, a plethora of techniques have been proposed in the literature to improve the spectral confinement of OFDM signals [7]. These are usually classified according to the domain in which they are applied: frequency domain techniques are usually

applied to the constellation symbols prior to the inverse discrete Fourier transform (IDFT) block; time domain techniques are applied after the IDFT block, that is, once the carries have been modulated with their corresponding symbols. In the first group of techniques, we find spectral precoding and active interference cancellation (AIC). From the second group, pulse-shaping, time-domain filtering and adaptive symbol transition (AST) techniques, among others, are frequently used.

A myriad of spectral precoding methods have been proposed in the literature. They mainly consist in coding the data into the symbols transmitted by the active carriers with the purpose of reducing the out-of-band emission (OOBE) produced by the OFDM signal. To that end, it is typical to design the optimal precoder coefficients so that the spectrum of the resulting signal is null in a set of strategically selected frequencies [8] [9] [10]. While these techniques achieve great performance in terms of OOBE reduction, they have a threefold problem. First, some data carriers are usually employed to convey precoder redundancy [10] [9], incurring a data rate degradation whose magnitude depends on the coding rate of the precoder (i.e., the ratio of the number of data carriers to the number of active carriers in use). In second place, the complexity of the transmitter is notably increased with respect to (w.r.t.) the conventional OFDM one. Moreover, noise enhancement occurs if the precoding matrix is not orthogonal, even when the receiver is aware of the applied precoding [11]. Finally, spectral precoding cannot be applied seamlessly, as many of these schemes require the receiver to decode the received symbols. This procedure further increases the computational complexity of the technique and requires modifications to the conventional receiver. Alternatively, other approaches obtain the coefficients of the precoder subject to the coded vector having minimum distance to the original data symbols [8]. This practice allows the symbols conveyed by the data carriers to be received without decoding them with limited impact on the bit error rate (BER) provided that low-density constellations are used.

As for the AIC techniques, they consist in reserving a subset of carriers exclusively to cancel the OOBE produced by the data carriers in the system [12] [11] [13]. The first subset of carriers is known as cancellation carriers (CC), which is disjoint from the set of carriers that convey data symbols. This technique can be seen as a particularization of spectral precoding, where data carriers convey uncoded data symbols and the CC transmit symbols that are a linear combination of those transmitted by the data carriers. This technique then incurs the same data rate penalty as spectral precoding, as some data carriers are typically used as CC. Although there can be CC located within the frequency regions where OOBE needs to be reduced, their spectral shaping capability is generally lower than that of in-band CC. Since the CC are orthogonal to the data carriers, this technique can be used without requiring any further modification in the receiver, as the symbols they carry can be disregarded after the discrete Fourier transform (DFT). Moreover, [12] and [11] propose AIC techniques whose solution can be obtained offline.

Among time-domain techniques, pulse-shaping consists in modifying the shape of the transmitted OFDM symbols to enhance the spectral confinement of the resulting signal. This can be done in several ways: by tapering the boundaries of the rectangularly-shaped transmission pulses conventionally used in OFDM, technique also known as weighted overlap and add based OFDM (WOLA-OFDM) [14]; or by designing these boundaries through an optimization procedure [11]. Additionally, an additive term can be used to modify the boundaries of the transmitted OFDM symbol, obtained as a linear combination of the transmitted data. This technique, known as AST, can be implemented by designing a single term for each OFDM symbol, as in [15], or a different term for each data carrier, as it was proposed in [16]. While the former requires recalculating it for every OFDM symbol, the latter is data independent. These techniques are as well transparent to the receiver, as the boundaries are discarded along with the cyclic prefix. However, to accommodate these AST terms/tapered boundaries it is necessary to either shorten the effective length of the cyclic extension of the OFDM symbol, or to extend the symbol period. The former impacts the robustness of OFDM in frequency-selective scenarios, and the latter decreases the symbol rate.

Filtering is another widely used spectral shaping technique from the time-domain group, in which the transmitted signal is filtered prior to transmission to reduce its OOBE [17] [18]. Nonetheless, filtering has high computational cost, even with short filters [19]. The latter work proposes performing part of the filtering process in the frequency domain, with lower computational cost. Finally, filtering techniques introduce distortion in the signal, degrading the error rate, and are not suitable for CR applications where the available spectrum is non-contiguous and changes dynamically.

Many works propose strategies that combine AIC and time-domain pulse shaping to reduce the OOBE of OFDM signals, as both techniques are transparent to the receiver. For instance, in [20] AIC is combined with a windowed pulse with smooth transitions, though the solution is data-dependent. Alternatively, in [16] a new pulse referred to as generalized pulse is proposed, which combines AIC and AST techniques. This pulse is different for each carrier, and can be obtained offline. In [11] a similar combination is proposed, only that the pulse design term is common to all data carriers, yielding lesser degrees of freedom than the former technique. Consequently, lower OOBE reductions can be expected.

1.1 Objectives

This thesis focuses on spectral shaping techniques for OFDM signals. In this context, three objectives have been defined:

- Provide a strategy to reduce the computational cost of state-of-the-art spectral shaping techniques. Typically, the higher the computational complexity of these techniques,

the higher the performance they are expected to provide. The goal is to devise a strategy to reduce their complexity while having minimal impact on their performance.

- Provide a framework to shape the spectrum of OFDM signals in scenarios where the power emission requirements change dynamically. This kind of scenario can be found in CR paradigm, where one or several secondary CR systems are allowed to use some frequency subbands allocated to a primary system as long as the latter is not making use of them.
- Provide a solution to the data rate degradation of AIC techniques. The issue with this technique is that it typically requires using some data carriers inside the passband as CC in order to achieve satisfactory OOBE reductions. However, this practice yields some data rate penalty due to the carriers that are not being used to convey data.

1.2 Outline of the thesis

This compilation thesis is organized into four main chapters and one Appendix section. Chapter 1, the current chapter, contains the introduction and motivation of this thesis, the objectives it pursues and the organization of the document. In Chapter 2 some necessary background is provided for the understanding of the main contributions of this thesis. In it, a group of commonly used spectral shaping techniques is reviewed to establish the foundation on which the following chapter is built. Chapter 3 contains a summary of the contributions of the publications compiled in this thesis, along with the discussion of the main results. In Chapter 4, some conclusions to the work are provided and several future work lines are laid out. Finally, in the Appendix A proof about different topics is provided, in Appendix B section the publications that support this thesis are arranged and in Appendix C a summary of the contributions is provided in Spanish.

1.3 Publications

This compilation thesis comprises the following list of publications:

- [21] J. Giménez, J. A. Cortés, F. Javier Cañete, E. Martos-Naya and L. Díez, "A Modified Pulse and Design Framework to Halve the Complexity of OFDM Spectral Shaping Techniques," in *IEEE Communications Letters*, vol. 28, no. 9, pp. 2146-2150, Sept. 2024,
- J. Giménez, J. A. Cortés, F. J. Cañete, E. Martos-Naya and L. Díez, "Low-complexity Spectral Shaping Method for OFDM Signals with Dynamic Transmission Band Location," *IEEE International Symposium on Power Line Communications and its Applications* (Presented in the *Recent Results* session), Oct. 2021.

- [22] J. Giménez, J. A. Cortés and L. Díez, "Low-Complexity Spectral Shaping Method for OFDM Signals With Dynamically Adaptive Emission Mask," in *IEEE Transactions on Communications*, vol. 71, no. 4, pp. 2351-2363, April 2023.
- J. Giménez, J. A. Cortés and L. Díez, "A Low-Complexity Spectral Shaping Method for OFDM Signals with Dynamically Defined Emission Mask: Optimization Procedure," *14th Workshop for Power Line Communications*, Sept. 2023.
- [23] J. Giménez, J. A. Cortés, E. Martos-Naya and L. Díez, "Spectral Shaping Method for OFDM Combining Time-Shifted Active Interference Cancellation and Adaptive Symbol Transition," in *IEEE Open Journal of the Communications Society*, vol. 6, pp. 4476-4490, 2025.

Chapter 2

Background

This chapter provides an essential background that will serve as the basis for the main contents of this thesis. To that end, in Section 2.1 some general notation is presented. In Section 2.2, some background on convex optimization is given, along with two effective procedures to control the magnitude of the decision variables. Section 2.3 introduces OFDM signals, where the main assets of this modulation are outlined. Also, a general signal model that will serve as the foundation for subsequent sections is provided. In Section 2.4 some of the most commonly used spectral shaping strategies for OFDM signals are briefly described. Section 2.5 gives an overview on a particular pulse that embeds a combination of two spectral shaping techniques for OFDM, referred to as *generalized pulse*. This particular waveform is fundamental for the contributions of this thesis. Then, a further generalization of this pulse that embodies more techniques is presented. It is proved how this pulse can be particularized for each individual technique, along with their implementation cost.

2.1 Notation

Notation for sets

j	Imaginary unit, $\sqrt{-1}$
$\mathrm{Re}\{\cdot\}$, $(\cdot)^{\Re}$	Real part
$\mathrm{Im}\{\cdot\}$, $(\cdot)^{\Im}$	Imaginary part
$\mathbb{R}, \mathbb{C}, \mathbb{Z}, \mathbb{N}^{+}$	Real, complex, integer and positive natural numbers sets
$\mathcal{A}, \mathcal{B}$, etc.	Calligraphic letters denote sets
$\lvert \cdot \rvert$	Cardinality of a set
$\mathcal{A} \setminus \mathcal{B}$	Set difference of $\mathcal{A}$ and $\mathcal{B}$
$\emptyset$	Empty set

Notation for used functions

$\stackrel{\text{def}}{=}$	Defined as
$\log_n(\cdot)$	Logarithm base n
$\min\{\cdot\}, \max\{\cdot\}$	Minimum and maximum of an expression
$\arg\min\{\cdot\}$	Argument that minimizes an expression
$\arg\max\{\cdot\}$	Argument that maximizes an expression
$\lvert\cdot\rvert$	Absolute value
$\lVert\cdot\rVert_2$	Euclidean norm
$\lfloor\cdot\rfloor, \lceil\cdot\rceil, \lceil\cdot\rfloor$	Floor, ceiling and round functions
$a \bmod b$	Remainder of the division of a by b
$a \equiv b (\text{mod } n)$	a is congruent to b modulo n (i.e., $a \bmod n = b \bmod n$)

Matrix-vector notation

$\mathbf{x}, \mathbf{X}$	Boldface letters denote vectors (lowercase) and matrices (uppercase)
$\mathbb{R}^{M\times N}, \mathbb{C}^{M\times N}$	Sets of real and complex $M \times N$ matrices, respectively
$(\cdot)^*, (\cdot)^{\mathrm{T}}, (\cdot)^{\mathrm{H}}$	Conjugate, transpose and conjugate transpose operators, respectively
$\mathbf{X}^\dagger$	Pseudo-inverse of matrix $\mathbf{X}$ [24, App. A.5.4]
$\mathbf{I}_M$	$M \times M$ identity matrix
$\mathbf{J}_M$	$M \times M$ exchange/backward identity matrix
$\mathbf{0}_{M\times N}$	$M \times N$ all-zeroes matrix
$\mathbf{1}_{M\times N}$	$M \times N$ all-ones matrix
$\text{diag}\big([x_1, \ldots, x_M]\big)$	$M \times M$ diagonal matrix with elements $[x_1, \ldots, x_M]$
$\mathbf{A}[i, j]$	(i, j)-th element of the matrix $\mathbf{A}$
$\mathbf{x}^{\mathrm{b}}$	*Backward* of the vector $\mathbf{x}$ (i.e., $\mathbf{x}^{\mathrm{b}} = \mathbf{J}_M\mathbf{x}^* = \left[x^*_{M-1}, \ldots, x^*_0\right]^{\mathrm{T}}$)
$\mathbf{X}^{\mathrm{b}}$	*Backward* of the matrix $\mathbf{X}$ (i.e., $\mathbf{X}^{\mathrm{b}} = \mathbf{J}_M\mathbf{X}^*\mathbf{J}_N = \left[x^*_{M-i-1,N-j-1}\right] \in \mathbb{C}^{M\times N}$)
$\mathbf{W}_N$	N-point IDFT matrix (i.e., $\mathbf{W}_N = \left[\mathbf{w}^0_N, \ldots, \mathbf{w}^{N-1}_N\right]$)
$\mathbf{w}^k_N$	k-th column of the IDFT matrix (i.e., $\mathbf{w}^k_N = \left[w^{k\cdot 0}_N, \ldots, w^{k\cdot(N-1)}_N\right]^{\mathrm{T}}$)
w^{kn}_N	$e^{j\frac{2\pi}{N}kn}$

2.2 Quadratic optimization problems

This section introduces two tools for convex optimization that will be used in the current and following chapters.

In many areas of engineering, it is common to encounter an optimization problem that seeks to minimize the squared norm of some residual in the form of

$$\arg\min_{\mathbf{x}} \left\{ \|\mathbf{A}\mathbf{x} - \mathbf{b}\|_2^2 \right\}. \tag{2.1}$$

This is a well-known convex optimization problem, with several names depending on the application (e.g., regression analysis or least squares approximation). This unconstrained problem has an analytical solution

$$\mathbf{x} = \mathbf{A}^{\dagger}\mathbf{b} \tag{2.2}$$

where $\mathbf{A}^{\dagger}$ is the pseudo-inverse of $\mathbf{A}$.

Many applications require that these problems apply some constraints to the vector $\mathbf{x}$. In particular, in this thesis we use constraints that limit either the norm of $\mathbf{x}$ or the magnitude of its components, as it is described in the following subsections:

Tikhonov Regularization

Regularization methods [24, Sec. 6.3.2] are used to solve this kind of optimization problem in which two criteria involving the same unknown, $\mathbf{x}$, need to be met. The Tikhonov regularization allows formulating this type of problems as a convex quadratic optimization problem,

$$\min_{\mathbf{x}} \left\{ \|\mathbf{A}\mathbf{x} - \mathbf{b}\|_2^2 + \lambda \|x\|_2^2 \right\} = \min_{\mathbf{x}} \left\{ \mathbf{x}^{\mathrm{H}} \left(\mathbf{A}^{\mathrm{H}}\mathbf{A} + \lambda \mathbf{I} \right) \mathbf{x} - 2\mathbf{b}^{\mathrm{H}}\mathbf{A}\mathbf{x} + \mathbf{b}^{\mathrm{H}}\mathbf{b} \right\}, \tag{2.3}$$

where $\lambda > 0$, is a problem parameter that determines how much the norm of $\mathbf{x}$ penalizes the cost function. The analytical solution for the Tikhonov regularization problem is

$$\mathbf{x} = \left(\mathbf{A}^{\mathrm{T}}\mathbf{A} + \lambda \mathbf{I} \right)^{-1} \mathbf{A}^{\mathrm{T}}\mathbf{b}, \tag{2.4}$$

where no assumptions are required on the matrix $\mathbf{A}$ or vector $\mathbf{b}$. An optimal value of λ will depend on the desired trade-off between the cost function value and the magnitude of the coefficients. However, it has to be obtained heuristically.

Constrained Real and Imaginary Parts

An alternative to the Tikhonov regularization consists in solving the least squares (LS) problem in (2.1) subject to the following constraints

$$\begin{cases} |\mathrm{Re}\{x_i\}| \leq \psi_i \\ |\mathrm{Im}\{x_i\}| \leq \psi_i \end{cases} \quad \text{with } i \in \{1, \ldots, N\} \tag{2.5}$$

where $\mathbf{x} = [x_1, x_2, \ldots, x_N]^{\mathrm{T}}$, which for generality is assumed to be complex-valued. The LS problem in (2.1) subject to these constraints is also convex.

Note that while in the Tikhonov regularization there is only one parameter to adjust, λ, in this approach there are N, each controlling the magnitude of the real and imaginary parts of one of the decision variables involved in the optimization. This end provides a greater number of degrees of freedom.

2.3 OFDM signals

This section gives a brief overview of OFDM systems and provides the signal model that will serve as a basis for the ideas presented in the forthcoming chapters of this thesis.

OFDM is a multi-carrier digital modulation scheme, in which the allocated transmission band is divided into a set of N orthogonal and equally spaced carriers. Each carrier can be used as an independent subchannel where complex symbols are transmitted using a passband pulse amplitude modulation (PAM) scheme. These carriers are first divided into two sets: the set of active carriers, $\mathcal{K}$, contain those with allocated power that are used to transmit symbols, and the set of null carriers, with no allocated power, normally used as guard bands. The active carriers are classified according to the type of symbols they convey, which can be data or auxiliary modulating symbols. The purpose of the latter can be diverse, e.g., pilots for channel, carrier frequency offset (CFO) and sampling frequency offset (SFO) estimation [25] [26]. However, within the scope of this thesis they are exclusively used to reduce the OOBE of the transmitted signal. Consequently, two sets of carriers are defined: $\mathcal{D} = \{d_0, \ldots, d_{|\mathcal{D}|-1}\}$, set containing the indices of the data carriers, and $\mathcal{C} = \{c_0, \ldots, c_{|\mathcal{C}|-1}\}$ for the auxiliary (or redundant) carriers. These sets are such that no redundant carrier can be a data carrier, i.e., $\mathcal{D} \cap \mathcal{C} = \emptyset$, and $\mathcal{K} = \mathcal{D} \cup \mathcal{C}$.

Let the discrete-time low-pass equivalent expression of an OFDM signal be

$$x(n) = \sum_{u=-\infty}^{\infty} x_u(n - uN_{\mathrm{s}}). \tag{2.6}$$

where $N_{\mathrm{s}} = N + N_{\mathrm{GI}}$ is the symbol period, N_{GI} the number of samples in the guard interval and $x_u(n)$ is the u-th transmitted OFDM symbol. Its expression for a conventional OFDM

system, where the set of auxiliary carriers is empty (i.e., $\mathcal{C} = \emptyset \Rightarrow \mathcal{K} = \mathcal{D}$), is

$$x_u(n) = \sum_{k \in \mathcal{D}} p_k(n) s_k(u), \tag{2.7}$$

where $s_k(u)$ denotes the u-th modulating data symbol transmitted on carrier k, and $p_k(n)$ is the transmission pulse used by that carrier, referred to as *base pulse*. The latter is expressed as

$$p_k(n) = g(n) w_N^{k(n-N_{\mathrm{GI}})}, \tag{2.8}$$

where $g(n)$ is a shaping pulse whose only nonzero samples lie in the range $n \in [0, L-1]$, where $L = N_{\mathrm{s}} + \beta$, and $w_N^{kn} = e^{j\frac{2\pi}{N}kn}$. When $\beta = 0$, $g(n)$ is the rectangular pulse used conventionally in OFDM systems. The poor spectral confinement of the latter can be improved by choosing $\beta \neq 0$, so a shaping pulse with tapered transitions on $n \in [0, \beta - 1]$ and $n \in [N_{\mathrm{s}}, L-1]$ can be used, as the one shown in Fig. 2.1.

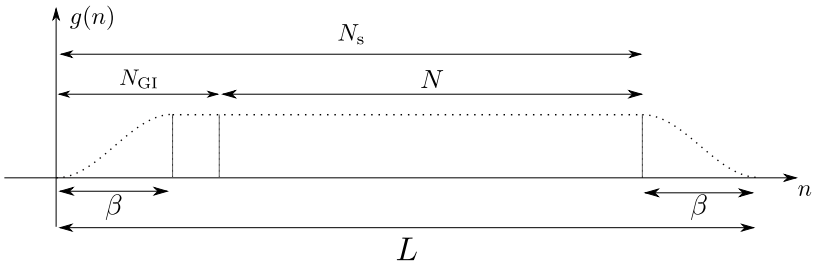

Figure 2.1: Shaping pulse $g(n)$ with smooth transitions and non-zero samples only in the interval $n \in [0, L-1]$.

In practice, OFDM symbols are directly generated in the discrete-time domain: data and auxiliary symbols are modulated at the transmitter using an N-samples IDFT, and demodulated from the received signal using an N-samples DFT. When transmitted over a frequency selective channel with impulse response length of L_{ch} samples, the transmitted symbols experience intersymbol interference (ISI) (i.e., interference from previous OFDM symbols) and intercarrier interference (ICI) (i.e., interference from other carriers). To avoid this effects, a guard interval of $N_{\mathrm{GI}} \geq L_{\mathrm{ch}}$ samples is prepended to each OFDM symbol. This guard interval contains a copy of the OFDM symbol's N_{GI} last samples, which is why it is also referred to as cyclic prefix. Note that the tapered transition at the beginning of the pulse overlaps with the one at the end of the preceding OFDM symbol, leading to a reduction of β samples in the effective length of the cyclic prefix. Then, to avoid ICI and ISI it is required that $N_{\mathrm{GI}} \geq L_{\mathrm{ch}} + \beta$.

For convenience, the u-th OFDM symbol can be expressed in matrix form as

$$\mathbf{x}_u = \mathbf{G}\boldsymbol{\Delta}_{N_{\mathrm{GI}},\beta} \mathbf{W}_N^{\mathcal{D}} \mathbf{s}_{\mathcal{D}}(u), \tag{2.9}$$

where $\mathbf{G} = \mathrm{diag}\big([g(0), \ldots, g(L-1)]\big)$ shapes the boundaries of the transmitted symbol, $\mathbf{W}_N^{\mathcal{D}} = \left[\mathbf{w}_N^{d_0}, \ldots, \mathbf{w}_N^{d_{|\mathcal{D}|-1}}\right]$, with $\mathbf{w}_N^k = \left[w_N^{k\cdot 0}, \ldots, w_N^{k\cdot(N-1)}\right]^{\mathrm{T}}$, perform the IDFT of the

symbols conveyed by the data carriers. Finally, $\mathbf{\Delta}_{N_{\mathrm{GI}},\beta}$ is defined as

$$\mathbf{\Delta}_{N_{\mathrm{GI}},\beta} = \begin{pmatrix} \mathbf{0}_{N_{\mathrm{GI}},N-N_{\mathrm{GI}}} & \mathbf{I}_{N_{\mathrm{GI}}} \\ \mathbf{I}_N & \\ \mathbf{I}_\beta & \mathbf{0}_{\beta,N-\beta} \end{pmatrix}, \tag{2.10}$$

which performs the cyclic extension of the transmitted symbol for the guard interval at the beginning and for the tapered extension at the end.

Assuming that the modulating symbol sequence $s_k(u)$ transmitted in each carrier is white (i.e., flat power spectral density (PSD) and zero mean), with variance σ_k^2, and that sequences transmitted in different carriers are independent, the PSD of the resulting OFDM signal (2.6) can be analytically computed as

$$S(f) = \frac{1}{N_{\mathrm{s}}} \sum_{k\in\mathcal{D}} \sigma_k^2 \left|P_k(f)\right|^2, \tag{2.11}$$

where $P_k(f)$ is the Fourier transform of $p_k(n)$. The latter pulse can be expressed in matrix form as $\mathbf{p}_k = [p_k(0), \ldots, p_k(L-1)]^{\mathrm{T}}$, which enables a compact expression for its Fourier transform as,

$$P_k(f) = \mathbf{f}_L^{\mathrm{H}}(f)\mathbf{p}_k, \tag{2.12}$$

where $\mathbf{f}_L(f) = \left[1, e^{j2\pi f}, \ldots, e^{j2\pi f(L-1)}\right]^{\mathrm{T}}$.

In order to evaluate the total power emitted outside of the transmission band, let us define the mask function $M(f)$ such that $M(f) = 0$ for the frequencies inside the band allocated for the subject OFDM system, and $M(f) = 1$ elsewhere. Accordingly, let us define the power of the OOBE, i.e., the power of the unwanted emissions outside the allocated passband, as

$$P_{\mathrm{OOBE}} = \int_{-1/2}^{1/2} M(f)S(f)df = \frac{1}{N_{\mathrm{s}}} \sum_{k\in\mathcal{D}} \sigma_k^2 \int_{-1/2}^{1/2} M(f)\left|P_k(f)\right|^2 df. \tag{2.13}$$

In some cases, it is interesting from the OOBE minimization point of view to custom-weight different frequency regions, so that reducing the power emitted into some areas of the spectrum has more priority than in others. For example, we might want the OOBE to be lower in the frequencies neighbouring to the passband than in the rest of frequencies. To that end, the range of the mask functions, $M(f)$, is not restricted to 1 and 0, but in-between values can be used.

When $M(f)$ takes values only in $\{0, 1\}$, a set that contains the frequencies where $M(f) = 1$ can be defined as $\mathcal{B} = \left\{f \in (-\frac{1}{2}, \frac{1}{2}] : M(f) = 1\right\}$. Let this set of frequencies be referred to as *notched band*, that is, the range of frequencies where power emissions from the signal should be avoided. Accordingly, a simpler formulation of the OOBE power can be used,

$$P_{\mathrm{OOBE}} = \int_{\mathcal{B}} S(f)df = \frac{1}{N_{\mathrm{s}}} \sum_{k\in\mathcal{D}} \sigma_k^2 \int_{\mathcal{B}} \left|P_k(f)\right|^2 df. \tag{2.14}$$

2.4 Spectral shaping techniques

This section provides background on some of the most widely used spectral shaping methods for OFDM signals. In particular, pulse-shaping, AST, AIC and spectral precoding techniques are reviewed due to their relevance to the contributions of this thesis.

2.4.1 Pulse-shaping

This technique consists in modifying the time-domain shape of the pulse using some window with tapered transitions to enhance the spectral confinement of the resulting OFDM signal. It can be accomplished by employing (2.8) with $g(n)$ using $\beta > 0$. In that case, the u-th OFDM symbol can be expressed as

$$x_u(n) = \sum_{k\in\mathcal{D}} s_k(u)g(n)w_N^{k(n-N_{\mathrm{GI}})}, \tag{2.15}$$

which is an equivalent expression to (2.7). However, the implementation of pulse-shaping is performed after the OFDM symbol is generated and the guard interval is prepended. The latter is shown in expression (2.9).

This technique requires little modifications in the transmitter. As for the receiver, besides the downside of reducing in the effective length of the cyclic prefix, it can be applied transparently. It is noted that the symbol period is N_{s} while the length of the shaping pulse is $L = N_{\mathrm{s}} + \beta$. This results in the tapered transition at the end of one OFDM symbol overlapping with the one at the beginning of the subsequent symbol, which mitigates the transmission efficiency loss.

2.4.2 AIC techniques

In these techniques, a set of auxiliary carriers in $\mathcal{C}$ are designated to reduce the OOBE produced by the data carriers, which is why they are referred to as cancellation carriers (CC). To that end, they are modulated by a set of complex values that are specifically determined to make the spectrum of these CC cancel the aggregate spectrum of the data carriers in the notched band. The expression of the u-th OFDM symbol when CC are used can be written as

$$x_u(n) = \sum_{k\in\mathcal{D}} p_k(n)s_k(u) + \sum_{i\in\mathcal{C}} p_i(n)\theta_i(u) \tag{2.16}$$

where $\theta_i(u) \in \mathbb{C}$ denotes the complex symbol that modulates the i-th CC in the u-th OFDM symbol.

If no constraint is imposed on the amplitudes of $\theta_i(u)$, they can be obtained by linearly combining the constellation symbols transmitted in the data carriers [27]. The coefficients of

the linear combinations are equal for all OFDM symbols and independent of the transmitted data [28].

However, using this procedure generally causes large peaks in the PSD of the transmitted signal. To avoid them, a constrained optimization of $\theta_i(u)$ has to be performed [20], which obliges to solve the optimization problem for each OFDM symbol in the communication device (online). In the following, we will see a practical implementation of the AIC techniques, in which the solutions are independent of the data while PSD peaks are avoided.

AIC techniques require little changes in the transmitter, since the symbols that modulate the CC are input into the IDFT block like the data symbols. The u-th OFDM symbol can be compactly expressed as

$$\mathbf{x}_u = \mathbf{G}\boldsymbol{\Delta}_{N_{\mathrm{GI}},\beta}\big(\mathbf{W}_N^{\mathcal{D}}\mathbf{s}_{\mathcal{D}}(u) + \mathbf{W}_N^{\mathcal{C}}\boldsymbol{\theta}_{\mathcal{C}}(u)\big), \tag{2.17}$$

where $\mathbf{W}_N^{\mathcal{C}} = \left[\mathbf{w}_N^{i_0}, \ldots, \mathbf{w}_N^{i_{|\mathcal{C}|-1}}\right]$ perform the IDFT of the symbols conveyed by the CC, which are contained in $\boldsymbol{\theta}_{\mathcal{C}}(u) = \left[\theta_{i_0}, \theta_{i_1}, \ldots, \theta_{i_{|\mathcal{C}|-1}}\right]^{\mathrm{T}}$.

At the receiver, the symbols conveyed by the CC are discarded, as they are orthogonal to the data carriers. Hence, this techniques can be applied without interfering with the regular operation of the receiver. Nonetheless, even in cases where carrier orthogonality is lost due to receiver limitations (e.g. CFO, Doppler, insufficient cyclic prefix (CP)) the use of AIC does not have a noticeable negative impact on symbol reception. This is because the CC comprise only a small set of carriers: those located within the passband were previously data carriers, and those out-of-band are allocated much less power than the data carriers, thus contributing negligibly to the ICI.

2.4.3 Spectral precoding

This spectral shaping method can be seen as a generalization of the AIC techniques in which the set of carriers used to reduce the OOBE, formerly limited to the CC in $\mathcal{C}$, is extended to the set of active carriers, $\mathcal{K}$. This means that all the active carriers assume the task of reducing the OOBE of the signal, including those that convey data (i.e., those in $\mathcal{D}$). The expression of the u-th OFDM symbol when spectral precoding is applied, can be written as

$$x_u(n) = \sum_{k\in\mathcal{K}} p_k(n) d_k(u), \tag{2.18}$$

where $d_k(u)$ is the complex symbol that modulates de the k-th active carrier in the u-th OFDM symbol. It can be also obtained as a linear combination of the data symbols transmitted in the corresponding OFDM symbol. For precoding schemes, the precoding operation is conventionally formulated in matrix form

$$\mathbf{d}_{\mathcal{K}}(u) = \mathbf{A}_{\mathcal{D}\to\mathcal{K}}\mathbf{s}_{\mathcal{D}}(u), \tag{2.19}$$

where $\mathbf{d}_{\mathcal{K}}(u) = \left[d_{k_0}(u), d_{k_1}(u), \ldots, d_{k_{|\mathcal{K}|-1}}(u)\right]^{\mathrm{T}}$ and $\mathbf{A}_{\mathcal{D}\to\mathcal{K}} \in \mathbb{C}^{|\mathcal{K}|\times|\mathcal{D}|}$ is the *precoding matrix*. Its coefficients are obtained to minimize the OOBE generated by the resulting OFDM signal. Different criteria can be used to accomplish that: force nulls in the signal spectrum at some strategically designated frequencies [9] [10]; or minimize the leaked power in the whole notched band [11]. It should be noted that the achievable performance of the precoding scheme depends on the precoder redundancy, defined as $|\mathcal{K}| - |\mathcal{D}|$.

Spectral precoding increases the transmitter complexity due to the precoding of the data symbols. Then these symbols are input into the IDFT block as in conventional OFDM. Let the u-th OFDM symbol be expressed in matrix form as

$$\mathbf{x}_u = \mathbf{G}\mathbf{\Delta}_{N_{\mathrm{GI}},\beta}\mathbf{W}_N^{\mathcal{K}}\mathbf{A}_{\mathcal{D}\to\mathcal{K}}\mathbf{s}_{\mathcal{D}}(u), \tag{2.20}$$

where $\mathbf{W}_N^{\mathcal{K}} = \left[\mathbf{w}_N^{k_0}, \ldots, \mathbf{w}_N^{k_{|\mathcal{K}|-1}}\right]$ perform the IDFT of the symbols conveyed by the active carriers.

Note that each active carrier conveys a weighted combination of all the data symbols, so a decoding procedure is normally required at the receiver to obtain these symbols with minimum error [9]. The latter operation usually entails noise enhancement, which can be avoided by designing the precoding matrix to be orthogonal. Nonetheless, some precoding schemes avoid decoding the received symbols by imposing some conditions on the precoding matrix, $\mathbf{A}_{\mathcal{D}\to\mathcal{K}}$. For instance, by minimizing the Euclidean distance between the data symbols and the precoded ones [8], the error vector magnitude (EVM) can be kept under control without complicating the receiver.

2.4.4 AST techniques

These techniques achieve OOBE reduction by adaptively designing the transitions between consecutive OFDM symbols. Similar to pulse shaping, this technique aims to smooth these transitions, but it provides a larger number of degrees of freedom. It is accomplished by prepending an additive term to each OFDM symbol. Accordingly, the u-th OFDM symbol can be expressed as

$$x_u(n) = \sum_{k\in\mathcal{D}} p_k(n)s_k(u) + a_u(n), \tag{2.21}$$

where $a_u(n)$ is the additive term that is only non-zero in the transition between consecutive OFDM symbols. In this case, the u-th AST term is non-zero for $n \in [u\cdot N_{\mathrm{s}}, u\cdot N_{\mathrm{s}} + \beta - 1]$, i.e., at the beginning of the u-th OFDM symbol. It is noted that this term overlaps with the first β samples of the OFDM symbol, which extends from $n = 0$ to $n = L - 1$, where $L = N_{\mathrm{s}} + \beta$. Consequently, it reduces the effective length of the guard interval.

The β samples that constitute the AST term are designed to minimize the OOBE of the transmitted signal. To that end, in [15] both the u-th and $(u-1)$-th symbols take part in the computation of $a_u(n)$, where a LS problem is solved subject to a quadratic inequality.

This solution is necessarily dependent on the data being transmitted. Hence, it has to be computed for each OFDM symbol. At the receiver, it is discarded along with the guard interval and it remains unaffected by the loss of orthogonality between carriers.

In what follows, a simpler implementation of the AST technique that does not require performing an optimization procedure for every OFDM symbol is proposed.

2.5 The generalized pulse

This section reviews a novel waveform for OFDM signals proposed in [16], which forms the foundation for the objectives pursued in this thesis. The proposed pulse is referred to as *generalized pulse*, since it generalizes and unifies many AIC and AST techniques, which can be obtained as particular cases of it. The generalized pulse has two key features: it does not depend on the data and can be used without interfering with the regular reception of the OFDM symbols. Hence, in order to use the generalized pulse, no modifications of the conventional OFDM receiver are needed, nor does the optimal solution have to be recalculated for each OFDM symbol.

Let the generalized pulse used by the k-th data carrier be expressed as [16]

$$h_k(n) = p_k(n) + \sum_{i \in \mathcal{C}} \alpha_{i,k} p_i(n) + t_k(n), \quad k \in \mathcal{D}, \tag{2.22}$$

where the first term on the right hand side (RHS) is the base pulse used in conventional OFDM, and the second and third terms are the AIC and AST components, respectively. In this way, the generalized pulse includes cancellation terms that allow each data carrier that uses this pulse to self-limit its OOBE. The AIC term consists of the weighted sum of the pulses used by the CC in the set $\mathcal{C}$, where $\alpha_{i,k} \in \mathbb{C}$ is the weight assigned to the i-th CC for the data carrier k. The spectra of these CC are conveniently combined to cancel the sidelobes of the base pulse's spectrum. The AST term, $t_k(n)$, is also referred to as *transition pulse*. It is nonzero for the starting and ending boundaries of the pulse, that is, in $n \in [0, \beta - 1] \cup [L - \beta, L - 1]$, overlapping with the tapered transitions of $g(n)$. This way, it smooths the transitions between OFDM symbols, enhancing the spectral confinement of the signal.

For compactness, the generalized pulse can be expressed in its matrix form

$$\mathbf{h}_k = \mathbf{p}_k + \mathbf{P}_{\mathcal{C}} \boldsymbol{\alpha}_k + \mathbf{t}_k, \tag{2.23}$$

where $\mathbf{P}_{\mathcal{C}} = \left[\mathbf{p}_{i_0}, \ldots, \mathbf{p}_{i_{|\mathcal{C}|-1}}\right]$ is an $L \times |\mathcal{C}|$ matrix whose column vectors are pulses corresponding to the CC, $\boldsymbol{\alpha}_k = \left[\alpha_{i_0,k}, \ldots, \alpha_{i_{|\mathcal{C}|-1},k}\right]^{\mathrm{T}}$ is the vector of coefficients that weight the CC for the k-th data carrier and $\mathbf{t}_k = [t_k(0), \ldots, t_k(L-1)]^{\mathrm{T}}$ is the transition pulse in

vector form. Since the latter is nonzero just for the starting and ending β samples, it can be expressed as

$$\mathbf{t}_k = \underbrace{\begin{bmatrix} \mathbf{I}_\beta & & \mathbf{0}_{\beta,\beta} \\ & \mathbf{0}_{L-2\beta,2\beta} & \\ \mathbf{0}_{\beta,\beta} & & \mathbf{I}_\beta \end{bmatrix}}_{\mathbf{T}} \boldsymbol{\zeta}_k, \tag{2.24}$$

where $\boldsymbol{\zeta}_k = [\zeta_k(0), \ldots, \zeta_k(2\beta-1)]^{\mathrm{T}}$ contain the nonzero samples of $t_k(n)$. Alternatively, it can be expressed as

$$\mathbf{t}_k = \begin{bmatrix} \mathbf{I}_\beta \\ \mathbf{0}_{L-\beta,\beta} \end{bmatrix} \boldsymbol{\zeta}_k^{\mathrm{s}} + \begin{bmatrix} \mathbf{0}_{L-\beta,\beta} \\ \mathbf{I}_\beta \end{bmatrix} \boldsymbol{\zeta}_k^{\mathrm{e}}, \tag{2.25}$$

where the coefficients $\boldsymbol{\zeta}_k$ are separated in two vectors, $\boldsymbol{\zeta}_k^{\mathrm{s}} = [\zeta_k(0), \ldots, \zeta_k(\beta-1)]$ and $\boldsymbol{\zeta}_k^{\mathrm{e}} = [\zeta_k(\beta), \ldots, \zeta_k(2\beta-1)]$, representing the starting and ending samples of the transition pulse, respectively. For compactness, $\mathbf{h}_k$ can be expressed as

$$\mathbf{h}_k = \mathbf{p}_k + \underbrace{\begin{bmatrix} \mathbf{P}_{\mathcal{C}} & \mathbf{T} \end{bmatrix}}_{\boldsymbol{\Pi}} \underbrace{\begin{bmatrix} \boldsymbol{\alpha}_k \\ \boldsymbol{\zeta}_k \end{bmatrix}}_{\boldsymbol{\gamma}_k}. \tag{2.26}$$

It can be easily proved that the generalized pulse can be particularized into the AIC and AST techniques proposed in Sec. 2.4. For the latter, the starting and ending nonzero regions of $\mathbf{t}_k$ can be identified as the contribution of the k-th data carrier and the u-th OFDM symbol to the terms $a_u(n)$ and $a_{u+1}(n)$, respectively (as defined in (2.21)). For the AIC techniques, the complex symbol $\theta_i(u)$ used in (2.16) can be expressed in terms of the coefficients of the generalized pulse, $\alpha_{i,k}$, as

$$\theta_i(u) = \sum_{k \in \mathcal{D}} \alpha_{i,k} s_k(u) \quad \forall i \in \mathcal{C}. \tag{2.27}$$

See Appendix A.2 for a more detailed proof.

Note that the total OOBE emitted by an OFDM signal is dominated by the data carriers located closest to the regions of the spectrum where emissions should be avoided. The remaining data carriers produce negligible emissions into those regions, so they do not need to use the generalized pulse in (2.22). As a consequence, let us define the subset of data carriers that employ this pulse as $\mathcal{D}^{\mathrm{h}} \subseteq \mathcal{D}$.

In that case, the u-th OFDM symbol can be expressed as

$$x_u(n) = \sum_{k \in \mathcal{D} \setminus \mathcal{D}^{\mathrm{h}}} p_k(n) s_k(u) + \sum_{k \in \mathcal{D}^{\mathrm{h}}} h_k(n) s_k(u). \tag{2.28}$$

Then, the PSD of the resulting OFDM signal is

$$S(f) = \frac{1}{N_{\mathrm{s}}} \sum_{k \in \mathcal{D} \setminus \mathcal{D}^{\mathrm{h}}} \sigma_k^2 \left| P_k(f) \right|^2 + \frac{1}{N_{\mathrm{s}}} \sum_{k \in \mathcal{D}^{\mathrm{h}}} \sigma_k^2 \left| H_k(f) \right|^2, \tag{2.29}$$

where $H_k(f)$ is the Fourier transform of the modified pulse $h_k(n)$, i.e., $H_k(f) = \mathbf{f}_L^{\mathrm{H}}(f)\mathbf{h}_k$. The power emitted into the notched band $\mathcal{B}$ can be obtained disregarding the one produced by the data carriers that do not use the generalized pulse (those $\mathcal{D} \setminus \mathcal{D}^{\mathrm{h}}$), as

$$P_{\mathrm{OOBE}} = \int_{\mathcal{B}} S(f)df \approx \frac{1}{N_{\mathrm{s}}} \sum_{k \in \mathcal{D}^{\mathrm{h}}} \sigma_k^2 E_{k,\mathcal{B}}, \tag{2.30}$$

where $E_{k,\mathcal{B}}$ is the energy that the generalized pulse used by the k-th data carrier emits into $\mathcal{B}$. The expression of the latter is

$$E_{k,\mathcal{B}} = \mathbf{h}_k^{\mathrm{H}} \mathbf{\Phi}_{\mathcal{B}} \mathbf{h}_k = (\mathbf{p}_k + \mathbf{\Pi}\boldsymbol{\gamma}_k)^{\mathrm{H}} \mathbf{\Phi}_{\mathcal{B}} (\mathbf{p}_k + \mathbf{\Pi}\boldsymbol{\gamma}_k), \tag{2.31}$$

where $\mathbf{\Phi}_{\mathcal{B}} = \int_{\mathcal{B}} \mathbf{f}_L(f)\mathbf{f}_L^{\mathrm{H}}(f)df$.

We notice that P_{OOBE} is the weighted sum of the energy emitted into the notched band by each of the generalized pulses used in the signal. Since each $E_{k,\mathcal{B}}$ depends only on the generalized pulse $\mathbf{h}_k$ and the notched band $\mathcal{B}$, which is the same for all the carriers, to minimize the OOBE one just needs to obtain the pulse that makes $E_{k,\mathcal{B}}$ minimum for each data carrier in $\mathcal{D}^{\mathrm{h}}$. Hence, the OOBE minimization problem can be solved on a carrier-by-carrier basis. In that case, let the coefficients that minimize the leakage of the k-th generalized pulse be obtained as

$$\widehat{\boldsymbol{\gamma}}_k = \arg\min_{\boldsymbol{\gamma}_k} \{E_{k,\mathcal{B}}\}. \tag{2.32}$$

In [16], a closed expression for this optimization problem is provided, which involves minimizing a quadratic function over $\boldsymbol{\gamma}_k$, which is a convex optimization problem [24, p. 71]. The solution is given by

$$\widehat{\boldsymbol{\gamma}}_k = -\left(\mathbf{\Pi}^{\mathrm{H}} \mathbf{\Phi}_{\mathcal{B}} \mathbf{\Pi}\right)^{-1} \mathbf{\Pi}^{\mathrm{H}} \mathbf{\Phi}_{\mathcal{B}} \mathbf{p}_k. \tag{2.33}$$

However, this unconstrained optimization usually results in a solution that yields PSD peaks inside the transmission band. This can be avoided by introducing a second criterion in the optimization problem that limits the magnitude of the coefficients. In the problem proposed in (2.32) this can be done by using the Tikhonov regularization introduced in Section 2.2, which turns the optimization problem into

$$\widehat{\boldsymbol{\gamma}}_k = \arg\min_{\boldsymbol{\gamma}_k} \left\{(\mathbf{p}_k + \mathbf{\Pi}\boldsymbol{\gamma}_k)^{\mathrm{H}} \mathbf{\Phi}_{\mathcal{B}} (\mathbf{p}_k + \mathbf{\Pi}\boldsymbol{\gamma}_k) + \lambda \boldsymbol{\gamma}_k^{\mathrm{H}} \mathbf{I}_Q \boldsymbol{\gamma}_k\right\}. \tag{2.34}$$

where $Q = |\mathcal{C}| + 2\beta$. This problem has a closed-form solution

$$\widehat{\boldsymbol{\gamma}}_k = -\left(\mathbf{\Pi}^{\mathrm{H}} \mathbf{\Phi}_{\mathcal{B}} \mathbf{\Pi} + \lambda \mathbf{I}_Q\right)^{-1} \mathbf{\Pi}^{\mathrm{H}} \mathbf{\Phi}_{\mathcal{B}} \mathbf{p}_k. \tag{2.35}$$

for which an appropriate value for λ has to be obtained heuristically. This may oblige to compute expression (2.35) several times before reaching a solution that satisfies the requirements of the problem. Moreover, the relation between the regularization parameter

λ and the magnitude of the PSD peaks is not straightforward. Alternatively, the problem (2.32) can be solved with constraints imposed on the absolute value of the real and imaginary parts of $\boldsymbol{\alpha}_k$ and $\boldsymbol{\zeta}_k$, as it is introduced in Sec. 2.2,

$$\left.\begin{array}{l} |\mathrm{Re}\{\alpha_{c_i,k}\}| \leq \epsilon_{c_i,k} \\ |\mathrm{Im}\{\alpha_{c_i,k}\}| \leq \epsilon_{c_i,k} \end{array}\right\} \text{ for } i \in \{0,\ldots,|\mathcal{C}|-1\}$$
$$\left.\begin{array}{l} |\mathrm{Re}\{\zeta_k(r)\}| \leq \delta_k \\ |\mathrm{Im}\{\zeta_k(r)\}| \leq \delta_k \end{array}\right\} \text{ for } r \in \{0,\ldots,2\beta-1\}\,. \tag{2.36}$$

The latter approach yields more degrees of freedom, enabling a finer control over the trade-off between the OOBE reduction and the PSD peaks. To illustrate this end, Fig. 2.2 shows the normalized PSD of the signal obtained when the OOBE of a single data carrier needs to be reduced in the notch. The problem involves an extended version of the generalized pulse, proposed as one of the contributions of this thesis in Sec. 3.3, obtained in two different ways: using the closed expression (2.35), in blue, and obtained numerically solving (2.32) subject to (2.36), in yellow. The spectrum of the pulse with raised cosine (RC)-shaped tapered transitions (referred to as RC-shaped pulse) is shown as a reference, in red. Each of the pulses uses the same set of CC. The parameter λ and the limits in (2.36) are tuned to avoid PSD peaks in the passband. As a result, Fig. 2.2 shows that the solution obtained using (2.35) gives slightly higher PSD in the notch than the constrained numerical minimization (roughly 1.5 dB). It should be noted that the contribution of each data carrier to the OOBE is additive. Hence, when all of them are considered, the performance gap between both optimization criteria increases.

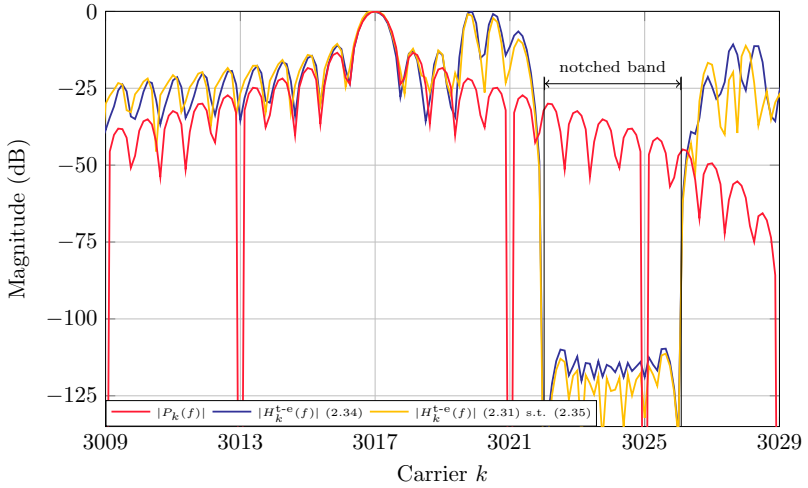

Figure 2.2: Magnitude of the generalized pulse when used by one data carrier located next to a notch band. In the comparison, two different ways of obtaining the optimal pulse are assessed: by using (2.35) subject to a parameter λ, and by numerically minimizing (2.32) subject to (2.36). The conventional RC pulse is shown (in red) as a reference.

2.5.1 Implementation of the generalized pulse

When the generalized pulse is used, the u-th OFDM symbol can be expressed as

$$\mathbf{x}_u = \mathbf{G}\boldsymbol{\Delta}_{N_{\mathrm{GI}},\beta}\Big(\mathbf{W}_N^{\mathcal{D}}\mathbf{s}_{\mathcal{D}}(u) + \mathbf{W}_N^{\mathcal{C}}\mathbf{A}_{\mathcal{D}\to\mathcal{C}}\mathbf{s}_{\mathcal{D}}(u)\Big) + \mathbf{T}\mathbf{Z}_{\mathcal{D}}\mathbf{s}_{\mathcal{D}}(u), \tag{2.37}$$

where $\mathbf{A}_{\mathcal{D}\to\mathcal{C}} = \Big[\boldsymbol{\alpha}_{d_0}, \ldots, \boldsymbol{\alpha}_{d_{|\mathcal{D}|-1}}\Big]$ and $\mathbf{Z}_{\mathcal{D}} = \Big[\boldsymbol{\zeta}_{\boldsymbol{d_0}}, \ldots, \boldsymbol{\zeta}_{\boldsymbol{d_{|\mathcal{D}|-1}}}\Big]$.

It is noted that for the k-th data carrier using the generalized pulse, only the CCs located close to the region where emissions need to be reduced are able to successfully compensate for the leakage the corresponding data carrier produces in the latter. Therefore, for each data carrier k, there is a subset of $\mathcal{C}$ that effectively contribute to the minimization of its OOBE. This subset, denoted as $\mathcal{C}(k) \subset \mathcal{C}$, might vary from one data carrier to another. This implies that only the coefficients corresponding to the CCs in the set $\mathcal{C}(k)$ are nonzero for data carrier k, i.e., $\alpha_{c_i,k} = 0, \forall c_i \in \mathcal{C} : c_i \notin \mathcal{C}(k), \forall k \in \mathcal{D}$. Moreover, it was proved in [16] that most of the OOBE reduction is attained with just 3 CC around each edge of the passband—2 inside the passband and 1 out-of-band.

An alternative and computationally simpler way to implement the transition pulse is proposed in [16]. It consists in expressing the nonzero samples of the transition pulse in terms o two IDFT of β samples. That is,

$$\mathbf{t}_k = \begin{bmatrix} \mathbf{W}_\beta \\ \mathbf{0}_{L-\beta,\beta} \end{bmatrix} \boldsymbol{\xi}_k^{\mathrm{s}} + \begin{bmatrix} \mathbf{0}_{L-\beta,\beta} \\ \mathbf{W}_\beta \end{bmatrix} \boldsymbol{\xi}_k^{\mathrm{e}}, \tag{2.38}$$

where $\mathbf{W}_\beta = \Big[\mathbf{w}_\beta^0, \ldots, \mathbf{w}_\beta^{\beta-1}\Big]$ is the β-samples IDFT matrix, and $\boldsymbol{\xi}_k^{\mathrm{s}} = [\xi_k^{\mathrm{s}}(0), \ldots, \xi_k^{\mathrm{s}}(\beta-1)]^{\mathrm{T}}$ and $\boldsymbol{\xi}_k^{\mathrm{e}} = [\xi_k^{\mathrm{e}}(0), \ldots, \xi_k^{\mathrm{e}}(\beta-1)]^{\mathrm{T}}$ are the samples corresponding to the β-DFT of the starting and ending boundaries of the transition pulse, respectively. Accordingly, the following matrix can be defined

$$\mathbf{T}_{\mathrm{h}} = \begin{bmatrix} \mathbf{W}_\beta & \mathbf{0}_{L-\beta,\beta} \\ \mathbf{0}_{L-\beta,\beta} & \mathbf{W}_\beta \end{bmatrix}, \tag{2.39}$$

so that

$$\mathbf{t}_k = \mathbf{T}_{\mathrm{h}} \begin{bmatrix} \boldsymbol{\xi}_k^{\mathrm{s}} \\ \boldsymbol{\xi}_k^{\mathrm{e}} \end{bmatrix}. \tag{2.40}$$

Finally, since the ending section of the transition pulse of one OFDM symbol overlaps with the starting section of the subsequent symbol's transition pulse, it is proved that the real-time implementation of this term can be done with only one β-DFT per OFDM symbol. This implementation of the transition pulse is referred to as *harmonically designed* AST or h-AST, for convenience.

Note that the DFT terms that contribute the most to reducing the OOBE are those corresponding to frequencies that are close to the region where the OOBE needs to be minimized.

Hence, only those terms should be considered, which allows the distant ones to be zeroed. This end makes $\boldsymbol{\xi}_k^{\mathrm{s}}$ and $\boldsymbol{\xi}_k^{\mathrm{e}}$ sparse vectors, reducing the computational complexity involved in optimizing and implementing the AST term. Naturally, the subset of effective DFT terms depend on the data carrier index, so let us denote it as $\mathcal{T}(k)$.

For simplicity in the notation, in the forthcoming chapter the regular implementation of the transition pulses is assumed. However, all the contributions in this thesis can benefit from the use of harmonically designed AST terms. Furthermore, most of the presented results are obtained with this particular implementation of the transition pulse. The corresponding works contain information about how this is accomplished.

2.5.2 Supergeneralized pulse

Among the spectral shaping techniques reviewed in Sec. 2.4, the generalized pulse unifies three of them within the same waveform: pulse shaping, AIC and AST techniques. Nevertheless, a new waveform can be proposed to include spectral precoding into the same formulation[1].

Let the expression of this new waveform be

$$h_k(n) = p_k(n) + \sum_{i \in \mathcal{K}; i \neq k} \alpha_{i,k} p_i(n) + t_k(n), \quad k \in \mathcal{D}, \tag{2.41}$$

which, like the generalized pulse, is used by the data carriers in $\mathcal{D}^{\mathrm{h}}$, replacing the base pulse $p_k(n)$. The first term on the RHS of (2.41) is the base pulse. The second term is a weighted sum, with $\alpha_{i,k} \in \mathbb{C}$, of the pulses transmitted in the remaining active carriers. In this way, every active carrier other than k contributes to reducing the leakage of the base pulse used by the latter carrier. The last term, $t_k(n)$, is the AST term.

The proposed pulse can be used in the same way the generalized pulse is employed, and shares with the latter one critical characteristic: optimal pulses do not depend on the data being transmitted, and can be computed offline. To that end, an optimization procedure like the one proposed in (2.32) can be solved for each data carrier, subject to constraints like the ones in (2.36) to avoid PSD peaks.

In Table 2.1 it is shown how this pulse can be particularized to obtain the spectral shaping techniques reviewed above. As indicated in the table notes, it is achieved by omitting and grouping specific terms in (2.41). The proposed expressions differ from those conventionally used for each of these spectral shaping techniques. However, in Appendix A.2 there is proof of how the ones proposed in Table 2.1 are related to the ones conventionally used.

[1]The formulation that encompasses the four spectral shaping techniques reviewed in Sec. 2.4 is a contribution of this thesis, but for convenience, and given its generality, it is presented in this chapter. In particular, the new formulation is proposed in the work [21].

Table 2.1: Particularized expressions of the supergeneralized pulse in (2.41) for each of the reviewed spectral shaping methods for OFDM. The implementation complexity of each technique, given in number of complex products per OFDM symbol, is also provided.

Method	**Expression**	**Number of complex products/OFDM symbol**
Pulse-shaping[a]	$h_k(n) = p_k(n)$	2β
AIC[b]	$h_k(n) = p_k(n) + \sum_{i\in\mathcal{C}(k)} \alpha_{i,k} p_i(n)$	$\sum_{k\in\mathcal{D}} \lvert\mathcal{C}(k)\rvert$
Precoding[cd]	$h_k(n) = \sum_{i\in\mathcal{K}} \alpha_{i,k} p_i(n)$	$\lvert\mathcal{K}\rvert\lvert\mathcal{D}\rvert$
AST[e]	$h_k(n) = p_k(n) + t_k(n)$	$2\beta\lvert\mathcal{D}\rvert$
h-AST[e]		$\sum_{k\in\mathcal{D}} 2\lvert\mathcal{T}(k)\rvert + \frac{\beta}{2}\log_2(\beta)$

[a] When $\beta \neq 0$ the shaping pulse $g(n)$ has two tapered boundaries of β samples each.
[b] The summation is particularized to the set of CC, $\mathcal{C}(k)$, and $t_k(n)$ is omitted.
[c] It is assumed that $\alpha_{k,k} = 1$, $\forall k \in \mathcal{D}$, and the first two terms are grouped. Also, $t_k(n)$ is omitted.
[d] For the complexity, its straightforward implementation is considered, involving the product between the precoding matrix and the data symbols. Furthermore, $\lvert\mathcal{K}\rvert\lvert\mathcal{D}\rvert$ additional products might be required at the receiver in some precoding strategies.
[e] The summation (second) term in (2.41) is omitted.

The reviewed spectral shaping methods require just minimal modifications at the transmitter for their implementations. Meanwhile, for most of them, with the exception of most implementations of spectral precoding, the receiver can remain unmodified. The number of complex products per OFDM symbol required to implement each of the spectral shaping methods described in this section is given in Table 2.1. The implementation cost of each technique has to be added to that of conventional OFDM, involving a single N-samples IDFT, which can be assumed to be $\frac{N}{2}\log_2(N)$.

Note that pulse-shaping involves tapering just the starting and ending boundaries of the pulse, of β samples each, as it is portrayed in Fig. 2.1. The remaining central samples of the pulse are left untouched. In addition, it is recalled that, for the AIC method, $\mathcal{C}(k)$ is the subset of CCs that are used to minimize the OOBE of data carrier k. Likewise, $\mathcal{T}(k)$ denotes the number of frequency terms used in the design of the starting and ending terms of the h-AST. The implementation of the latter involves performing a β-DFT, whose cost is included as $\frac{\beta}{2}\log_2(\beta)$. Finally, the implementation cost for the spectral precoding method is obtained assuming its straightforward implementation, which involves a product with the precoding matrix. Nonetheless, in the literature there is a wide range of approaches with lower implementation costs [29]. Some precoding schemes also require modifications at the receiver: for instance, orthogonal precoding multiply the received symbols with a $\lvert\mathcal{K}\rvert \times \lvert\mathcal{K}\rvert$ matrix; for other precoding methods, a suboptimal iterative decoding procedure like the one

originally proposed in [30] can be used. Alternatively, precoding can be applied transparent to the receiver at the expense of an increase in the BER [8].

In Table 2.2 we qualitatively compare the performance and complexity of spectral precoding and of the combined AIC and AST techniques. The latter combination achieves higher performance (comparable to that of spectral precoding) when both techniques are used together. It is shown that AIC+AST have a greater capability to generate deep notches within the passband than spectral precoding. Conversely, the latter yields faster-decaying sidelobes in the sidebands compared to the AIC+AST technique, which produces spectra with steep notches near the passband edges but with more slowly decaying sidelobes. As for the complexity of these two techniques, the AIC+AST technique is transparent to the receiver, while its implementation at the transmitter involves a low-to-moderate increase in the number of complex multiplications. Meanwhile, spectral precoding involves a high increase in computational complexity at both the transmitter and the receiver.

Table 2.2: Performance and complexity comparison between the combined AIC+AST techniques and spectral precoding.

Method	**Performance**		**Complexity**	
	In-band notch	**Sideband**	**Transmitter**	**Receiver**
AIC+AST	Good	Moderate	Low-Moderate	Transparent
Precoding	Moderate	Good	High	High[a]

[a] Most implementations of precoding require a decoding procedure at the receiver to avoid negatively impacting the BER and the EVM.

Chapter 3

Contributions and Summary of Results

This chapter contains a summarized review of the contributions made in this thesis and a selection of its most relevant results. The contributions are threefold:

i) A new waveform and a design framework are proposed to shape the spectrum of OFDM signals. Their use leads to substantial reductions in the computational cost of both the optimization procedures involved and the real-time implementation of several spectral shaping techniques commonly used in OFDM systems.

ii) A second design framework is proposed to reduce the real-time implementation cost of AIC and AST spectral shaping techniques for OFDM systems that operate in scenarios with dynamically changing PSD emission requirements.

iii) A spectral shaping strategy that combines AIC and AST techniques, generalized by extending their influence to previous and subsequent symbols. This generalization improves their performance by further diminishing the OOBE and by mitigating the data rate penalty yielded by the first technique.

These contributions comprise a set of tools for the design of low-complexity and receiver-agnostic spectral shaping solutions for OFDM systems. The following exposition will focus on each of the contributions separately. At the end of this chapter, some insight is provided on how they can be combined to accomplish different results.

The chapter organization is as follows. First, in Section 3.1 the new waveform and the first design framework is proposed, as it allows a wider range of techniques to reduce their optimization and implementation cost, such as spectral precoding, AIC and AST techniques. Section 3.2 summarizes the second spectral shaping framework, this one oriented just to the

generalized pulse (which, it is recalled, generalizes other AIC- and AST- based techniques). Finally, in Section 3.3 the generalization for AIC and AST techniques is provided.

3.1 Novel pulse and design framework to reduce the complexity of spectral shaping methods

This first section makes a twofold contribution:

- First, a new pulse with Hermitian symmetry is proposed to replace the conventional OFDM one. It enables notable reductions in the implementation cost of several commonly used spectral shaping techniques.
- Second, an optimization framework for this new waveform is devised. It defines a problem template that grants a reduction of up to 50% in both the optimization cost and the cost of its real-time implementation.

In addition, a compilation of existing spectral shaping strategies from the literature that benefit from these proposals is provided to demonstrate its utility.

This set of contributions is presented in

[21] J. Giménez, J. A. Cortés, F. Javier Cañete, E. Martos-Naya and L. Díez, "A Modified Pulse and Design Framework to Halve the Complexity of OFDM Spectral Shaping Techniques," in *IEEE Communications Letters*, vol. 28, no. 9, pp. 2146-2150, Sept. 2024,

attached in Appendix B.1.1.

The first contribution involves modifying the conventional OFDM signal by forcing symmetry on the pulse transmitted by each carrier. This is carried out by replacing $p_k(n)$ with its Hermitian-symmetric[1] counterpart,

$$\widetilde{p}_k(n) = g(n+\eta)w_N^{kn}, \tag{3.1}$$

where $\eta = (L-1)/2$ and $g(n)$ is the shaping pulse with tapered transitions introduced in Chapter 2. To illustrate the purpose of this replacement, Fig. 3.1 depicts the imaginary part of the carriers with indices $k = 1, 2, 3$ both when the conventional OFDM pulse is employed (a), and when the proposed pulse $\widetilde{p}_k(n)$ proposed in (3.1) is used (b). Note that the phase origin (phase equal to zero) for all carriers of a conventional OFDM signal is at sample $n = N_{\mathrm{GI}}$. When the proposed pulse is used, the phase origin for all carriers is placed at the sample $n = \frac{L-1}{2} = \eta$, achieving an OFDM symbol that has Hermitian symmetry.

[1] A discrete-time function $x(n)$ has Hermitian symmetry (also known as conjugate symmetry [31, Sec. 5.3.4]) if $x(-n) = x(n)^*$. The Fourier transform of a Hermitian-symmetric function is real valued by virtue of the conjugate and duality properties.

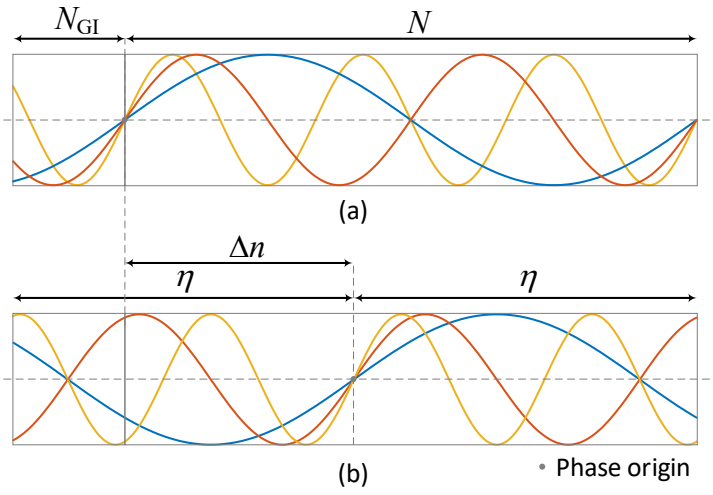

Figure 3.1: Illustrative representation of the (a) conventional OFDM and (b) OFDM with the proposed pulse. For the sake of clarity, only the imaginary part is depicted using continuous line and a rectangular shaping pulse is assumed.

Replacing the conventional pulse with the proposed Hermitian-symmetric one involves minor changes in the transmitter. For the former, symmetry can be attained by multiplying the inputs of the IDFT by the phasor $e^{-\frac{j2\pi}{N}k(\eta-N_{\mathrm{GI}})} = e^{-\frac{j2\pi}{N}k\frac{(N-N_{\mathrm{GI}}+\beta-1)}{2}} = e^{-\frac{j2\pi}{N}k\Delta n}$. However, the properties of the IDFT allow obtaining this same result by circularly rotating its output to the right by $\Delta n = \frac{(N-N_{\mathrm{GI}}+\beta-1)}{2}$ samples. This operation is depicted in Fig. 3.2. Since the time origin is arbitrary (the key aspect is that the phase origin is placed at the central sample of the OFDM symbol) the resulting signal will be equal to the one generated with the pulse $\widetilde{p}_k(n)$ given in (3.1).

At the receiver, this reordering of samples translates into a rotation in the carriers' constellations. This can be strictly compensated for by performing a circular shift to the left of Δn samples, which requires the receiver to be aware of the spectral shaping techniques performed on the signal. Alternatively, this rotation can be absorbed as part of the channel response by the frequency equalizer (FEQ) typically used in OFDM systems. Hence, this change in the transmitted signal can be transparent to the receiver.

At the end of Chapter 2, we showed that a range of widely used spectral shaping techniques—spectral precoding, AIC and AST—can be unified under a single pulse. This pulse, defined in (2.41), serves as a general formulation from which each individual technique can be derived by combining or excluding specific terms. When $\widetilde{p}_k(n)$ is used to replace $p_k(n)$, the pulse in

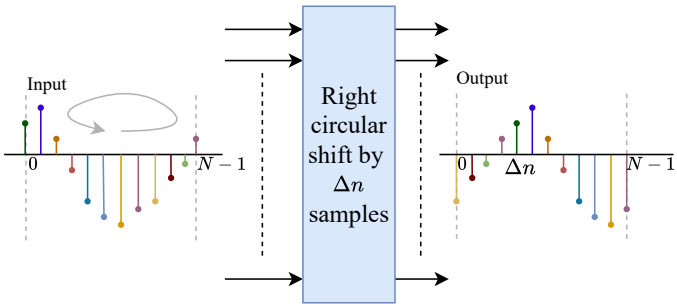

Figure 3.2: Detail of the right circular shift applied to the IDFT output samples.

(2.41) can be rewritten as

$$\widetilde{h}_k(n) = \widetilde{p}_k(n) + \sum_{i\in\mathcal{K};i\neq k} \widetilde{\alpha}_{i,k}\widetilde{p}_i(n) + \widetilde{t}_k(n). \tag{3.2}$$

where $\widetilde{\alpha}_{i,k}$ and $\widetilde{t}_k(n)$ are the weight for the i-th CC and the transition pulse of this new waveform, respectively. These coefficients should be obtained with the objective of minimizing the OOBE of the resulting OFDM signal. Moreover, to avoid the appearance of PSD peaks, some constraints should be applied to the optimization problem.

Let us introduce the following problem model for the optimization of the modified pulses proposed in (3.2),

$$\begin{aligned} &\widehat{\widetilde{\mathbf{H}}}_{\mathcal{D}} = \arg\min_{\widetilde{\mathbf{H}}_{\mathcal{D}}} \left\{ \sum_{k\in\mathcal{D}} \sigma_k^2 \int_{-1/2}^{1/2} M_0(f) \left|\widetilde{H}_k(f)\right|^2 df \right\} \\ &\text{s.to.} \\ &\quad \sum_{k\in\mathcal{D}} \sigma_k^2 \int_{-1/2}^{1/2} M_j(f) \left|\widetilde{H}_k(f)\right|^2 df \leq \delta_j, \quad 1 \leq j \leq R, \end{aligned} \tag{3.3}$$

where $M_j(f)$ is the j-th mask function, δ_j the value to which the j-th summation is bounded, and R is the number of constraints that will be applied. Typically, $M_j(f)$ is defined such that they equal 1 in the frequency regions where the energy emissions have to be controlled and 0 elsewhere. Nonetheless, values in between can be considered to custom-weight different regions of the spectrum with different purposes, as it was previously stated. Both the cost function and the constraints refer to the energy emitted by the set of data carriers at the frequencies indicated by the mask functions $M_j(f)$ when the pulse in (3.2) is used. A practical goal is to minimize the leakage in the notched band while the constraints are set to, for instance, limit the the total transmission power of the signal (when $M_1(f) = 1$ $\forall f \in [-1/2, 1/2)$), or avoid PSD peaks in the passband, a recurring restriction when using AIC techniques [11] [16], among others.

The proposed template encompasses a wide range of problems where the cost function and the constraints share a common trait: they involve the energy of the transmission pulse. The energy spectral density of the latter can be expanded as

$$\left|\widetilde{H}_k(f)\right|^2 = \left(\widetilde{H}_k^{\Re}(f)\right)^2 + \left(\widetilde{H}_k^{\Im}(f)\right)^2, \tag{3.4}$$

where, given that $\widetilde{p}_k(n)$ has Hermitian symmetry, $\widetilde{P}_k(f)$ is real-valued,

$$\begin{aligned} \widetilde{H}_k^{\Re}(f) &= \widetilde{P}_k(f) + \sum_{i\in\mathcal{K};i\neq k} \widetilde{\alpha}_{i,k}^{\Re}\widetilde{P}_k(f) + \widetilde{T}_k^{\Re}(f), \\ \widetilde{H}_k^{\Im}(f) &= \sum_{i\in\mathcal{K};i\neq k} \widetilde{\alpha}_{i,k}^{\Im}\widetilde{P}_k(f) + \widetilde{T}_k^{\Im}(f). \end{aligned} \tag{3.5}$$

Minimizing the cost function in (3.3) means that (3.4) has to be minimized in the frequency region determined by $M_0(f)$. To accomplish the latter, $\widetilde{H}_k^{\Im}(f)$ must be zero, as only the cancellation terms have a contribution to its expression. The latter result involves that $\widetilde{\alpha}_{i,k}$ and $\widetilde{T}_k(n)$ are real valued, with $i \in \mathcal{K}$, $k \in \mathcal{D}$, which means that $\widetilde{t}_k(n)$ must have Hermitian symmetry. Both results imply that the number of coefficients to be obtained in the optimization procedure, as well as the number of products required to implement the transmission pulse, is halved or almost halved. It should be noted that these conditions do not interfere with the constraints in (3.3), which also benefit from setting the term $\widetilde{H}_k^{\Im}(f)$ equal to zero.

The pulse in (3.1) and the model proposed in (3.3) comprise the first contribution of this section: using the former pulse and optimizing it following the latter model, is a sufficient condition for $\widetilde{\alpha}_{i,k}$ to be real valued and $\widetilde{t}_k(n)$ to have Hermitian symmetry, with $i \in \mathcal{K}$ and $k \in \mathcal{D}$. Strategies that adopt this approach obtain optimization and real-time implementation cost reductions. However, some spectral shaping techniques that do not comply with (3.3) can still benefit from these cost reductions provided that the pulse with Hermitian symmetry given in (3.1) is used. A collection of methods that fit this description is reviewed in the numerical results subsection.

We present an overview of the computational complexity reduction achieved for each of the reviewed spectral shaping techniques. We show that the number of real products per OFDM symbol involved in the real-time implementation of AIC and spectral precoding techniques is halved. For the AST technique, it is also reduced by 50% with its regular implementation, while for h-AST the reduction is lower because the complexity of the β-point IDFT that is required per OFDM symbol is not halved. To understand these reductions it is key to note that a product with complex operands involves 4 real products, but only 2 real products when one operand is real-valued. Similarly, if a pair of complex conjugate values is multiplied by the same complex value in two separate operations, only 4 real products are required. As for the complexity reductions in the optimization procedure, the number of real-valued coefficients to be computed is halved for all the methods, which impacts the computational cost of obtaining them.

Finally, there are some spectral shaping techniques that cannot benefit from the real-time implementation cost reduction, due to the impossibility of using a Hermitian-symmetric pulse, but can still benefit from the simplifications in the optimization procedure. This is the case of some strategies whose optimization problem can be expressed as in (3.3) but cannot use the proposed pulse in (3.2). Under these conditions, the solution to the spectral shaping problem with non-symmetric pulses in (2.41) can be computed from the solutions to (3.3) as

$$\alpha_{i,k} = \widetilde{\alpha}_{i,k} e^{j\frac{2\pi}{N}(k-i)(\eta-N_{\mathrm{GI}})}, \qquad \mathbf{t}_k = \widetilde{\mathbf{t}}_k e^{j\frac{2\pi}{N}k(\eta-N_{\mathrm{GI}})}. \tag{3.6}$$

3.1.1 Numerical results and discussion

The first goal of this subsection is to provide a compilation of existing spectral shaping methods from the literature that benefit from the proposed pulse and design framework. In addition, it is proved that the use of the proposed strategy does not impact the performance of some of these existing techniques.

To address the first goal, Table 3.1 contains a selection of spectral shaping methods found in the literature that benefit from using the pulse in (3.1). Some of these techniques approach their optimization problem in a similar way to the one we propose in (3.3). However, since complying with this optimization framework is just a sufficient condition to enjoy important reductions in the implementation complexity, we include some other spectral shaping methods that enjoy the latter while not satisfying the former condition. To do this, all that is required is to use the pulse in (3.1).

In second place, it is proved that the use of the proposed pulse and framework does not affect the performance of the spectral shaping techniques. To that end, the PSD attained by the selected techniques is calculated in two cases: when using regular OFDM pulses, and when using the Hermitian-symmetric pulse in (3.1). The selected methods are the one by Díez *et al.* [16] and the one by Hussain and López-Valcarce [11], that combine AIC and AST techniques, and the spectral precoding methods by Zhou *et al.* [9] (particularized to the single-user scenario), by van de Beek [8] and by Ma *et al.* [10]. Their PSD is plotted in Fig. 3.3, where the goal is to prove that the performance of each individual technique remains unchanged when the pulse proposed in (3.1) replaces the one conventionally used in OFDM systems, rather than to compare the performance of the different techniques. Interestingly, [9] and [8] yield different precoding matrices but lead to the same PSD, although their BER will be different [9]. The former result is proved in Appendix A.1.

The PSD of the different methods is obtained using the analytical expressions in [16, eq. (8)], [11, eq. (10)], [9, eq. (10)] and [8, eq. (6)], respectively. While [10] does not provide an analytical expression for the PSD, it can be obtained using [9, eq. (10)]. The considered system uses $N = 4096$, $N_{\mathrm{GI}} = 1024$. The methods that use AST employ $\beta = 511$. A

Table 3.1: Spectral shaping methods for OFDM signals that would benefit from using the Hermitian-symmetric pulse proposed in this work.

Reference(s)	**Proof**
[16, eqs. (18)-(20)] [28, eqs. (6)-(8)] [13, eq. (3)] [22, eqs. (12)-(13)]	The optimization in [16, eqs. (18)-(19)] and [22, eqs. (12)-(13) and (30)-(31)] are essentially identical to the one in (3.3). Hence, when $\widetilde{p}_k(n)$ in (3.1) is used, the optimal coefficients of the AIC terms must be real-valued and the optimal AST term must have Hermitian-symmetry. Since [16] generalizes [28] and [13], as proven therein, the latter also benefit from this perk.
[32, eq. (9)] [33, eq. (10)] [34, eq. (27)]	Their optimization problems are very similar to the one in (3.3), plus the constraints imposed to preserve the correct operation of the receiver. The problems are solved by means of iterative algorithms in which, given that all the terms are real-valued (out-of-band radiation matrices; identity, selection and permutation matrices; etc.), lead to real-valued solutions.
[11, eqs. (17)-(18)]	It proposes two spectral shaping problems: [11, eq. (17)] for orthogonal precoding and [11, eq. (18)] for an AIC-based solution. For the first one, the optimal precoding matrix is real-valued when $\widetilde{p}_k(n)$ in (3.1) is used because it is made of the eigenvectors of a matrix that will be real and symmetric. For the second, the optimal matrix is also computed out of the same real-valued matrix, an identity matrix and a selection matrix, which are also real-valued. In both cases, a shaping window that can be proven to have Hermitian symmetry when using $\widetilde{p}_k(n)$ in (3.1) is employed.
[29, eq. (16)]	The optimal precoding matrix is made up of the eigenvectors of the matrix in [29, eq. (16)], which can be easily proved to be real-valued and symmetric, as it results from adding matrices that are real and symmetric when $\widetilde{p}_k(n)$ in (3.1) is employed.
[35, eq. (12)]	The closed-form expression for the optimal precoding matrix is obtained by inverting a matrix that can be easily proved to be real-valued, as it results from the addition of matrices computed out of the Fourier transform of $\widetilde{p}_k(n)$ in (3.1).
[9, eq. (15)]	The closed-form expression of the optimal precoding matrix per user consists of a subset of the right-singular vectors of a real-valued matrix. Hence, the optimal matrix is real-valued.
[36, below eq. (7)] [8, eq. (12)]	The optimal precoding matrix in [36, below eq. (7)] is real-valued matrix because it is obtained as the product of real-valued matrices (an identity matrix, a matrix of real weights and one that contains the Fourier transform of the pulses). In [8, eq. (12)] only an identity matrix and the one containing the Fourier transform of the pulses appear, and both are real-valued.
[10, eq. (12)]	The optimal precoding matrix is real-valued, as it is obtained out of the singular value decomposition (SVD) of a matrix that contains the Fourier transform of $\widetilde{p}_k(n)$ in (3.1), and an arbitrary matrix, which can be chosen to be real as well.

scenario where the OOBE is to be reduced in the bands corresponding to carrier indices $\mathcal{B} = \{0, \ldots, 1024\} \cup \{3022, \ldots, 3026\} \cup \{3072, \ldots, 4095\}$ is assumed in [16].

The method in [16] uses a shaping pulse $g(n)$ with RC transitions, 3 CC by each edge of the passband (2 inband and 1 out-of-band) and regular transition pulses. This same set of

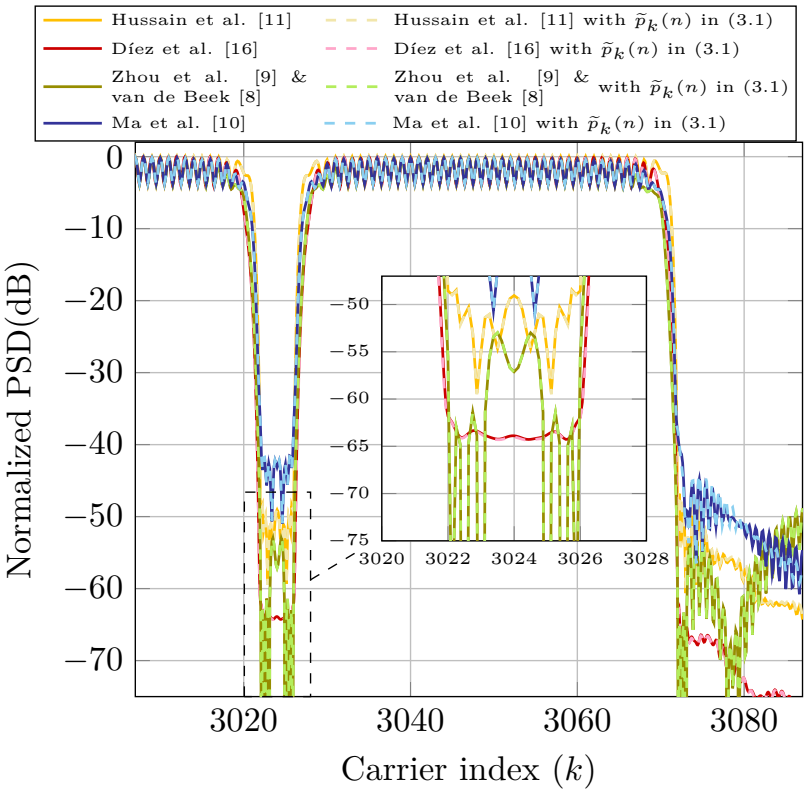

Figure 3.3: Normalized PSD given by several methods taken from Table 3.1 when using the conventional OFDM pulse and $\widetilde{p}_k(n)$ in (3.1). Since [9] and [8] yield the same PSD (see proof in Appendix A.1), a single curve is depicted for both of them.

CC is used with [11], whose solution is obtained after 16 iterations with the regularization term configured to avoid PSD peaks in the passband. The techniques in [9] and [10] are configured with a coding rate of $\lambda = \frac{2026}{2042}$. The former uses the following set of 16 normalized frequencies to notch the PSD, $\phi = \{-\phi_1, 0.2378, 0.2379, 0.2380, 0.2385, 0.2386, 0.2387, \phi_1\}$, with $\phi_1 = \{0.250, 0.2501, 0.2502, 0.2515, 0.2518\}$, which is also used for [8]. For the method in [10], the notched band $\mathcal{B}$ is evenly sampled with 10 samples per subcarrier spacing.

Results show that the PSD of the assessed methods are unaffected when the proposed pulse is used. On the other hand, employing the proposed pulse allows implementing the 5 considered spectral shaping techniques with just 50% of the number of real products per symbol needed with the conventional OFDM pulse. Similarly, the peak-to-average power ratio (PAPR) of the resulting signals can be analyzed. In Fig. 3.4 the complementary cumulative distribution function (CCDF) of the PAPR of the assessed spectral shaping methods is plotted. The same two cases are considered for each method: one using the regular OFDM pulses and another using the proposed pulse, $\widetilde{p}_k(n)$ in (3.1). The same parameters used to obtain PSD of each method in Fig. 3.3 are used to obtain the PAPR.

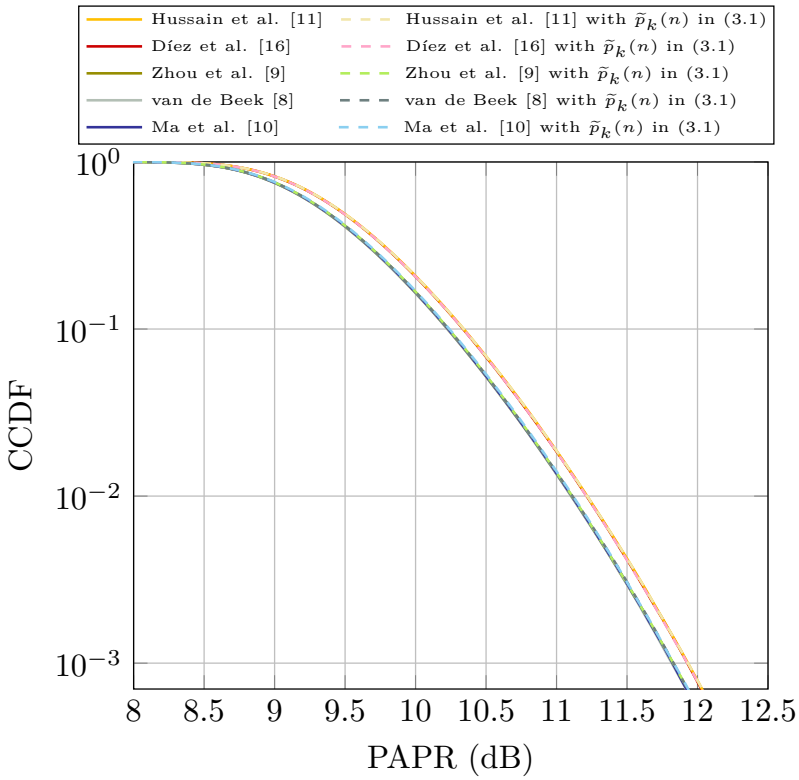

Figure 3.4: PAPR of the five spectral shaping techniques assessed in this numerical results section when the conventional OFDM pulse is used, and when $\widetilde{p}_k(n)$ in (3.1) is employed.

The curves have been obtained using 10^7 OFDM symbols. Fig. 3.4 show that for each method, the curve obtained with the proposed pulse (3.1) overlaps with the one obtained with the conventional OFDM pulse.

Even though the goal of this section is not to compare the assessed methods, two interesting results can be drawn from Fig. 3.4. First, methods of the same type yield the same PAPR: the curves of the AIC+AST methods by Hussain *et al.* [11] and by Díez *et al.* [16] fully overlap; also for the precoding methods by Zhou *et al.* [9], van de Beek [8] and Ma *et al.* [10]. In second place, the PAPR of the AIC+AST techniques is slightly higher than the one given by the precoding methods. This is due to the AST techniques generally yielding larger PAPR than AIC and precoding methods.

3.2 Spectral shaping design paradigm for dynamically adaptive emission masks

The CR paradigm gives communication systems the opportunity to transmit in frequency subbands allocated to a primary system when the latter is not using them. The region of the spectrum where transmission is allowed for the secondary systems can change dynamically, in accordance with the requirements of the primary system. Consequently, systems that abide by the CR paradigm face a major difficulty when spectral shaping is applied to their signals: every time the emission mask changes, the solutions to the spectral shaping problem must be adapted accordingly. The purpose of this section is to propose a cost-effective solution to this problem. In that direction, the contributions are threefold:

- The formulation of a paradigm that allows the dynamic adaptation of precomputed spectral shaping solutions to changes in the emission mask.
- The proposal of an efficient implementation of the operations performed by the transmitter to seamlessly adapt the set of precomputed spectral shaping solutions to changes in the scenario.
- The definition of an optimization framework to obtain the set of solutions that will serve as a source for the adaptation operation. For the latter, two optimization approaches are proposed with different complexity and performance.

These contributions have been proposed in three separate works. The first one is a conference contribution where a preliminary result was presented: the possibility of adapting some precomputed solutions to a different problem. In second place, in a journal paper this idea was further developed and the whole design framework was devised, which included an optimization procedure. Finally, in a workshop contribution, we presented an alternative optimization method to obtain the set of precomputed solutions. The references to these works are, respectively,

- J. Giménez, J. A. Cortés, F. J. Cañete, E. Martos-Naya and L. Díez, "Low-complexity Spectral Shaping Method for OFDM Signals with Dynamic Transmission Band Location," *IEEE International Symposium on Power Line Communications and its Applications* (Presented in the *Recent Results* session), Oct. 2021.

[22] J. Giménez, J. A. Cortés and L. Díez, "Low-Complexity Spectral Shaping Method for OFDM Signals With Dynamically Adaptive Emission Mask," in *IEEE Transactions on Communications*, vol. 71, no. 4, pp. 2351-2363, April 2023.

- J. Giménez, J. A. Cortés and L. Díez, "A Low-Complexity Spectral Shaping Method for OFDM Signals with Dynamically Defined Emission Mask: Optimization Procedure," *14th Workshop for Power Line Communications*, Sept. 2023.

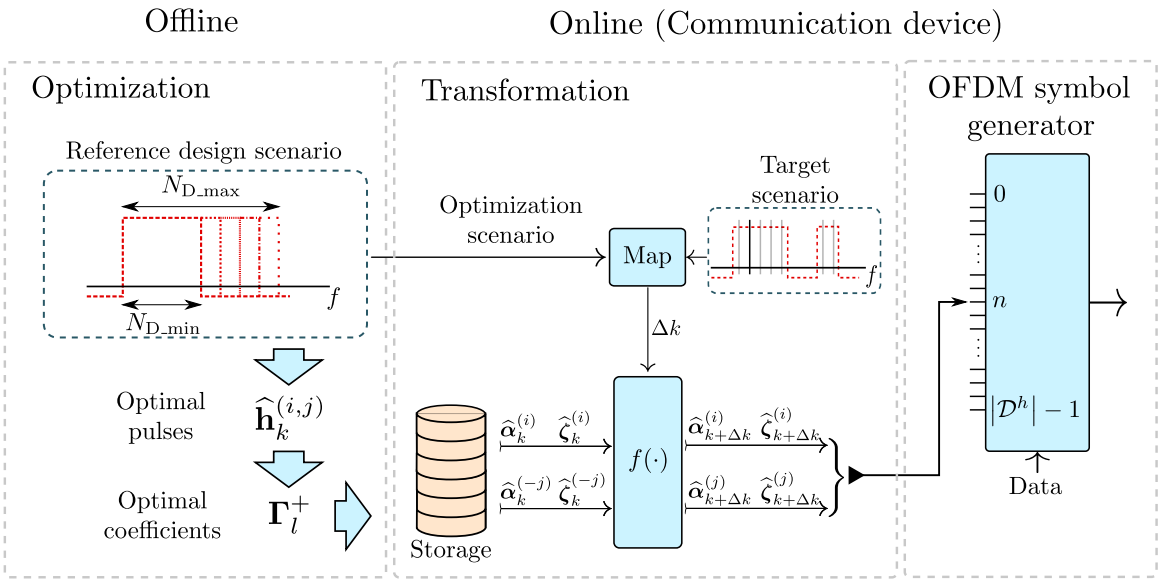

Figure 3.5: Diagram describing the spectral shaping paradigm proposed in this section. It consists of three phases: 1) optimization of the precomputed set of coefficients; 2) transformation of the original solutions; 3) generation of the OFDM symbol. The first phase if performed offline, while the other two are performed online in the communications device.

attached in Appendix B.1.2, B.1.3 and B.1.4, respectively.

The spectral shaping paradigm we propose consists of three phases, depicted in Fig. 3.5:

1) An original set of optimal solutions is obtained offline through an optimization procedure for a generic scenario. This procedure is carried out offline.

2) The original set of solutions is stored in the communication device. Then, when the system is online, they are transformed to adapt them to the current scenario.

3) The transformed solutions are employed to compute the OFDM symbol.

We call this paradigm the *dynamically adaptive* spectral shaping method.

For a more straightforward exposition of the matter, we first solve a simpler approach to the problem that consists in shaping the spectrum of an isolated arbitrarily wide passband. To that end, the type of solutions that this problem requires, i.e., the pulses that we use to minimize the OOBE in that problem, are presented. Next, we propose a method through which the optimal solutions can be obtained. Finally, we provide a set of elementary operations that allow one to transform the precomputed pulses to adapt them to solve a shifted version of the scenario.

After that, the proposal is extended to more complex scenarios with multiple passbands with arbitrary widths and locations. In that context, two alternative optimization procedures are proposed to obtain a set of solutions whose efficacy upon transformation extends to any arbitrary scenario.

The proposed framework is founded on the generalized pulse in (2.22), due to its reasonable performance for a limited computational cost increase. Consequently, these contributions are restricted to AIC and AST spectral shaping techniques (as from now, precoding is out of the picture). It is recalled that the generalized pulse is only used in the data carriers located closest to the edges of the passband, as the OOBE of further ones is negligible. Let us define N_{h} as the number of data carriers that use the generalized pulse close to each edge of a passband. In the same fashion, the cancellation terms employed by the generalized pulses could be limited to those located close to where the emissions need to be minimized.

3.2.1 Adaptive solutions for wide passbands

Let us start by considering the scenario portrayed in Fig. 3.6. It depicts a single passband flanked by two notched bands, $\mathcal{B}_{\mathrm{n}}^{+}(l_{\mathrm{l}})$ and $\mathcal{B}_{\mathrm{n}}^{-}(l_{\mathrm{r}})$. The width of the passband is such that no data carrier lies sufficiently close to both edges simultaneously to cause non-negligible spectral leakage in both notched bands. As for the notched bands, $\mathcal{B}_{\mathrm{n}}^{+}(l_{\mathrm{l}})$ starts at carrier index l_{l}, $\mathcal{B}_{\mathrm{n}}^{-}(l_{\mathrm{r}})$ at l_{r}, and each has a nominal frequency span of B_{n}. This width is the same regardless of the location of the passband, so in the cases where they extend beyond the $f \in \left(-\frac{1}{2}, \frac{1}{2}\right]$ limits, the portion of the notched band that exceeds one of the limits appears at the other end of the spectrum.

A key observation of the proposed paradigm is that data carriers that lie in the same position w.r.t. the closest edge of the passband produce the same OOBE, even if their passbands have different frequency locations. Consequently, the respective solutions should be somehow related. Hence, it is convenient to introduce in the notation of the generalized pulse a reference to the position that the corresponding data carrier occupies w.r.t. the closest edge of the passband. That allows to transform the solutions to one problem into

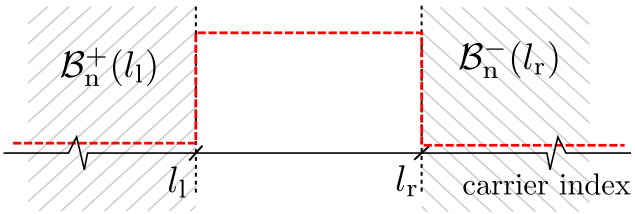

Figure 3.6: Transmitter PSD mask with passband left and right edges in l_{l} and l_{r}, respectively. $\mathcal{B}_{\mathrm{n}}^{+}(l_{\mathrm{l}})$ and $\mathcal{B}_{\mathrm{n}}^{-}(l_{\mathrm{r}})$ denote the notched bands.

the solutions to a different one. Let us redefine the generalized pulse as follows

$$\begin{aligned} \mathbf{h}_k^{(i)} &= \mathbf{p}_k + \mathbf{C}_{k-i}^{+}\boldsymbol{\alpha}_k^{(i)} + \mathbf{t}_k^{(i)}, \quad i > 0, \\ \mathbf{h}_k^{(i)} &= \mathbf{p}_k + \mathbf{C}_{k-i}^{-}\boldsymbol{\alpha}_k^{(i)} + \mathbf{t}_k^{(i)}, \quad i < 0, \end{aligned} \tag{3.7}$$

where i is the distance, given in number of carriers, between carrier k and the carrier located at the passband edge (either l_l or l_r in Fig. 3.6). Note that the pulse above, with $i > 0$, is used by data carriers located close to the left edge of a passband (with $k > l_\mathrm{l}$). Similarly, the pulse with $i < 0$ is used by data carriers located close to the right edge of a passband (with $k < l_\mathrm{r}$). Another important variation in the notation w.r.t. the generalized pulse in (2.23) is the introduction of matrices $\mathbf{C}_l^{+}$ and $\mathbf{C}_l^{-}$, in replacement of $\mathbf{P}_\mathcal{C}$. These are defined as

$$\begin{aligned} \mathbf{C}_l^{+} &= \left[\mathbf{p}_{l-N_\mathrm{co}}, \ldots, \mathbf{p}_l, \ldots, \mathbf{p}_{l+N_\mathrm{ci}}\right], \\ \mathbf{C}_l^{-} &= \left[\mathbf{p}_{l-N_\mathrm{ci}}, \ldots, \mathbf{p}_l, \ldots, \mathbf{p}_{l+N_\mathrm{co}}\right], \end{aligned} \tag{3.8}$$

where N_ci and N_co are two design parameters that denote the number of CC located inside the passband and out-of-band, respectively. The total number of CC, which includes one located right at the corresponding edge of the passband (carrier index l), is denoted as $N_\mathrm{CC} = N_\mathrm{ci} + N_\mathrm{co} + 1$. It is important to note that the CC in $\mathbf{C}_l^{+}$ and $\mathbf{C}_l^{-}$ are the ones that surround the left and right edges of the passband, respectively. This asset is crucial for the utility of the pulse, as the closer the CC are to the notched band, the more capable they are to control the OOBE.

The AST term, $\mathbf{t}_k^{(i)}$, is also identified with the superindex (i). It can be realized using any of the implementations proposed in Sec. 2.5. However, for simplicity, this summary only considers the regular implementation. For details on how the harmonically designed AST term can be implemented within the proposed framework, we kindly refer the reader to [22].

Let Fig. 3.7 complete the description of the scenario: the carriers in yellow represent the CC; the data carriers that use the generalized pulses in (3.7) are in blue, where N_h of them are defined by each edge (next to the N_ci CC inside de passband); the remaining data carriers inside the passband, in black, use the regular base pulse as their OOBE is considered unimportant. Hence, the value of N_h represents the trade-off between computational cost and OOBE reduction, so it may vary according to needs. However, its maximum value is determined by the number of data carriers located near each edge of the passband that are considered to produce relevant out-of-band emissions. In other words, increasing N_h in one implies that an additional data carrier uses the generalized pulse to limit its leakage. There will be a point in which the use of the generalized pulse in an additional carrier yields a negligible reduction in the global OOBE. Let us denote $N_\mathrm{h\_max}$ as the maximum number of data carriers whose OOBE is worth controlling. Finally, let us denote the total number of carriers within the passband by N_D.

Given the defined scenario, the power that the OFDM signal emits into the notched bands is approximately equal to the OOBE produced only by the data carriers that use the generalized pulse, as stated in (2.30). The leakage produced by the remaining data carriers is

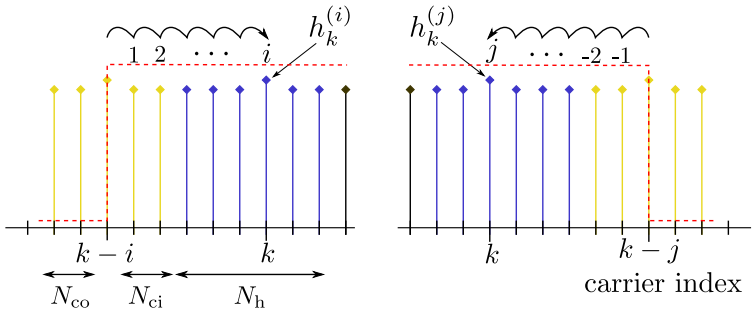

Figure 3.7: Detailed representation of the carriers at the left and right edges of a passband.

considered negligible. Hence,

$$P_{\text{OOBE}} = \int_{\mathcal{B}_n^+(l_{\text{l}})\cup\mathcal{B}_n^-(l_{\text{r}})} S(f)df \approx \frac{1}{N_{\text{s}}} \sum_{k=l_{\text{l}}+N_{\text{ci}}+1}^{l_{\text{l}}+N_{\text{ci}}+N_{\text{h}}} \sigma_k^2 E_k^{(k-l_{\text{l}})} + \frac{1}{N_{\text{s}}} \sum_{k=l_{\text{r}}-N_{\text{ci}}-N_{\text{h}}}^{l_{\text{r}}-N_{\text{ci}}-1} \sigma_k^2 E_k^{(k-l_{\text{r}})}, \tag{3.9}$$

where the term $E_k^{(i)}$ denotes the energy emitted by the k-th generalized pulse into the closest notched band, and is defined as

$$E_k^{(i)} = \begin{cases} \displaystyle\int_{\mathcal{B}_{\text{n}}^+(k-i)} \left|H_k^{(i)}(f)\right|^2 df = (\mathbf{h}_k^{(i)})^{\text{H}} \mathbf{\Phi}_{\mathcal{B}_{\text{n}}^+(k-i)} \mathbf{h}_k^{(i)}, & i > 0, \\ \displaystyle\int_{\mathcal{B}_{\text{n}}^-(k-i)} \left|H_k^{(i)}(f)\right|^2 df = (\mathbf{h}_k^{(i)})^{\text{H}} \mathbf{\Phi}_{\mathcal{B}_{\text{n}}^-(k-i)} \mathbf{h}_k^{(i)}, & i < 0. \end{cases} \tag{3.10}$$

Optimization of the pulses

As stated above, each generalized pulse has the ability to minimize the OOBE produced by the corresponding carrier. Hence, the pulse of one carrier can be optimized independently of the others, leading to the optimal coefficients of the k-th generalized pulse being obtained as

$$\widehat{\boldsymbol{\gamma}}_k^{(i)} = \begin{bmatrix} \widehat{\boldsymbol{\alpha}}_k^{(i)} \\ \widehat{\boldsymbol{\zeta}}_k^{(i)} \end{bmatrix} = \arg \min_{\boldsymbol{\alpha}_k^{(i)}, \boldsymbol{\zeta}_k^{(i)}} \left\{ E_k^{(i)} \right\}. \tag{3.11}$$

To avoid having PSD peaks in the passband, this problem has to be solved with limits applied on the magnitude of the real and imaginary parts of the coefficients $\boldsymbol{\alpha}_k^{(i)}$ and $\boldsymbol{\zeta}_k^{(i)}$, as explained in Section 2.5

The solution to this optimization is a pulse designed to locally minimize the OOBE of a given data carrier in the predefined passband. The pulses that result from this procedure are also appropriate for any other passband with the same characteristics, i.e., one that is

wide enough such that the leakage of one data carrier is relevant in, at most, one notched band. The following subsection describes the operations that allow computing the optimal pulses for a given scenario from the solutions to the problem (3.11).

3.2.2 Frequency transformations

Let us consider again the scenario with a single passband portrayed in Fig. 3.6. If this passband is shifted in frequency Δk carriers to the right, it can be easily proved that the OOBE of the first scenario is identical to that of the second. Furthermore, it can also be proved that the spectral shaping solutions to the latter scenario are closely related to that in the first one. Namely, those of the latter can be obtained from those in the former through the following equations

$$\boldsymbol{\alpha}_{k+\Delta k}^{(i)} = \boldsymbol{\alpha}_{k}^{(i)}, \qquad \mathbf{t}_{k+\Delta k}^{(i)} = \boldsymbol{\Omega}_{\Delta k}\mathbf{t}_{k}^{(i)}, \tag{3.12}$$

where $\Omega_{\Delta k} = \mathrm{diag}\Big([w_N^{\Delta k(0-N_{\mathrm{GI}})}, \ldots, w_N^{\Delta k(L-1-N_{\mathrm{GI}})}]\Big)$.

Similarly, it can be easily proved that the power emitted by the OFDM signal into $\mathcal{B}_{\mathrm{n}}^{+}(l_{\mathrm{l}})$ is identical to that emitted into $\mathcal{B}_{\mathrm{n}}^{-}(l_{\mathrm{r}})$. Hence, pulses that minimize the OOBE beyond the left edge must have some relation to those that minimize beyond the right edge. In fact, the first ones can be obtained from the other, and vice versa, through the following relations,

$$\boldsymbol{\alpha}_{k}^{(-i)} = (\boldsymbol{\alpha}_{k}^{(i)})^{*}, \qquad \mathbf{t}_{k}^{(-i)} = \boldsymbol{\Omega}_{2k-N}(\mathbf{t}_{k}^{(i)})^{*}. \tag{3.13}$$

Proof of these relations can be found in [21].

It is important to note that the superindices in (3.12) are identical on both sides of the equation, and in (3.13) they have the same absolute value but opposite sign. This means that these transformations involve solutions for data carriers that are at the same distance to the edge of their respective passband. In that case, it is convenient to arrange the optimal coefficients corresponding to one edge in a single matrix. In this way, it comprises the set of spectral shaping solutions for one edge of the passband, which can be transformed to obtain that of another passband. Let us define

$$\begin{aligned} \boldsymbol{\Gamma}_{l}^{+} &= \left[\boldsymbol{\gamma}_{l+N_{\mathrm{ci}}+1}^{(N_{\mathrm{ci}}+1)}, \ldots, \boldsymbol{\gamma}_{l+N_{\mathrm{ci}}+N_{\mathrm{h}}}^{(N_{\mathrm{ci}}+N_{\mathrm{h}})}\right], \\ \boldsymbol{\Gamma}_{l}^{-} &= \left[\boldsymbol{\gamma}_{l-N_{\mathrm{ci}}-1}^{(-N_{\mathrm{ci}}-1)}, \ldots, \boldsymbol{\gamma}_{l-N_{\mathrm{ci}}-N_{\mathrm{h}}}^{(-N_{\mathrm{ci}}-N_{\mathrm{h}})}\right], \end{aligned} \tag{3.14}$$

containing the coefficients for the left and right edges of a wide passband whose boundary is at carrier index l. Note that one matrix is related to the other through (3.13).

3.2.3 Bandwidth adaptive solutions for arbitrary scenarios

The previous approach is useful for scenarios where only wide passbands are present, but not for those where the passbands are arbitrarily narrow. The reason is the solutions to the problem in (3.11) being obtained assuming that the leakage of one data carrier was relevant in just one notched band. Since in narrow passbands its relevance might extend to both notched bands, a new approach that focuses on finding solutions for the narrow-band scenarios is required. It should comprise pulses that allow each data carrier to minimize its OOBE beyond both edges of the passband it occupies simultaneously, regardless of how narrow the latter is. To that end, let us first redefine the modified pulse as

$$\mathbf{h}_k^{(i,j)} = \mathbf{p}_k + \underbrace{\mathbf{C}_{k-i}^{+}\boldsymbol{\alpha}_k^{(i)} + \mathbf{t}_k^{(i)}}_{\mathbf{r}_k^{(i)}} + \underbrace{\mathbf{C}_{k-j}^{-}\boldsymbol{\alpha}_k^{(j)} + \mathbf{t}_k^{(j)}}_{\mathbf{r}_k^{(j)}}, \quad \begin{matrix} i > 0 \\ j < 0, \end{matrix} \tag{3.15}$$

where $i > 0$ denotes that carrier k is the i-th one above the left edge of the passband and $j < 0$ that it is the j-th one below the right edge. Accordingly, $\mathbf{r}_k^{(i)}$ and $\mathbf{r}_k^{(j)}$ comprise the cancellation terms used to minimize the OOBE beyond the left and the right edges, respectively.

The goal now is to find a unique set of coefficients, similar to those in (3.14), that can be used to shape the spectrum of the OFDM signal in any scenario by virtue of the transformations in (3.12) and (3.13). To accomplish this end, this unique set must be obtained through an optimization procedure that takes into account a wide variety of bandwidths. Consider the set of passband widths depicted in Fig. 3.8, ranging from $N_{\text{D\_min}} = N_{\text{h\_min}} + 2N_{\text{ci}}$ carriers, the narrowest, to $N_{\text{D\_max}} = N_{\text{h\_max}} + 2N_{\text{ci}}$, the widest. Regarding the first, $N_{\text{D\_min}}$ is a design parameter that determines the minimum bandwidth for which the proposed spectral shaping framework will be effective. For the widest passband, $N_{\text{h\_max}}$ has been defined as the maximum number of consecutive data carriers that need to use a generalized pulse at each of the passband edges. The value of $N_{\text{D\_max}}$ can be obtained from the latter.

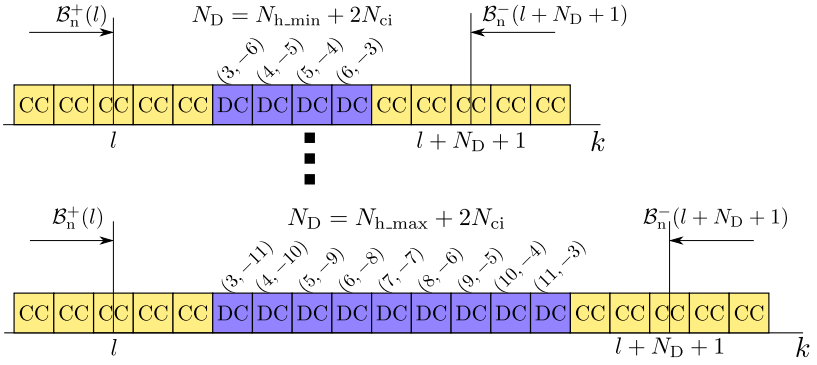

Figure 3.8: Illustrative location of the data carriers (DC) and CC in passbands of width ranging from $N_{\text{D\_min}}$ to $N_{\text{D\_max}}$.

It is important to note that the transformations proposed in (3.12) and (3.13) can also be applied to the coefficients used in $\mathbf{h}_k^{(i,j)}$. Also, the optimal solutions for this pulse can be stored in the matrices defined in (3.14), which are related to each other by means of the transformations in (3.13). Consequently, it is enough to obtain one of them. In that direction, we adopt the convention that the reference point is at the left edge of the passbands, so we seek to obtain the matrix $\mathbf{\Gamma}_l^+$. Also, the index of the left edge is located on the same carrier for all of them, for convenience.

Two different optimization procedures are proposed to obtain the set of original coefficients for our framework:

- Incremental method: this approach iteratively increases the considered bandwidth in one carrier and computes the coefficients of the additional pulse.
- Direct method: this approach takes into account all the bandwidths at the same time and directly obtains the set of optimal coefficients that minimizes the averaged OOBE of the considered cases.

Incremental method

This first optimization procedure assumes that $\mathbf{r}_k^{(i)}$ can be obtained independently of $\mathbf{r}_k^{(j)}$ for each carrier k. A simple yet effective optimization method is proposed to obtain the set of original coefficients for the framework. As we focus on the left edge of the passband, let us redefine for convenience the notched band $\mathcal{B}_\mathrm{c} = \mathcal{B}_\mathrm{n}^+(l)$ as the *contiguous notched band*, and $\mathcal{B}_\mathrm{o} = \mathcal{B}_\mathrm{n}^-(l + N_\mathrm{D} + 1)$ as the *opposite notched band*. Then, the optimal coefficients for the k-th data carrier, such that $k = l + i$, are obtained as

$$\widehat{\boldsymbol{\gamma}}_k^{(i)} = \begin{bmatrix} \widehat{\boldsymbol{\alpha}}_k^{(i)} \\ \widehat{\boldsymbol{\zeta}}_k^{(i)} \end{bmatrix} = \arg \min_{\boldsymbol{\alpha}_k^{(i)}, \boldsymbol{\zeta}_k^{(i)}} \left\{ (1-a) E_{k,\mathcal{B}_\mathrm{c}}^{(i)} + a E_{k,\mathcal{B}_\mathrm{o}}^{(i)} \right\}, \tag{3.16}$$

where

$$E_{k,\mathcal{B}_\mathrm{c}}^{(i)} = \int_{\mathcal{B}_\mathrm{c}} \left| P_k(f) + R_k^{(i)}(f) \right|^2 df; \qquad E_{k,\mathcal{B}_\mathrm{o}}^{(i)} = \int_{\mathcal{B}_\mathrm{o}} \left| R_k^{(i)}(f) \right|^2 df, \tag{3.17}$$

where $R_k^{(i)}(f)$ is the Fourier transform of $\mathbf{r}_k^{(i)}$, and the parameter a is used to tune the relevance that we give to each component in the cost function. Note that $E_{k,\mathcal{B}_\mathrm{c}}^{(i)}$ is the total OOBE emitted into the contiguous notched band, while $E_{k,\mathcal{B}_\mathrm{o}}^{(i)}$ represents the energy leaked by the cancellation terms into the opposite notched band. Consequently, the optimal $\mathbf{r}_k^{(i)}$ is the one that minimizes the OOBE produced by the k-th data carrier in the contiguous notched band while leaking as little as possible into the opposite notched band.

The problem in (3.16) needs to be constrained in order to avoid the appearance of PSD peaks in the passband. Let some limits be applied on the magnitude of the real and imaginary parts of the coefficients, similar to those in (2.36).

The optimization procedure we propose in this section takes into account the range of passbands in Fig. 3.8. It starts with the narrowest bandwidth, for which $\boldsymbol{\gamma}_k^{(i)}$ is obtained for all its data carriers using (3.16). Then, as the width is increased iteratively, $\boldsymbol{\gamma}_k^{(i)}$ is obtained just for the rightmost data carrier in each instance. The procedure ends when the iteration reaches the greatest bandwidth. Note that since the left edge of all passbands is fixed at carrier l, the opposite notched band shifts as the number of carriers, N_{D}, increases.

The procedure is described in Algorithm 1. The result is the set $\boldsymbol{\Gamma}_l^+$ that contains the optimal coefficients for the $N_{\mathrm{h\_max}}$ data carriers located closest to the left edge of the passband.

Algorithm 1 Incremental method

1: Consider the passband with $N_{\mathrm{D}} = N_{\mathrm{D\_min}}$
2: Obtain $\widehat{\boldsymbol{\gamma}}_k^{(i)}$ for all its $N_{\mathrm{h\_min}}$ data carriers solving (3.16) constrained to (2.36)
3: Store the optimal coefficients in $\boldsymbol{\Gamma}_l^+$
4: **while** $N_{\mathrm{D}} < N_{\mathrm{D\_max}}$ **do**
5: Consider the passband with one additional data carrier: $N_{\mathrm{D}} = N_{\mathrm{D}} + 1$
6: Obtain $\widehat{\boldsymbol{\gamma}}_k^{(i)}$ just for the rightmost data carrier in the passband by solving (3.16) constrained to (2.36)
7: Store the optimal coefficients in $\boldsymbol{\Gamma}_l^+$
8: **end while**

Direct method

In this approach, the whole set of original coefficients $\boldsymbol{\Gamma}_l^+$ is obtained through a procedure that takes into account all the bandwidths in the range from $N_{\mathrm{D\_min}}$ to $N_{\mathrm{D\_max}}$ simultaneously. To that end, the total OOBE produced in this range of scenarios is set as the figure to minimize. In this direction, let the energy emitted into $\mathcal{B}_{\mathrm{n}}^+(l_{\mathrm{l}})$ and $\mathcal{B}_{\mathrm{n}}^-(l_{\mathrm{r}})$ by one of the generalized pulses in (3.15) be

$$E_k^{(i,j)} = \left(\mathbf{h}_k^{(i,j)}\right)^{\mathrm{H}} \left(\boldsymbol{\Phi}_{\mathcal{B}_{\mathrm{n}}^+(k-i)} + \boldsymbol{\Phi}_{\mathcal{B}_{\mathrm{n}}^-(k-j)}\right) \mathbf{h}_k^{(i,j)}, \qquad \begin{matrix} i > 0 \\ j < 0, \end{matrix} \tag{3.18}$$

which depends on $\boldsymbol{\gamma}_k^{(i)}$ and $\boldsymbol{\gamma}_k^{(j)}$. However, the latter is related to $\boldsymbol{\gamma}_k^{(-j)}$ by means of the proposed transformations.

The energy leaked into the notched bands by the N_{D} data carriers of a passband whose left edge is at carrier index l is

$$F_l^{(N_{\mathrm{D}})} = \sum_{m=1}^{N_{\mathrm{h}}} E_{l+N_{\mathrm{ci}}}^{(N_{\mathrm{ci}}+m,-N_{\mathrm{D}}-1+N_{\mathrm{ci}}+m)}, \tag{3.19}$$

which involves the coefficients $\boldsymbol{\gamma}_{l+i}^{(i)}$ for $i \in \{2N_{\mathrm{ci}}+1, \ldots, 2N_{\mathrm{ci}}+N_{\mathrm{h}}\}$, and where $N_{\mathrm{h}} = N_{\mathrm{D}} - 2N_{\mathrm{ci}}$.

In the same fashion, the energy emitted out-of-band by the whole range of passbands is included in the following term

$$F_l(\boldsymbol{\Gamma}_l^+) = \sum_{n_{\mathrm{D}}=N_{\mathrm{D\_min}}}^{N_{\mathrm{D\_max}}} F_l^{(n_{\mathrm{D}})} \tag{3.20}$$

which depends on the whole set of coefficients $\boldsymbol{\Gamma}_l^+$. Finally, we are interested in finding the set of coefficients that minimize the sum of the OOBE in all these scenarios. This optimal set is obtained as

$$\widehat{\boldsymbol{\Gamma}}_l^+ = \arg\min_{\boldsymbol{\Gamma}_l^+} \left\{ F_l(\boldsymbol{\Gamma}_l^+) \right\}. \tag{3.21}$$

To avoid PSD peaks within the passband, the optimization problem must be solved with constraints such as those in (2.36).

Implementation cost of the method

The first stage of the proposed spectral shaping paradigm involves applying one of the introduced optimization procedures to obtain the matrix of original coefficients. Regardless of the optimization method of choice, the computational cost of this phase is irrelevant for the communication device, as it is performed offline. In the second phase, the original solutions, which have been stored in the transmitter, are adapted to shape the spectrum of the OFDM signal in the current scenario. To that end, two different schemes can be adopted:

A) Compute the transformed coefficients just once at the beginning and every time the transmission mask changes. The resulting set of coefficients is stored in the transmitter and replaced by a new one when there is a change in the PSD mask.

B) Compute the transformed coefficients for every transmitted symbol, saving memory at the cost of higher computational cost.

The computational cost per OFDM symbol and memory requirements involved in the second phase of the framework is given in Table 3.2. It is expressed in terms of the number of complex products per OFDM symbol, for the former metric, and the number of stored complex coefficients, for the latter. The first one is the cost of applying the operations in (3.12) and (3.13). The pulse in (3.15) is the one considered, as it is the worst-case scenario in terms of memory and complexity.

Table 3.2: Computational cost and memory requirements per OFDM symbol

	Number of complex products	Number of complex coefficients to be stored
Scheme A	–	$2\lvert\mathcal{D}^{\mathrm{h}}\rvert(N_{\mathrm{CC}}+2\beta)$
Scheme B	$4\lvert\mathcal{D}^{\mathrm{h}}\rvert\beta$	$N_{\mathrm{h\_max}}(N_{\mathrm{CC}}+2\beta)$

Note: For this table, the regular implementation of AST technique is assumed. While details about how h-AST technique is implemented within the context of the proposed paradigm are omitted for simplicity, the reader is kindly referred to [22] for a detailed explanation on how the latter are implemented.

In scheme A, the computational cost associated with the transformations applied to adapt the precomputed solutions to the ones employed in the considered scenario has been neglected because they are performed only when the transmission mask changes, and it is reasonable to assume that the frequency of these changes is far below the frequency at which OFDM symbols are transmitted. Scheme B does not require storing many coefficients, although there is some additional computational cost in the transmission of every OFDM symbol that corresponds to the transformation of the transition pulses.

The computational cost of the third phase can be found in Table 2.1, in the entries corresponding to AIC and AST techniques. The total cost involved in implementing the framework results from adding the number of complex products in that table to those in Table 3.2. As shown, both phases depend on the number of carriers that employ the modified pulse, $|\mathcal{D}^{\mathrm{h}}|$, yielding a trade-off between complexity and performance. While other spectral shaping strategies in the literature report lower implementation costs, e.g. [15], [11] and [20], they require performing the first phase for every OFDM symbol or, at best, every time the emission mask changes. In contrast, in the proposed method this phase is performed offline and only once, which yields a lower overall cost, since solving the optimization problem is much more costly than the operations in Table 3.2.

3.2.4 Numerical results and discussion

In this section, we assess the performance of the proposed framework, focusing exclusively on the approach designed for arbitrarily narrow passbands, referred to as *bandwidth adaptive*, due to its broader applicability and higher complexity. The assessment is performed in two ways. First, we evaluate the effect that the parameter $N_{\mathrm{h\_min}}$ has on its performance for the two optimization methods we propose. In second place, we compare it to other spectral shaping techniques from the literature in a common scenario.

The influence of the parameter $N_{\mathrm{h\_min}}$ is evaluated with the *incremental* and the *direct* optimization methods. To this end, the optimization is performed with $N_{\mathrm{h\_min}} \in \{1, 2, \ldots, 5\}$, $N_{\mathrm{h\_max}} = 13$, $N_{\mathrm{ci}} = 2$ and $N_{\mathrm{co}} = 0$. An OFDM system like the one defined in ITU-T Rec.

G.9960 is employed [37]. It uses $N = 4096$, $N_{\mathrm{GI}} = 1024$ and $\beta = 512$. The β samples at both edges of $g(n)$ are shaped using an RC window. Pulses with two types of OOBE reduction terms are considered: the one with just the AIC term, denoted as $h_k(\mathrm{CC})$, and the one with AIC and harmonically designed AST terms, denoted as $h_k(\mathrm{CC}, t_k\text{-h})$, with $N_{\mathrm{q}} = 2$. Each of the resulting sets of coefficients (one per value of $N_{\mathrm{h\_min}}$ and type of pulse) are applied to two different passbands: the narrowest passband for each $N_{\mathrm{h\_min}}$, i.e., one with $N_{\mathrm{D}} = N_{\mathrm{h\_min}} + 2N_{\mathrm{ci}}$, and a wider passband of $N_{\mathrm{D}} = N_{\mathrm{h\_max}} + 2N_{\mathrm{ci}}$.

In the assessment, the largest value of the normalized PSD in the notched bands, denoted as $\mathrm{PSD}_{\mathrm{max}}$, is used as figure of merit. In each scenario, this value is usually attained in the frequencies closest to the passband edges. To obtain it, the PSD is analytically computed using (2.29). These values are plotted in Fig. 3.9 (a) when the solutions are evaluated in the passband with $N_{\mathrm{D}} = N_{\mathrm{h\_min}} + 2N_{\mathrm{ci}}$ and in Fig. 3.9 (b) when they are evaluated in the $N_{\mathrm{D}} = N_{\mathrm{h\_max}} + 2N_{\mathrm{ci}}$ passband.

As expected, $h_k(\mathrm{CC}, t_k\text{-h})$ outperforms $h_k(\mathrm{CC})$, since the former has more degrees of freedom. Also, both figures show that increasing the value of $N_{\mathrm{h\_min}}$ leads to better OOBE reduction for both types of pulse. The selection of $N_{\mathrm{h\_min}}$ involves a trade-off between the minimum OOBE attained in narrow passbands and that obtained in wider passbands. Increasing $N_{\mathrm{h\_min}}$ reduces the range of bandwidths to be considered in the optimization, which relaxes the referred trade-off, and leads to better performance in the passbands considered in the optimization. However, such solutions yield a suboptimal OOBE reduction when evaluated in a passband with $N_{\mathrm{D}} < N_{\mathrm{D\_min}}$. It can be seen that $N_{\mathrm{D}} = N_{\mathrm{h\_max}} + 2N_{\mathrm{ci}}$ (b) yields lower $\mathrm{PSD}_{\mathrm{max}}$ than $N_{\mathrm{D}} = N_{\mathrm{h\_min}} + 2N_{\mathrm{ci}}$ (a), which is because the wider the passband, the lower the OOBE emitted by the optimized pulses at the farthest edge of the passband. However, the rate at which the $\mathrm{PSD}_{\mathrm{max}}$ decreases as $N_{\mathrm{h\_min}}$ increases is more pronounced in the narrower passband than in the wider. This is because the width of the former grows as $N_{\mathrm{h\_min}}$ increases, while for the latter it is fixed.

It can be observed that the curves for the incremental and direct methods are very similar. This means that both methods produce similar solutions, but there are still some aspects that need explanation. First, for the $h_k(\mathrm{CC})$ pulse, the direct method outperforms the incremental method for almost every $N_{\mathrm{h\_min}}$. This is due to the former approach being more comprehensive than the latter by considering all the bandwidths at once. In contrast, for the pulse $h_k(\mathrm{CC}, t_k\text{-h})$, when evaluated in the narrowest band (a), there is not a clear better option. Meanwhile, when evaluated in the wider passband (b), the incremental method outperforms the direct method. Both results can be attributed to the large number of degrees of freedom that take part in the direct optimization in comparison to the incremental method. The greater the problem, the more difficult it is to find an appropriate solution without getting stuck in suboptimal solutions.

The value of $N_{\mathrm{h\_min}}$ is determined to ensure that the OOBE level attained in the narrowest passband is below the required limit. Fig. 3.9 can be used to perform this selection. For

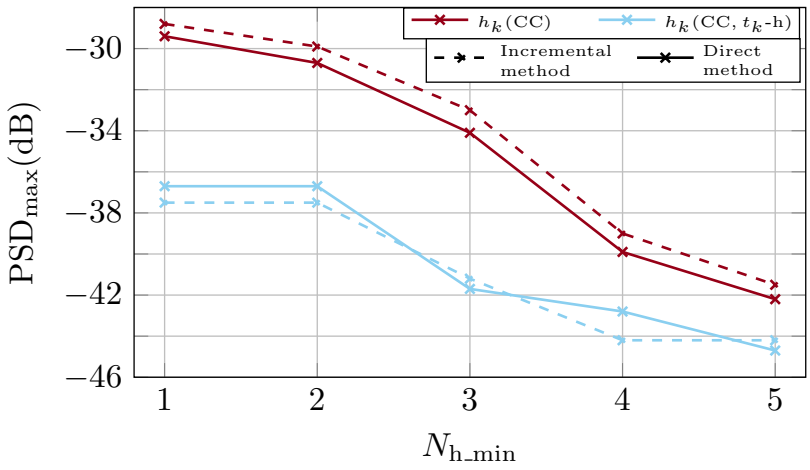

(a)

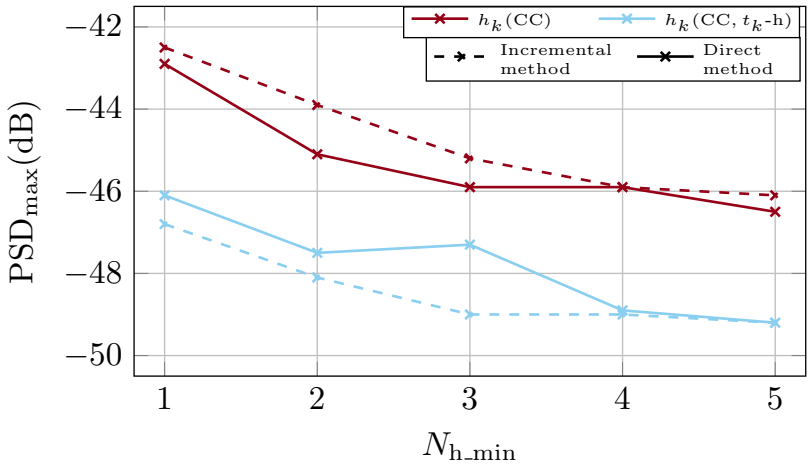

(b)

Figure 3.9: $\text{PSD}_{\max}$ attained by $h_k(\text{CC})$ and $h_k(\text{CC}, t_k\text{-h})$ when the proposed framework is applied using the *incremental* optimization method and the *direct* optimization method. Each set of solutions is applied in a passband of width $N_{\text{D}} = N_{\text{h\_min}} + 2N_{\text{ci}}$ (a) and in another of $N_{\text{D}} = N_{\text{h\_max}} + 2N_{\text{ci}}$, where $N_{\text{h\_max}} = 13$ (b).

instance, in order to guarantee that $\text{PSD}_{\max} \leq -41$ dB with $h_k(\text{CC})$, $N_{\text{h\_min}} \geq 5$ must be employed, while with $h_k(\text{CC}, t_k\text{-h})$ this can be attained with $N_{\text{h\_min}} \geq 3$.

The proposed framework is now compared with other strategies in a scenario with notched bands at carrier indices $\mathcal{B} = \{0, \ldots, 1024\} \cup \{3022, \ldots, 3026\} \cup \{3072, \ldots, 4095\}$ used in the previous section. The comparison includes the time-domain method by Mahmoud and Arslan [15] and the methods that combine AIC and time-domain strategies by Brandes *et al.* [20], Hussain and López-Valcarce [11] and the one in [16], henceforth referred to as *ad hoc*, as the generalized pulses are optimized ad hoc for a given scenario.

The PSD obtained with the methods in [15] and [20] is computed applying the Welch's averaged periodogram method with a 16384-sample Hanning window and 4096-sample overlap to an OFDM signal consisting of 2000 QPSK modulated symbols. The PSD for the method in [11] is obtained analytically using [11, eq. (10)]. Pulses optimized with the proposed framework and the ad hoc [16] method are designed using $N_{\mathrm{ci}} = 2$, $N_{\mathrm{co}} = 0$ and $N_{\mathrm{q}} = 2$. Likewise, the method in [11] is configured to use the same set of CC as the aforementioned strategies and the tapered transitions also span β samples. Its solution is obtained after 16 iterations and the regularization term is configured to avoid PSD peaks in the passband. For the proposed framework, the direct optimization method is applied with $N_{\mathrm{h\_min}} = 4$ and $N_{\mathrm{h\_max}} = 13$. The ad hoc design also uses $N_{\mathrm{h}} = 13$. While the latter can give lower PSD values by using larger N_{h} as shown in [16, Fig. 4], this will increase the computational cost of the third phase, since a larger number of optimized pulses would be employed.

Fig 3.10 shows the normalized PSD attained in the aforesaid scenario. The RC pulse-shaping case is shown as a reference. It can be observed that reducing the OOBE in the spectral hole is more challenging than in the sideband. In the former, the bandwidth adaptive method gives $\mathrm{PSD}_{\mathrm{max}} = -48$ dB, outperforming the technique in [15] by 14.93 dB and the one in [20] by more than 20 dB. It attains similar emissions to the method in [11]. As expected, the latter performs worse than the ad hoc method, which generalizes [11] by optimizing the transition pulse to be used in each carrier (instead of optimizing a single one for all carriers). The performance loss of the bandwidth adaptive method w.r.t. the ad hoc one is about 10.3 dB. However, this loss is paid in exchange for an easy recomputation of the solutions whenever the spectral emission mask changes. Hence, if the notched band between carriers 3022 and 3026 is to be dynamically created without prior knowledge of the receiver, the proposed method determines the optimized pulses to be used by applying simple transformations to the ones already employed in the data carriers closest to the rightmost edge of the band (carriers 3056 to 3068), while costly optimization problems have to be solved online in the ad hoc one. In the notched band starting in carrier 3072, the bandwidth adaptive method attains $\mathrm{PSD}_{\mathrm{max}} = -49$ dB, which is 24 dB lower than the one given by [15] and roughly 2.2 dB lower than the one in [11]. Note that the bandwidth adaptive method slightly outperforms [11], even though the pulses of the latter are optimized for the considered spectral mask and in the former they are obtained by adapting a precomputed solution. The performance improvement obtained is due to the additional degree of freedom, with respect to [11], given by the use of a different transition pulse in each of the $|\mathcal{D}^{\mathrm{h}}|$ data carriers.

It should be mentioned that, in the considered scenario, the bandwidth adaptive method can achieve $\mathrm{PSD}_{\mathrm{max}}$ below -50 dB by increasing $N_{\mathrm{h\_min}} = 10$, at the cost of penalizing its performance in passband widths narrower than 14 carriers. Finally, it must be highlighted that the PAPR of the signal designed with the bandwidth adaptive method is similar to that obtained with the ad hoc solution, being the latter lower than the one resulting with [15] and [20] [16, Fig. 6(b)].

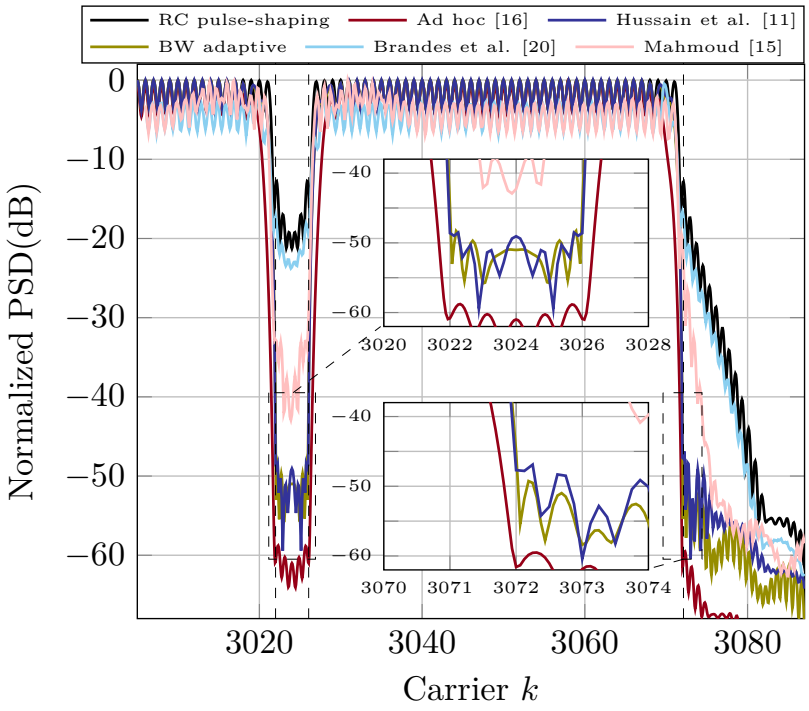

Figure 3.10: Normalized PSD attained by the proposed method and other taken from the literature. For those that use the proposed pulses, only $h_k(\mathrm{CC}, t_k\text{-h})$ is considered.

3.3 Enhancing spectral confinement by adding time-shifted OOBE-cancelling terms

In this third section, we propose an innovative way to increase the number of degrees of freedom of spectral shaping methods based on the generalized pulse reviewed in Sec. 2.5 by adding time-advanced and delayed versions of the AIC and AST terms. The additional flexibility can be used in a twofold way:

- To mitigate the data-rate penalty of AIC techniques and to lessen the amount of effective cyclic prefix that is shortened due to the tapered transitions and the AST term, while still attaining the same OOBE level.
- To reduce the OOBE of the OFDM signal while keeping data-rate loss and the effective cyclic extension unchanged.

This contribution is presented in deeper detail in

[23] J. Giménez, J. A. Cortés, E. Martos-Naya and L. Díez, "Spectral Shaping Method for OFDM Combining Time-Shifted Active Interference Cancellation and Adaptive Symbol

Transition," in *IEEE Open Journal of the Communications Society*, vol. 6, pp. 4476-4490, 2025.

attached in the Appendix B.1.5.

The idea of extending the generalized pulse arises after noticing that its cancellation terms can be shifted by an integer number of symbol periods without affecting the receiver operation, i.e., while still being orthogonal to the data being transmitted. The result is a pulse, referred to as *time-expanded pulse*, with M_{a} advanced and M_{d} delayed cancellation terms, with the following expression

$$\mathbf{h}_k^{\text{t-e}} = \underbrace{\begin{bmatrix} \mathbf{0}_{M_{\mathrm{a}}N_{\mathrm{s}},1} \\ \mathbf{p}_k \\ \mathbf{0}_{M_{\mathrm{d}}N_{\mathrm{s}},1} \end{bmatrix}}_{\stackrel{\text{def}}{=}\mathbf{p}_k^{\text{t-e}}} + \sum_{i=-M_{\mathrm{a}}}^{M_{\mathrm{d}}} \underbrace{\begin{bmatrix} \mathbf{0}_{(M_{\mathrm{a}}+i)N_{\mathrm{s}},|\mathcal{C}|} \\ \mathbf{P}_{\mathcal{C}} \\ \mathbf{0}_{(M_{\mathrm{d}}-i)N_{\mathrm{s}},|\mathcal{C}|} \end{bmatrix}}_{\stackrel{\text{def}}{=}\mathbf{P}_{\mathcal{C},i}^{\text{t-e}}} \boldsymbol{\alpha}_{k,i} + \sum_{i=-M_{\mathrm{a}}}^{M_{\mathrm{d}}+1} \underbrace{\begin{bmatrix} \mathbf{0}_{(M_{\mathrm{a}}+i)N_{\mathrm{s}},\beta} \\ \mathbf{I}_{\beta} \\ \mathbf{0}_{(M_{\mathrm{d}}-i+1)N_{\mathrm{s}},\beta} \end{bmatrix}}_{\stackrel{\text{def}}{=}\mathbf{T}_i^{\text{t-e}}} \boldsymbol{\zeta}_{k,i}, \quad k \in \mathcal{D}^{\mathrm{h}}, \tag{3.22}$$

where the symbols $\mathbf{p}_k^{\text{t-e}}$, $\mathbf{P}_{\mathcal{C},i}^{\text{t-e}}$ and $\mathbf{T}_i^{\text{t-e}}$ are defined for convenience to represent the base pulse, the time-shifted matrix of CC and the time-shifted identity matrix for the transition pulses, respectively. The pulse that results when $M_{\mathrm{a}} = M_{\mathrm{d}} = 0$ is the generalized pulse in (2.22), comprising the AIC terms with $i = 0$ and the AST terms with $i = 0$ and $i = 1$, the latter two corresponding to the starting and ending segments of the transition pulse ($\boldsymbol{\zeta}_k^{\mathrm{s}}$ and $\boldsymbol{\zeta}_k^{\mathrm{e}}$), respectively. The remaining terms, i.e., the AIC terms for $i \in \{-M_{\mathrm{a}}, \ldots, -1, 1, \ldots, M_{\mathrm{d}}\}$ as well as the AST terms for $i \in \{-M_{\mathrm{a}}, \ldots, -1, 2, \ldots, M_{\mathrm{d}}+1\}$, are novel.

For illustrative purposes, Fig. 3.11 depicts the waveform of the base pulse, $p_k(n)$, of a regular generalized pulse, $h_k(n)$, and of the proposed pulse with $M_{\mathrm{a}} = M_{\mathrm{d}} = 1$, $h_k^{\text{t-e}}(n)$. The shaded regions define the time duration of the AIC and AST terms in (3.22). The time-shifted cancellation terms are labeled as AIC with $i \in \{-1, 1\}$ and AST with $i \in \{-1, 2\}$, and extend to the preceeding and subsequent symbol periods. The ripple in the flat regions of $h_k(n)$ and $h_k^{\text{t-e}}(n)$ is due to the CC and their shape in the boundaries between symbols is mainly due to the transition pulses.

For convenience, let us rewrite the proposed time-expanded pulse in (3.22) as

$$\mathbf{h}_k^{\text{t-e}} = \mathbf{p}_k^{\text{t-e}} + \boldsymbol{\Pi}_k^{\text{t-e}} \boldsymbol{\gamma}_k^{\text{t-e}}, \tag{3.23}$$

where $\boldsymbol{\Pi}_k^{\text{t-e}}$ and $\boldsymbol{\gamma}_k^{\text{t-e}}$ are defined for compactness

$$\begin{aligned} \boldsymbol{\Pi}_k^{\text{t-e}} &= \left[\mathbf{P}_{\mathcal{C},-M_{\mathrm{a}}}^{\text{t-e}} \cdots \mathbf{P}_{\mathcal{C},M_{\mathrm{d}}}^{\text{t-e}} \mid \mathbf{T}_{-M_{\mathrm{a}}}^{\text{t-e}} \cdots \mathbf{T}_{M_{\mathrm{d}}+1}^{\text{t-e}}\right], \\ \boldsymbol{\gamma}_k^{\text{t-e}} &= \left[\boldsymbol{\alpha}_{k,-M_{\mathrm{a}}}^{\mathrm{T}} \cdots \boldsymbol{\alpha}_{k,M_{\mathrm{d}}}^{\mathrm{T}} \mid \boldsymbol{\zeta}_{k,-M_{\mathrm{a}}}^{\mathrm{T}} \cdots \boldsymbol{\zeta}_{k,M_{\mathrm{d}}+1}^{\mathrm{T}}\right]^{\mathrm{T}}. \end{aligned} \tag{3.24}$$

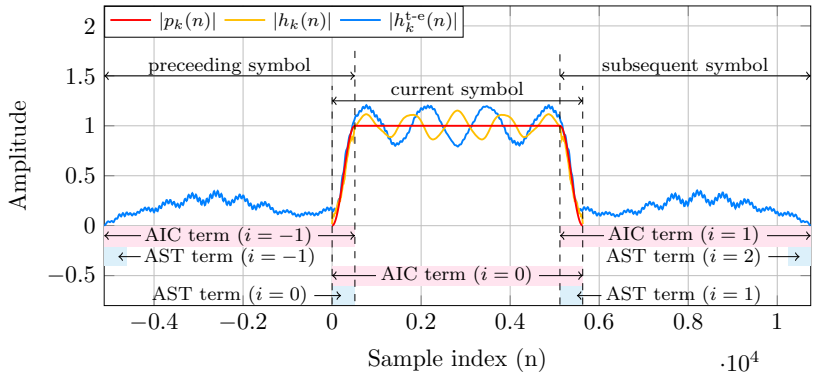

Figure 3.11: Waveform of the time-expanded pulse, the generalized pulse and the basic one. They have been generated with $N = 4096$, $N_{\text{GI}} = 1024$, $\beta = 512$ and a shaping pulse $g(n)$ with RC transitions. The proposed pulse employs $M_{\text{a}} = M_{\text{d}} = 1$. The shaded regions highlight the time extent of the AIC and AST terms in (3.22).

The coefficients in $\boldsymbol{\gamma}_k^{\text{t-e}}$ can be obtained through the following optimization procedure to minimize the OOBE,

$$\widehat{\boldsymbol{\gamma}}_k^{\text{t-e}} = \arg\min_{\boldsymbol{\gamma}_k^{\text{t-e}}} \{E_{k,\mathcal{B}}\} = \arg\min_{\boldsymbol{\gamma}_k^{\text{t-e}}} \left\{ \left(\mathbf{h}_k^{\text{t-e}}\right)^{\text{H}} \boldsymbol{\Phi}_{\mathcal{B}}^{\text{t-e}} \mathbf{h}_k^{\text{t-e}} \right\}, \qquad k \in \mathcal{D}^{\text{h}}, \tag{3.25}$$

where $\boldsymbol{\Phi}_{\mathcal{B}}^{\text{t-e}} = \int_{\mathcal{B}} \mathbf{f}_{L'}(f) \mathbf{f}_{L'}^{\text{H}}(f) df$, and $L' = L + \left(M_{\text{a}} + M_{\text{d}}\right) N_{\text{s}}$ is the number of samples of the new time-expanded pulse.

The problem in (3.25) is solved for each data carrier in $\mathcal{D}^{\text{h}}$, offline, as it is independent of the data. It is recalled that, even though there is a closed-form solution for this problem, it may lead to PSD peaks in the passband. To avoid them, the Tikhonov regularization can be applied to the problem, as explained in Section 2.5, which had a closed-form solution too. Nonetheless, it is preferred to solve the problem in (3.25) while constraining the magnitude of the real and imaginary parts of the coefficients involved as

$$\left.\begin{aligned} |\text{Re}\{\alpha_{k,i}(l)\}| &\leq \epsilon_{k,i} \\ |\text{Im}\{\alpha_{k,i}(l)\}| &\leq \epsilon_{k,i} \end{aligned}\right\} \text{ for } \begin{aligned} &i \in \{-M_{\text{a}}, \ldots, M_{\text{d}}\}, \\ &l \in \{1, \ldots, |\mathcal{C}|\}, \end{aligned}$$
$$\left.\begin{aligned} |\text{Re}\{\zeta_{k,i}(r)\}| &\leq \delta_{k,i} \\ |\text{Im}\{\zeta_{k,i}(r)\}| &\leq \delta_{k,i} \end{aligned}\right\} \text{ for } \begin{aligned} &i \in \{-M_{\text{a}}, \ldots, M_{\text{d}}+1\}, \\ &l \in \{1, \ldots, \beta\}. \end{aligned} \tag{3.26}$$

for $k \in \mathcal{D}^{\text{h}}$. These constraints require resorting to numerical methods to find the minimum-energy solution, but the relation between the imposed limits and the potential PSD peaks is quite straightforward.

3.3.1 Numerical results and discussion

The performance of the time-expanded pulse is assessed using two actual OFDM scenarios with rather different characteristics: the 5G NR and the wired system defined in the ITU-T Rec. G.9960 for in-home broadband PLC already used in a previous section [38] [37]. Regarding the former, the standard defines a rectangularly windowed OFDM system whose number of carriers and cyclic prefix length depend on the employed subcarrier spacing (SCS) and channel bandwidth. For this assessment, the SCS is fixed to 15 kHz and three channel bandwidths, namely 5, 10 and 50 MHz, are considered. The number of resource blocks (RBs) is set to the maximum one allowed for each channel bandwidth [39, Table F.5.3.1]. The OOBE is quantified by means of the adjacent channel leakage ratio (ACLR), defined as the ratio of the transmitted power on the assigned channel to the power on the adjacent channel, and that must be kept over 45 dB [38]. To comply with this requirement, vendors have traditionally used pulses with tapered transitions [40]. Despite the standard defines a rectangularly windowed OFDM system, pulse-shaping can be employed provided that the specified EVM limit is not exceeded [38, Sec. 6.5.2.2]. It can be shown that pulse shaping does not impact the EVM, measured according to the procedure described in [38, Appendix B], if the tapered transitions are shorter or equal to half the length of the cyclic prefix, i.e., $\beta \leq N_{\mathrm{GI}}/2$.

Regarding the ITU-T Rec. G.9960, we recall that it defines a pulse-shaped OFDM system with $N = 4096$, $N_{\mathrm{GI}} = 1024$ and $\beta = 512$. The shaping pulse $g(n)$ is assumed to have RC transitions. In the European Union (EU), these systems have to comply with the EN 50561-1 [6], which defines 20 permanently excluded subbands plus 14 dynamic ones within the range 1.8–30 MHz. While the EN 50561-1 does not define the level of the PSD in these subbands, a drop by at least 43 dB for the ones below 5 MHz and by at least 39 dB for those located in the 5-30 MHz is typically employed by vendors. Furthermore, the PSD of ITU-T G.9960 devices must also drop at least 30 dB (w.r.t. the level within the passband) below 1.8 MHz and above 30 MHz [41]. This system has been selected because the severe emission mask highlights the potential of the time-expanded pulses to reduce the OOBE without the data rate penalty of AIC-based techniques.

In both scenarios, the optimization problem presented in (3.25) is solved subject to the constraints in (3.26). Additionally, the transition pulses of the proposed method are harmonically designed to reduce their optimization and implementation complexity. In [23] we provide details on how the implementation of these terms is carried out, which has been omitted in this summary. The PSD of the resulting OFDM signal is computed using (2.29) and normalized to its maximum value.

Parametrization of the proposed method

This subsection analyzes the influence that the number of advanced and delayed terms has on the performance of the proposed pulse. The 5G NR system is set up with a channel bandwidth of 5 MHz, $N = 512$, $N_{\mathrm{GI}} = 36$ and $\beta = 15$, which satisfies the constraint $\beta \leq N_{\mathrm{GI}}/2$ [38, Table 5.3.2-1]. The ITU-T Rec. G.9960 is configured to use the 2047 data carrier with indexes $1025 \leq k \leq 3071$. In both scenarios, the proposed method is employed to reduce the OOBE in the notched band $\mathcal{B}$ corresponding to the unused carriers. Two types of pulses are considered in both cases: one with the same number of advanced and delayed terms ($M_{\mathrm{a}} = M_{\mathrm{d}}$), and another that only has delayed terms ($M_{\mathrm{a}} = 0$, $M_{\mathrm{d}} \geq 0$). The number of data carriers using the proposed pulse is fixed at $|\mathcal{D}^{\mathrm{h}}| = 11$ in the ITU-T Rec. G.9960 case, and ranges from 20 to 40 in the 5G scenario depending on the values of M_{a} and M_{d}. Similarly, the number of CC is 5 in the ITU-T Rec. G.9960 case and ranges from 5 to 15 CC in the 5G scenario. None of the data carriers inside the passband are used as CC, which allows evaluating the ability of the time-expanded pulses to handle the OOBE without data rate penalty. The harmonic design of the transition pulses uses 6 terms in all cases.

Fig. 3.12 represents $\mathrm{PSD}_{\mathrm{max}}$ values for different number of extended terms and for the two aforementioned pulse types. M_{T} denotes the total number of advanced and delayed terms, i.e., $M_{\mathrm{T}} = M_{\mathrm{a}} + M_{\mathrm{d}}$. Both cases show a substantial gain when time-expanded terms are used w.r.t. the case where there are none ($M_{\mathrm{T}} = 0$). Interestingly, the $\mathrm{PSD}_{\mathrm{max}}$ decreases notably for $M_{\mathrm{T}} = 1$ and $M_{\mathrm{T}} = 2$, while small additional reductions are obtained with larger values of M_{T}. The time-expanded pulse that uses both advanced and delayed cancellation terms (in light blue in the figure) gives substantially lower $\mathrm{PSD}_{\mathrm{max}}$ than the pulse that only has delayed terms (in red).

It is interesting to note that $\mathrm{PSD}_{\mathrm{max}}$ attains a lower value in the 5G NR case than in the ITU-T Rec. G.9960, despite the latter using a larger β. The reason is that the minimum value of $\mathrm{PSD}_{\mathrm{max}}$ depends on the relation between β and the length of the base pulse $L = N_{\mathrm{s}} + \beta$, which determines how aligned are the maxima of the sidelobes of the canceling terms' spectrum with those of the base pulse's spectrum. The tighter the alignment, the lower the $\mathrm{PSD}_{\mathrm{max}}$ yielded by the method.

Fig. 3.12 shows that the most gain is attained when both advanced and delayed cancellation terms are used. However, delay-sensitive applications would require using only delayed terms, which still yield notable OOBE reductions without employing data carriers as CC.

Comparison With Previous Proposals

In this subsection, the performance of the proposed pulse is compared to that attained by the following techniques found in the literature: the generalized pulse in [16], the AST method

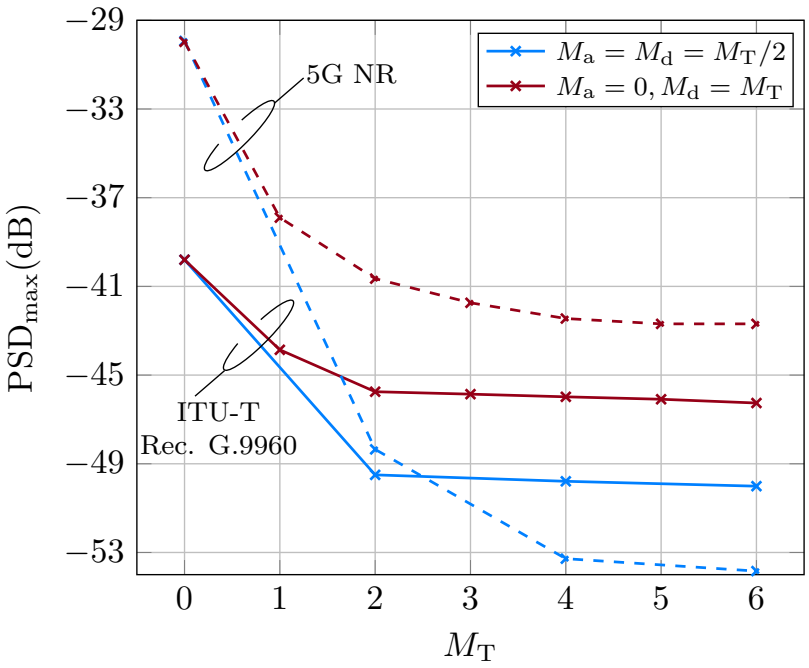

Figure 3.12: $\mathrm{PSD}_{\max}$ attained by the proposed method for different number of time-expanded pulses (M_{T}). Two cases are considered: one using pulses with the same number of advanced and delayed terms ($M_{\mathrm{a}} = M_{\mathrm{d}} = M_{\mathrm{T}}/2$), and another with pulses that counts only with delayed cancellation terms ($M_{\mathrm{a}} = 0; M_{\mathrm{d}} = M_{\mathrm{T}}$).

by Mahmoud and Arslan [15] and the method that combines AIC and AST by Hussain and López-Valcarce [11]. To this end, the normalized PSD of the signals that result from using each of the methods is computed and compared.

In order to assess the capability of the proposed pulse to create both deep notches in the passband and in the sidebands of the transmitted signal, the OFDM parameters of the ITU-T Rec. G.9960 are employed and the scenario with notched bands at carrier indices $\mathcal{B} = \{0, \ldots, 1024\} \cup \{3022, \ldots, 3026\} \cup \{3072, \ldots, 4095\}$ has been selected again. The excluded subband corresponding to carrier indexes $3022 \leq k \leq 3026$ allows assessing the ability of the method to create notches in the passband of the transmitted signal, while the ones with indexes $0 \leq k \leq 1024$ and $3072 \leq k \leq 4095$ judge its ability to reduce the OOBE in the sidebands. For the sake of simplicity, we focus on the reduction of the OOBE in the notch and in the right sideband.

For the method in [15], the PSD is estimated by means of the Welch's averaged periodogram with a 16384-sample Hanning window and an overlap of 4096 samples applied to an OFDM signal consisting of 2000 symbols modulated with QPSK. For the method in [11], it is obtained using the analytical expression in [11, eq. (10)]. Finally, the method in [16] is a particularization of the proposed one with $M_{\mathrm{a}} = M_{\mathrm{d}} = 0$, hence its PSD is obtained using

(2.29) as well.

First, we show that the proposed method is able to achieve lower OOBE than existing methods that also combine AIC and AST techniques, but without undergoing the data rate penalty of the latter. For the proposed pulse, a set of CC is defined, consisting of 8 out-of-band CC by the side band, 4 more out-of-band CC at the narrow notch, and no CC inside the passband. This set is denoted as $\mathcal{C}_1$ which does not incur a data rate penalty since it has none of its CC inside the passband. The transition pulses are harmonically designed using 10 terms, which are distributed as follows: 5 by the right side band and 5 around the notch. The method in [16], denoted as $h_k(\mathcal{C}_1)$, is parameterized in the same manner. As for the method in [11], a different set of CC is defined, consisting of 3 CC by each of the 3 edges of the passband where the OOBE is to be reduced. Out of these CC, only 1 is out-of-band, while 2 are inband. With this set, which is represented as $\mathcal{C}_2$, there is a data rate penalization due to the 6 data carriers employed as inband CC. The use of out-of-band carriers as CC entails no data rate penalty, as they cannot convey information. The solutions to the method in [11] are obtained after 16 iterations with the regularization term configured to avoid PSD peaks in the passband.

The normalized PSD attained by the aforesaid methods is plotted in Fig. 3.13. Only the narrow notched band and the upper sideband are presented, since the lower sideband is equivalent to this latter. The RC pulse-shaping case proposed in the standard is shown as a reference. As it can be observed, in the notch, the pulse $h_k^{\text{t-e}}(\mathcal{C}_1; M_\text{a} = M_\text{d} = 1)$ attains $\text{PSD}_\text{max} = -63.46$ dB, outperforming the method in [11] by 14.92 dB (and without incurring any data rate loss), the method $h_k(\mathcal{C}_1)$ by 20.87 dB and the one by Mahmoud and Arslan by more than 30 dB. In the sideband edge, the proposed pulse also outperforms the other methods.

The time-expanded pulse that only has delayed expanded terms, $h_k^{\text{t-e}}(\mathcal{C}_1; M_\text{a} = 0, M_\text{d} = 2)$, attains a lower performance than its anticausal counterpart both in the narrow notch and the sideband. However, it still outperforms the method in [11] by 2 dB in the sideband and gives similar performance in the notch. It must be highlighted that, while the PSD_max values are similar, the proposed method yields lower overall OOBE power than [11].

Performance Examples in Actual Scenarios

This section quantifies the benefits that can be obtained by using the proposed pulse in the 5G NR and the ITU-T Rec. G.9960 systems. In the latter we will highlight the potential of the proposal to nearly eliminate the data rate penalty of AIC-based methods due to the use of data carriers as CC, while in the former we emphasize the capacity of the time-expanded pulse to reduce both the guard band and the part of the cyclic prefix used to shape the spectrum of the signal.

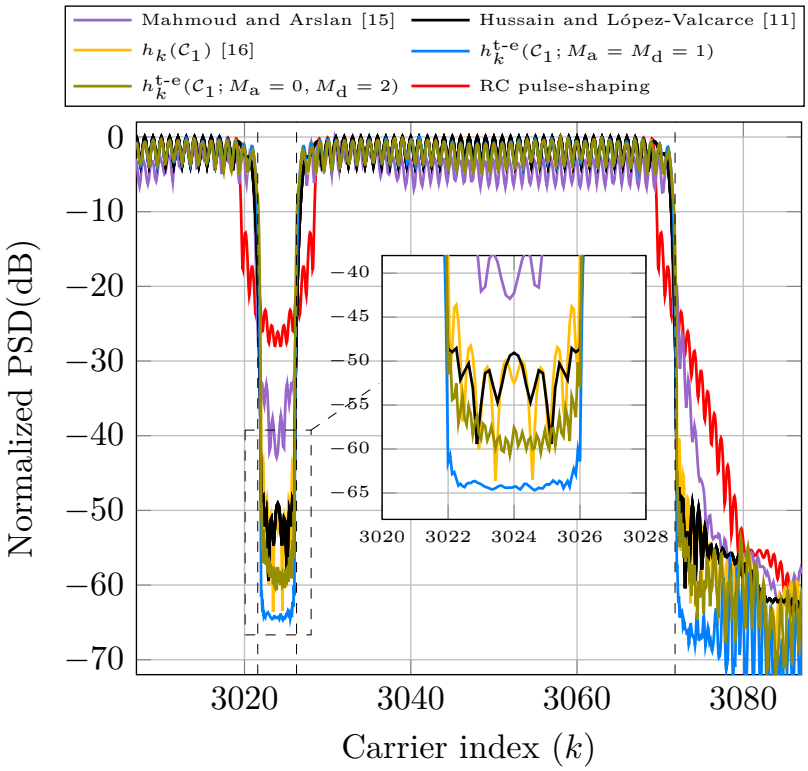

Figure 3.13: PSD obtained with the proposed method and others taken from the literature. While set $\mathcal{C}_1$ contains no inband CC to avoid the data rate degradation caused by the AIC term, the method in [11] uses 6 inband CC.

Wireless system: 5G NR. We herein consider channel bandwidths equal to 5, 10 and 50 MHz. The standard defines that part of these are used as guard band, in a percentage that ranges from 10% for the 5 MHz bandwidth to 2.8% for the 50 MHz one, which translates into a spectral efficiency loss that is particularly relevant for the narrowest channels.

For illustrative purposes, Fig. 3.14 depicts the PSD obtained in the 5 MHz bandwidth with the proposed pulse and with the RC pulse-shaping conventionally used for this purpose by vendors. In both cases, $\beta = 7$ and the guard bands are reduced to the minimum value that guarantees that ACLR > 45 dB. The number of data carriers using the proposed pulse on each side of the transmission bandwidth is 22 and a set of 5 out-of-band CC is used (no inband CC are employed). The transition pulses are harmonically designed using 3 non-zero terms and $M_\text{a} = M_\text{d} = 1$. As seen, the proposed pulse allows reducing the guard band to a single carrier (15 kHz) and its PSD falls below -45 dB at 502.5 kHz (33.5 times the SCS) from the passband edge. In contrast, the RC solution needs a guard band of 20 carriers (300 kHz) and its PSD falls below -45 dB only for frequencies farther than 832.5 kHz (55.5 times the SCS) from the passband edge. Moreover, the leftmost carriers of the adjacent channel suffer similar interference levels in both cases, with signal to interference ratio (SIR)

values around 30 dB. It can be noticed that the RC solution gives lower OOBE than the proposed method at distant frequencies from the transmission band edge. However, this gives no practical benefit, as it occurs for PSD values lower than −55 dB, which is well below the ACLR requirement.

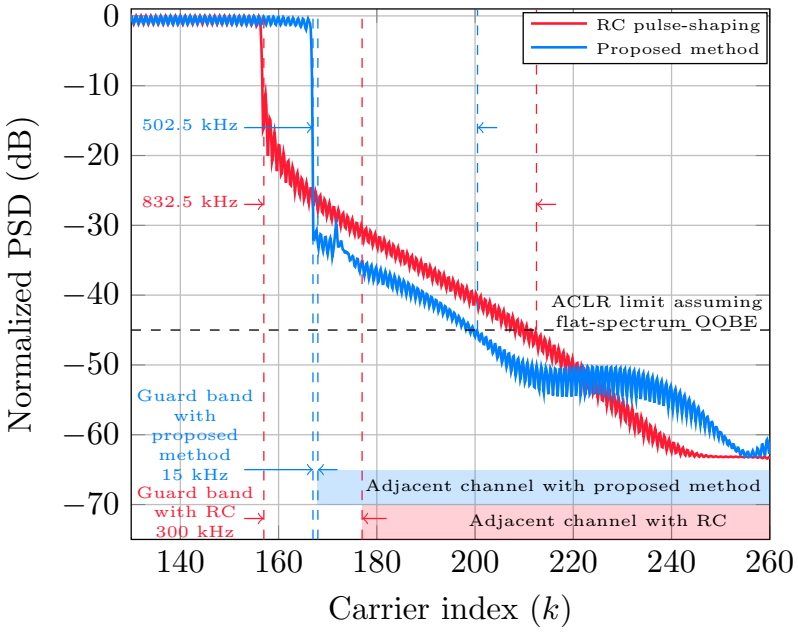

Figure 3.14: PSD obtained with the proposed method and the RC pulse-shaping in the 5 MHz bandwidth with SCS equal to 15 kHz and $\beta = 7$. The guard bands are reduced to the minimum value that guarantees that ACLR > 45 dB. The PSD limit that would be needed to comply with this requirement assuming an OOBE with flat spectrum is depicted for reference. The shaded regions highlight the limit of the adjacent channel with each solution.

Table 3.3 details the guard band reduction that can be achieved, while meeting the ACLR constraint and with EVM= 0, in the 5, 10 and 50 MHz channels when using the proposed method and the pulse-shaping one with RC pulse-shaping. The size of the DFT (N) is 512, 1024 and 4096, respectively. The guard interval (N_{GI}) contains 36, 72 and 288 samples, respectively. The number of data carriers at each edge of the transmission bandwidth using the proposed pulse ranges from 22 to 35 (depending on the channel bandwidth), while 5 CC are used in all cases. The number of terms in the harmonic design of the transition pulses ranges from 2 to 5. The computational cost of the proposed method is given in terms of the percentage increase of both the number of complex products per OFDM symbol and of the number of real products when the complexity reduction strategy described in Section 3.1 is employed. In both cases, the cost of the RC pulse-shaped OFDM system, assumed to be $\frac{N}{2}\log_2(N) + 2\beta$, is used as reference.

As shown, when $\beta = 3$ the ACLR condition cannot be satisfied for the 5 and 10 MHz

Table 3.3: Guard bandwidth reduction and complexity increment with the RC-windowed pulse and the proposed pulse when used in 5G NR signals.

		RC pulse	**Proposed method**		
Channel Bandwidth (MHz)	**Shaped samples (β)**	**Guard band reduction[a]**	**Guard band reduction[a]**	**Complex products/symbol increment (%)**	**Real products/symbol increment (%) (Hermitian symmetry)**
5	3	-	-56.3% (14/32)	+94%	+47.1%
	7	-37.5% (20/32)	-96.9% (1/32)	+51.7%	+26.1%
10	3	-	-35.7% (27/42)	+34.2%	+17.1%
	7	-38.1% (26/42)	-97.6% (1/42)	+34.1%	+17.1%
50	1	-46.2% (50/93)	-55.9% (41/93)	+6.6%	+3.3%
	7	-87.1% (12/93)	-98.9% (1/93)	+9.4%	+4.8%

[a] The values between brackets are the number of subcarriers of the reduced guard band/number of carriers of the guard band in the standard.

channels using the RC-shaped pulse, while the proposed method allows the guard band to be reduced by more than a half for the former, and by more than a third for the latter. For $\beta = 7$, the guard bands can be reduced in more than a third when the RC-windowed pulse is used, but can be almost entirely eliminated when the proposed method is employed. Relative differences in the guard band reduction between both pulses get smaller when the channel bandwidth increases. This is because augmenting the number of subcarriers, N, entails calculating the ACLR over a wider frequency region. Since the magnitude of the sidelobes decreases at distant frequencies, the wider the channel, the lower the ratio between the power leaked from adjacent channels and the transmitted power. Simultaneously, the relative cost of using the proposed pulse decreases as the number of subcarriers increases, as the complexity of the baseline system in the cases considered is dominated by N, while the one of the proposed pulse is dominated by β. Nevertheless, each percentage point increase in complexity provides percentage points reduction in the guard band ranging from 0.5 (for the 5 MHz channel with $\beta = 3$) to 8.5 (for the 50 MHz channel for $\beta = 1$). For $\beta = 7$ the aforementioned relations range from 1.9, for the 5 MHz channel, to 10.5, for 50 MHz. These values are nearly double when Hermitian-symmetric pulses are used.

Wired system: indoor broadband PLC In order to illustrate the strict requirements imposed by the EN 50561-1 and the considered PSD limits, Fig. 3.15 displays them in the frequency range corresponding to carrier indexes $500 \leq k \leq 630$, which correspond to frequencies 12.21 MHz $\leq f \leq$ 15.38 MHz. The PSD obtained with the proposed pulse, $h_k^{\text{t-e}}(\mathcal{C}_5, M_\text{a} = M_\text{d} = 1)$, and RC pulses are also shown, where $\mathcal{C}_5$ contains 6 inband CC and 186 out-of-band CC. As seen, the RC-pulse has to null a large number of data carriers in order to comply with the emission limits. This causes the depicted subbands with carrier

indexes $548 \leq k \leq 555$ and $570 \leq k \leq 573$ to have no active carriers at all. In contrast, the proposed pulse complies with the stringent mask while sacrificing just one of the data carriers in this frequency region.

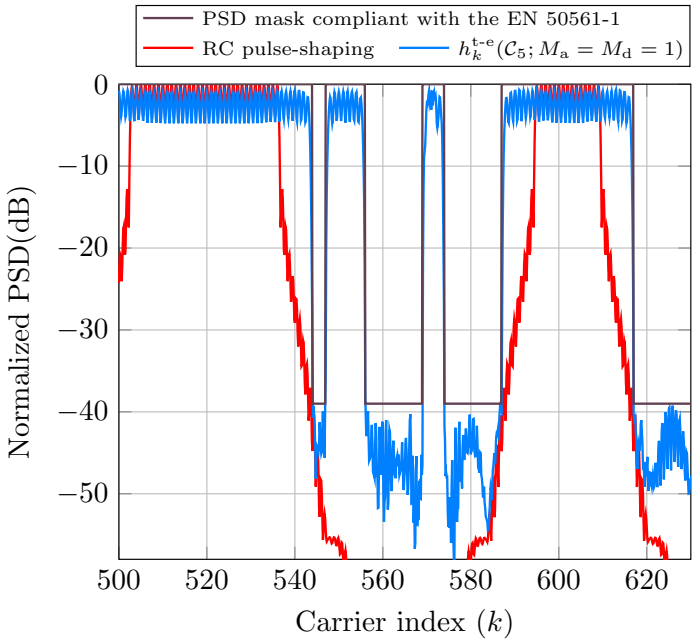

Figure 3.15: Detailed region of the PSD obtained with time-expanded pulse, $h_k^{\text{t-e}}(\mathcal{C}_5, M_a = M_d = 1)$, and the RC pulse-shaped one when complying with the notched bands imposed by the EN 50561-1 and the assumed emission mask.

In order to compare the capability of different spectral shaping methods to comply with the EN 50561-1 and the ITU-T Rec. G.9964, only the proposed method and the one in [16] will be now considered (in addition to the pulse-shaped one defined in the standard), as results in a previous subsection have shown that these give the lowest OOBE. Table 3.4 summarizes the data carriers loss (due to the use of inband CC) in the band up to 30 MHz and the increment in the number of products per OFDM symbol of the proposed method, $h_k^{\text{t-e}}(\mathcal{C}_5, M_a = M_d = 1)$, and the one in [16], $h_k(\mathcal{C}_6)$, w.r.t. the RC pulse-shaped solution. The set $\mathcal{C}_6$, used by the method in [16], contains 54 inband CC and 142 out-of-band CC, while $\mathcal{C}_5$ only contains 6 inband CC. Hence, the former causes greater data rate degradation. Table 3.4 also shows the complexity resulting when pulses with Hermitian symmetry are employed, given in terms of the percentage increment in real products per symbol w.r.t. the pulse-shaping method. As seen, the percentage of data carriers that have to be nulled when using the pulse-shaped OFDM system as the one defined in the standard exceeds 42% and is about 8% when using the method in [16], $h_k(\mathcal{C}_6)$. In contrast, the proposed method fulfills the imposed mask with almost no data carrier loss, keeping it below 1%.

Table 3.4: Data carrier loss and complexity of different spectral shaping methods when used to comply with the EN 50561-1 and the ITU-T Rec. G.9964.

Method	Data carriers loss (%)	Complexity increment per OFDM symbol	
		Complex products (%)	Real products (%) (Hermitian symmetry)
Pulse-shaping with RC window	42.49	0	0
$h_k(\mathcal{C}_6)$[a]	7.73	19.56	14.28
$h_k^{\text{t-e}}(\mathcal{C}_5; M_\text{a} = M_\text{d} = 1)$[b]	0.86	39.79	24.4

[a] $\mathcal{C}_6$ contains 54 inband CC and 142 out-of-band CC.
[b] $\mathcal{C}_5$ contains 6 inband CC and 186 out-of-band CC.

The aforementioned reduction in the data rate loss is achieved at the expense of increasing the implementation complexity. Hence, while the method $h_k(\mathcal{C}_6)$ requires a 19.56% increment in the number of complex products, the one with time-expanded pulses, $h_k^{\text{t-e}}(\mathcal{C}_5, M_\text{a} = M_\text{d} = 1)$, needs 39.79%. Nevertheless, when the complexity reduction strategy that exploits the Hermitian symmetry proposed in Section 3.1 is employed, the former reduces to 14.28% and the latter to 24.4% in terms of real products. Therefore, the proposed strategy lowers the data carrier loss by about 7 percentage-points at the price of a 10 percentage-point increment in the complexity.

Finally, it must be mentioned that benefit reported by the proposed method is achieved without increasing the PAPR, which is 0.011 dB lower than the one attained with the pulse-shaped OFDM signal at a 10^{-3} clipping rate.

3.4 Complementarity of the proposals

The purpose of this section is to show how the proposals in this thesis can be jointly employed. To that end, let us recall them first:

- A novel pulse and design framework that allows reducing the complexity of spectral shaping methods (Sec. 3.1)
- A spectral shaping design paradigm for dynamically adaptive emission masks (Sec. 3.2)
- A strategy to enhance the spectral confinement of OFDM signals by adding time-shifted OOBE-cancelling terms (Sec. 3.3)

They can be combined in different ways:

- The novel pulse and design framework to reduce the complexity of spectral shaping methods can be applied to the spectral shaping paradigm for dynamically adaptive emission masks and to the spectral shaping strategy based in adding time-shifted OOBE-cancelling terms. By using the Hermitian-symmetric pulse, the latter two proposals can benefit from the complexity reduction offered by the first contribution.

- The strategy that enhances the spectral confinement of OFDM signals by adding time-shifted OOBE-cancelling terms can be used in the spectral shaping design paradigm for dynamically adaptive emission masks. The latter can use the additional degrees of freedom provided by the former technique to enhance its OOBE reduction or to mitigate the data rate loss of AIC techniques.

The first statement has been proved in two different instances: in Table 3.1 it is explained that the spectral shaping design paradigm can benefit from using the novel pulse; in [23], it is proved that the spectral shaping strategy based on adding time-shifted OOBE-cancelling terms can benefit from using the novel Hermitian-symmetric pulse as well. However, the latter is not specified in Sec. 3.3, which is a summary of the aforesaid work.

For the second statement, it is recalled that the generalized pulse is used as the foundation for the design paradigm for dynamically adaptive emission masks. Also, that the strategy proposed in Sec. 3.3 adds time-shifted OOBE-cancelling terms to the generalized pulse to enhance its spectral shaping capabilities. Then, it can be proved that a pulse like the latter can be used in the design paradigm proposed in Sec. 3.2. To that end, let us define the time-expanded pulse used by the data carrier k, which is located i carriers apart from the left edge of the passband, as

$$\mathbf{h}_k^{(i)\,\text{t-e}} = \mathbf{p}_k^{\text{t-e}} + \sum_{m=-M_\text{a}}^{M_\text{d}} \underbrace{\begin{bmatrix} \mathbf{0}_{(M_\text{a}+m)N_\text{s},N_\text{CC}} \\ \mathbf{C}_{k-i,m}^{+} \\ \mathbf{0}_{(M_\text{d}-m)N_\text{s},N_\text{CC}} \end{bmatrix}}_{\mathbf{C}_{k-i,m}^{+\,\text{t-e}}} \boldsymbol{\alpha}_{k,m}^{(i)} + \sum_{m=-M_\text{a}}^{M_\text{d}+1} \underbrace{\begin{bmatrix} \mathbf{0}_{(M_\text{a}+m)N_\text{s},\beta} \\ \mathbf{I}_\beta \\ \mathbf{0}_{(M_\text{d}-m+1)N_\text{s},\beta} \end{bmatrix}}_{\mathbf{T}_m^{\text{t-e}}} \boldsymbol{\zeta}_{k,m}^{(i)}, \quad (3.27)$$

where, combining the notations in Sec. 3.2 and Sec. 3.3, $\boldsymbol{\alpha}_{k,m}^{(i)}$ contains the coefficients that the pulse $\mathbf{h}_k^{(i)\,\text{t-e}}$ assigns to the CCs of the m-th time-shifted AIC term. Likewise, $\boldsymbol{\zeta}_{k,m}^{(i)}$ are the samples of the m-th AST term for the same pulse. For convenience, the term comprising the m-th transition pulse for the k-data carrier is denoted as

$$\mathbf{t}_{k,m}^{(i)} = \mathbf{T}_m^{\text{t-e}} \boldsymbol{\zeta}_{k,m}^{(i)}. \quad (3.28)$$

The original set of solutions obtained in the first phase of the framework proposed in Sec. 3.2 should include the optimal coefficients for the time-shifted cancellation terms. Moreover, it

can be proved that the transformations that are used during the second phase are

$$\begin{aligned} \boldsymbol{\alpha}_{k+\Delta k,m}^{(i)} &= \boldsymbol{\alpha}_{k,m}^{(i)}, & \mathbf{t}_{k,m}^{(i)} &= \boldsymbol{\Omega}_{\Delta k}^{\text{t-e}} \mathbf{t}_{k,m}^{(i)}, \\ \boldsymbol{\alpha}_{k}^{(-i)} &= \left(\alpha_{k}^{(i)}\right)^{*}, & \mathbf{t}_{k,m}^{(-i)} &= \boldsymbol{\Omega}_{2k-N}^{\text{t-e}} \left(\mathbf{t}_{k,m}^{(i)}\right)^{*}, \end{aligned} \tag{3.29}$$

where $\boldsymbol{\Omega}_{\Delta k}^{\text{t-e}} = \text{diag}\left(\left[e^{-j\frac{2\pi}{N}\Delta k(M_{\text{a}}N_{\text{s}}+N_{\text{GI}})}, \ldots, e^{-j\frac{2\pi}{N}\Delta k(M_{\text{d}}N_{\text{s}}+L-1-N_{\text{GI}})}\right]\right)$. These relations are proved in Appendix A.3.

Chapter 4

Conclusions and Future Work

This chapter lays out the main conclusions that arise from the contributions of this thesis. In addition, some future lines are suggested.

4.1 Conclusions

This thesis has defined three distinct objectives aimed at improving the state-of-the-art spectral shaping techniques for OFDM signals.

The first objective pursued the reduction of the optimization and real-time implementation costs of some state-of-the-art spectral shaping techniques. This has been satisfactorily achieved through a twofold proposal: a new transmission pulse with Hermitian symmetry and a design framework that includes an optimization problem model, both applicable to a range of spectral shaping techniques. When the proposed waveform is used and the spectral shaping solutions are obtained following the proposed model, the complexity reductions materialize in:

- The number of real-valued parameters to be obtained in the optimization is reduced by 50% for spectral precoding, AIC and AST techniques.
- The number of real products required to implement spectral precoding and AIC techniques is reduced by 50%. For the AST method, this metric is also halved with its regular implementation, while for h-AST the reduction is lower.

Nonetheless, complying with the design framework is just a sufficient condition to benefit from the complexity reductions above. In this thesis, we have demonstrated how a collection of spectral shaping techniques found in the literature (mainly spectral precoding, AIC and AST based strategies) benefit from substantial complexity reductions in their respective

optimization and implementation procedures when using the proposed Hermitian-symmetric pulse.

Finally, it is also demonstrated that the use of the new waveform has no effect on the performance of the spectral shaping methods in terms of OOBE reduction and PAPR.

The second objective of this thesis was to reduce the cost involved in recalculating the solutions of a spectral shaping problem every time the power emission constraints change. This issue is experienced with most state-of-the-art spectral shaping techniques, which normally rely on a costly optimization procedure to obtain a new set of solutions. To fulfill this objective, a novel spectral shaping design paradigm, consisting of three phases, has been devised:

- The first phase is carried out offline, wherein a set of optimal solutions is obtained for a reference scenario through an optimization procedure and subsequently stored in the communication device.
- The second phase is performed while the system is online and involves transforming these precomputed solutions into a new set that satisfies the power emission constraints whenever they change.
- The third phase consists in generating the OFDM symbol using the transformed solutions.

To ensure the generality of the latter proposal, the generalized pulse is used as the basis for the proposed framework, as it is known to encompass many other AIC and AST techniques. Moreover, the framework benefits from two key characteristics of the generalized pulse: the spectral shaping solutions are data-independent, and it can be applied without modifying the conventional OFDM receiver or affecting the BER.

Numerical results have shown that the paradigm proposed yields OOBE levels that are close to those of other state-of-the-art techniques. Additionally, while some of these strategies found in the literature report lower implementation costs, they require performing the optimization phase for every OFDM symbol or, at best, every time the emission mask changes. In contrast, the proposed method performs this phase offline and only once. This yields a lower overall cost, since solving the optimization problem is much more costly than the implementation of the pulses. Moreover, it does not increase the PAPR of the OFDM signal.

The third objective of this thesis was twofold: to reduce the data rate penalty associated with AIC techniques, which arises from using data carriers as CC, and to mitigate the shortening of the effective cyclic-prefix caused by using pulse-shaping and AST techniques. In order to fulfill these goals without significantly increasing the OOBE, additional degrees of freedom are required. In this direction, an innovation is introduced into the generalized pulse, increasing its generality. The proposal is realized through the addition of novel AIC

and AST terms, like those in the generalized pulse, but time-shifted forward and backward by a discrete number of symbol periods. In this way, they remain orthogonal to the data and the other cancellation terms, at the same time they contribute to the OOBE-reduction goal. With this proposal, it is possible to attain the same OOBE levels that AIC techniques obtain with in-band CC without incurring the data rate penalty of the latter. This is accomplished in exchange for a somewhat higher computational cost.

The latter proposal poses an additional use: if the data rate penalty and the shortening of the effective cyclic prefix are not an issue, the additional cancellation terms can be used to further reduce the OOBE levels of the signal.

The proposed method has been evaluated in two real scenarios. First, in 5G NR the proposed time-expanded pulses allow to reduce the guard bands in more than 50 percentage points in narrow channels, compared to the RC-windowed pulse used by many vendors to comply with the ACLR constraint. In second place, it is evaluated in an indoor broadband PLC scenario where, in order to comply with a very stringent PSD mask, 42% of the data carriers need to be nullified when the conventional signal defined in ITU-T G.9960 is used. Meanwhile, the proposed method is able to create the 34 notches in the aforementioned PSD mask with almost no data rate loss.

Finally, one key characteristic of the contributions of this thesis is that they provide solutions to a spectral shaping problem that is data-independent and can be computed offline. In all cases, we have justified the need to set limits for the magnitude of the coefficients being obtained through the optimization procedure to avoid PSD peaks inside the passband. The procedure used to obtain these constraints is systematic: it involves tuning the constraints of the cancellation terms at the passbands where PSD peaks occur in order to suppress them. Similarly, we have established some criteria to determine which data carriers use the proposed pulses and which cancellation terms are used by each one of them. It mainly consists in selecting those that are closer to the region where the OOBE need to be reduced. Given the large number of possible combinations, it is not feasible to guarantee that the performance achieved with a given set of constraints is the best attainable overall. Moreover, the study of different types of constraints that simultaneously minimize the OOBE and control the PSD peaks, while preserving the convexity of the problem, has not been explored. Nonetheless, by defining the constraints in the proposed manner, it becomes straightforward to obtain a set of them that yields a satisfactory performance across a wide range of scenarios.

4.2 Future work

In the conclusion section, we have addressed how the constraints that are required to avoid PSD peaks within the passband are obtained through a systematic procedure. Also, the method used to determine the set of data carriers that use the proposed pulses and the set

of cancellation carriers follows a similar approach. Even though this method has shown to yield satisfactory solutions in all evaluated cases, there is room for further optimization of the resources employed.

In that direction, a future line can consist in the development of a design tool that carries out all the tasks involved in resolving the spectral shaping problem:

- Determine the data carriers that use the generalized pulses.
- Determine the cancellation terms used for each generalized pulse.
- Determine the constraints that limit the magnitude of the coefficients used for the cancellation terms
- Optimization of the coefficients

For the first three tasks a machine learning model can be trained. The tool would take the OFDM parameters and the PSD mask constraints as input. The output would be the solutions to the spectral shaping problem. The model should be trained subject to the existing trade-off between OOBE reduction and computational cost.

Another interesting line for future work can be defining a pulse-design method similar to the one described for the generalized pulse but for the receiving pulse in an OFDM system. In this thesis we have exploited the combination of AIC and AST techniques to minimize the OOBE produced by an OFDM signal. However, if our goal is to narrow the guard band between adjacent channels, the out-of-band power captured by the receivers of the adjacent channel's users should be taken into account, since conventional OFDM receivers use rectangular pulses with slow-decaying sidelobes. This multiple access interference does not occur when the signals involved are orthogonal. However, there are multiple phenomena that destroys orthogonality: the Doppler effect, CFO, an insufficient cyclic prefix or the use of a different numerology (as in 5G). In that case, pulses similar to the generalized pulse can be designed and used in the receiver to minimize the interference power present in the received symbols.

Finally, the effect that the non-linearity of the power amplifier has on the spectral-shaped signal can be studied. This effect has traditionally been compensated for by applying pre-distortion to the signal. However, the models used for the amplifier are usually memoryless and overly simplistic, so it could be interesting to carry out a more detailed study.

Appendices

Appendix A

Proofs

A.1 Proof of the equivalence between the spectral shaping solutions in [8] and [9]

This section analytically proves that the methods by van de Beek [8] and by Zhou *et al.* [9] give the same PSD (as shown in Fig. 3.3), despite they yield different precoding matrices. This fact is shown in [9], but by means of simulations.

Following the notation defined in Section 2.4, let $\mathcal{K}$ be the set of active carriers and $\mathcal{D}$ the set of data carriers. The methods in [8] and [9] are aimed at nulling the Fourier transform of each transmitted OFDM symbol at a set of selected frequencies denoted by $\{f_0, f_1, \ldots, f_{M-1}\}$. The method in [9] sets $|\mathcal{K}| - M = |\mathcal{D}|$, i.e., it uses M redundant carriers, while no redundant carriers are used in [8], i.e., $\mathcal{K} = \mathcal{D}$.

Let us define the vector $\mathbf{a}(f) = \Big[a_{k_0}(f), a_{k_1}(f), \ldots, a_{k_{|\mathcal{K}|-1}}(f)\Big]^{\mathrm{T}}$, where $a_k(f)$ is the Fourier transform of the pulse $p_k(t)$, which is the continuous-time version of $p_k(n)$ given in expression (2.8) of Chapter 2.

The PSD of a continuous-time OFDM signal employing precoding can be obtained as [9]

$$P(f) = \frac{1}{T}\mathbf{a}^{\mathrm{T}}(f)\mathbf{G}\mathbf{G}^{\mathrm{H}}\mathbf{a}^{*}(f), \tag{A.1.1}$$

where $\mathbf{G}$ is the precoding matrix and T is the symbol period.

Let us define the matrix $\mathbf{A} = [\mathbf{a}(f_0), \mathbf{a}(f_1), \ldots, \mathbf{a}(f_{M-1})]^{\mathrm{T}}$, which is of size $M \times |\mathcal{K}|$, and whose SVD is $\mathbf{A} = \mathbf{U}\mathbf{\Sigma}\mathbf{V}^{\mathrm{H}}$, where $\mathbf{U}$ is a unitary matrix of size $M \times M$, $\mathbf{\Sigma}$ is a real matrix of size $M \times |\mathcal{K}|$ and $\mathbf{V} = \big[\mathbf{v}_1, \mathbf{v}_2, \ldots, \mathbf{v}_{|\mathcal{K}|}\big]$ is a unitary matrix of size $|\mathcal{K}| \times |\mathcal{K}|$. Denoting the zero matrix of size $M \times |\mathcal{D}|$ by $\mathbf{0}_{M\times|\mathcal{D}|}$, the matrix $\mathbf{\Sigma}$ can be expressed as $\mathbf{\Sigma} = \Big[\widetilde{\mathbf{\Sigma}}, \mathbf{0}_{M\times|\mathcal{D}|}\Big]$, with $\widetilde{\mathbf{\Sigma}} = \mathrm{diag}\Big([\lambda_1, \lambda_2, \ldots, \lambda_M]\Big)$.

The precoding matrix given in [9] is formed by the last $|\mathcal{K}| - M = |\mathcal{D}|$ right singular vectors of $\mathbf{A}$,

$$\mathbf{G}_{[9]} = \left[\mathbf{v}_{M+1}, \mathbf{v}_{M+2}, \ldots, \mathbf{v}_{|\mathcal{K}|}\right]. \tag{A.1.2}$$

Expressing $\mathbf{V} = \left[\mathbf{v}_1, \mathbf{v}_2, \ldots, \mathbf{v}_{|\mathcal{K}|}\right] = [\mathbf{V}_\alpha\ \mathbf{V}_\beta]$, with $\mathbf{V}_\alpha = [\mathbf{v}_1, \mathbf{v}_2, \ldots, \mathbf{v}_M]$ and $\mathbf{V}_\beta = \left[\mathbf{v}_{M+1}, \mathbf{v}_{M+2}, \ldots, \mathbf{v}_{|\mathcal{K}|}\right]$,

$$\mathbf{G}_{[9]}\mathbf{G}_{[9]}^{\mathrm{H}} = \mathbf{V}_\beta\mathbf{V}_\beta^{\mathrm{H}}. \tag{A.1.3}$$

The precoding matrix in [8] is

$$\mathbf{G}_{[8]} = \mathbf{I} - \mathbf{A}^{\mathrm{H}}(\mathbf{A}\mathbf{A}^{\mathrm{H}})^{-1}\mathbf{A}. \tag{A.1.4}$$

Since $\mathbf{G}_{[8]}$ is an idempotent and Hermitian matrix, $\mathbf{G}_{[8]}\mathbf{G}_{[8]}^{\mathrm{H}} = \mathbf{G}_{[8]}$. Now, substituting $\mathbf{A} = \mathbf{U}\mathbf{\Sigma}\mathbf{V}^{\mathrm{H}} = \mathbf{U}\left[\widetilde{\mathbf{\Sigma}}, \mathbf{0}_{M,|\mathcal{D}|}\right][\mathbf{V}_\alpha\mathbf{V}_\beta]^{\mathrm{H}}$ and after some algebra,

$$\mathbf{G}_{[8]} = \mathbf{I} - \mathbf{V}_\alpha\mathbf{V}_\alpha^{\mathrm{H}}. \tag{A.1.5}$$

However, since $\mathbf{V}$ is a unitary matrix,

$$\mathbf{V}\mathbf{V}^{\mathrm{H}} = [\mathbf{V}_\alpha\ \mathbf{V}_\beta]\,[\mathbf{V}_\alpha\ \mathbf{V}_\beta]^{\mathrm{H}} = \mathbf{V}_\alpha\mathbf{V}_\alpha^{\mathrm{H}} + \mathbf{V}_\beta\mathbf{V}_\beta^{\mathrm{H}} = \mathbf{I}. \tag{A.1.6}$$

Since $\mathbf{G}_{[8]}\mathbf{G}_{[8]}^{\mathrm{H}} = \mathbf{I} - \mathbf{V}_\alpha\mathbf{V}_\alpha^{\mathrm{H}} = \mathbf{V}_\beta\mathbf{V}_\beta^{\mathrm{H}} = \mathbf{G}_{[9]}\mathbf{G}_{[9]}^{\mathrm{H}}$, both methods give the same PSD. However, while $\mathbf{G}_{[9]}$ is unitary, the spectral decoder at the receiver will not cause noise enhancement. In contrast, $\mathbf{G}_{[8]}$ is not unitary and the BER will be degraded if inverted at the receiver.

A.2 Proof of the supergeneralized pulse as a unifying framework for spectral shaping

We here prove that the different spectral shaping techniques (pulse-shaping, AIC, spectral precoding and AST) can be obtained as particular cases of the supergeneralized pulse proposed in Sec. 2.5.2. The expression of the aforesaid pulse used by the k-th data carrier is reproduced here for convenience,

$$h_k(n) = p_k(n) + \sum_{i\in\mathcal{K};i\neq k} \alpha_{i,k}p_i(n) + t_k(n), \quad k \in \mathcal{D}. \tag{A.2.1}$$

Table 2.1 in Sec. 2.5.2 contains the expression to which the supergeneralized pulse particularizes to embody each of the spectral shaping techniques. For convenience, we address each of the them separately.

A.2.1 AIC techniques

The particularized expression of the pulse for this technique is

$$h_k(n) = p_k(n) + \sum_{i \in \mathcal{C}} \alpha_{i,k} p_i(n). \tag{A.2.2}$$

When it is used, the u-th OFDM symbol is expressed in matrix form as

$$\mathbf{x}_u = \mathbf{G}\boldsymbol{\Delta}_{N_{\mathrm{GI}},\beta}\Big(\mathbf{W}_N^{\mathcal{D}}\mathbf{s}_{\mathcal{D}}(u) + \mathbf{W}_N^{\mathcal{C}}\mathbf{A}_{\mathcal{D}\to\mathcal{C}}\mathbf{s}_{\mathcal{D}}(u)\Big), \tag{A.2.3}$$

which is very similar to the expression in (2.17), which represents the u-th OFDM symbol obtained with the conventional notation of AIC techniques and that is reproduced below for convenience,

$$\mathbf{x}_{u\,(2.17)} = \mathbf{G}\boldsymbol{\Delta}_{N_{\mathrm{GI}},\beta}\big(\mathbf{W}_N^{\mathcal{D}}\mathbf{s}_{\mathcal{D}}(u) + \mathbf{W}_N^{\mathcal{C}}\boldsymbol{\theta}_{\mathcal{C}}(u)\big). \tag{A.2.4}$$

It can be easily proved that the proposed formulation for the AIC terms generalize the one introduced in Sec. 2.4.2. The symbols that modulate the CC in (A.2.3) can be identified with their analogue in (A.2.4), yielding the following equality

$$\boldsymbol{\theta}_{\mathcal{C}}(u) = \mathbf{A}_{\mathcal{D}\to\mathcal{C}}\mathbf{s}_{\mathcal{D}}(u). \tag{A.2.5}$$

A.2.2 Spectral precoding

The particularized pulse for this technique is

$$h_k(n) = \sum_{i \in \mathcal{K}} \alpha_{i,k} p_i(n), \tag{A.2.6}$$

with $\alpha_{k,k} = 1$, $\forall k \in \mathcal{D}$. When it is used, the u-th OFDM symbol is expressed in matrix form as

$$\mathbf{x}_u = \mathbf{G}\boldsymbol{\Delta}_{N_{\mathrm{GI}},\beta}\mathbf{W}_N^{\mathcal{K}}\mathbf{A}_{\mathcal{D}\to\mathcal{K}}\mathbf{s}_{\mathcal{D}}(u), \tag{A.2.7}$$

which is identical to the one proposed in (2.20). Then, the matrix $\mathbf{A}_{\mathcal{D}\to\mathcal{K}}$, which is such that $[\mathbf{A}_{\mathcal{D}\to\mathcal{K}}]_{i,k} = \alpha_{i,k}$, is the precoding matrix.

A.2.3 AST techniques

The particularized pulse for this technique is

$$h_k(n) = p_k(n) + t_k(n). \tag{A.2.8}$$

When it is used, the u-th OFDM symbol is expressed as

$$x_u(n) = \sum_{k\in\mathcal{D}} p_k(n)s_k(u) + \underbrace{\sum_{k\in\mathcal{D}} t_k(n)s_k(u)}_{t_u(n)}, \tag{A.2.9}$$

which is similar to the expression of the u-th OFDM symbol when the conventional implementation of the AST term is used, which is

$$x_u(n) = \sum_{k\in\mathcal{D}} p_k(n)s_k(u) + a_u(n). \tag{A.2.10}$$

In this case, $a_u(n)$ cannot be directly identified with $t_u(n)$, because the former is nonzero for $n \in [u\cdot N_\mathrm{s}, u\cdot N_\mathrm{s}+\beta-1]$, while the latter is nonzero for $n \in [u\cdot N_\mathrm{s}, u\cdot N_\mathrm{s}+\beta-1]\cup[(u+1)\cdot N_\mathrm{s}, (u+1)\cdot N_\mathrm{s}+\beta-1]$. Nonetheless, the latter can divided into its starting and ending sections, denoted as $t_u^\mathrm{s}(n)$ and $t_u^\mathrm{e}(n)$, respectively. That is, $t_u^\mathrm{s}(n) = t_u(n)$ for $n \in [u\cdot N_\mathrm{s}, u\cdot N_\mathrm{s}+\beta-1]$, and $t_u^\mathrm{e}(n) = t_u(n)$ for $n \in [(u+1)\cdot N_\mathrm{s}, (u+1)\cdot N_\mathrm{s}+\beta-1]$, so $t_u(n) = t_u^\mathrm{s}(n) + t_u^\mathrm{e}(n)$. In that case, $a_u(n)$ can be identified with $t_{u-1}^\mathrm{e}(n) + t_u^\mathrm{s}(n)$. This idea is reinforced by the fact that, in the work [15], $a_u(n)$ is obtained taking into account the data transmitted in the $(u-1)$-th and u-th OFDM symbols, as the term that results from the superposition of $t_{u-1}^\mathrm{e}(n)$ and $t_u^\mathrm{s}(n)$ also depends on both OFDM symbols.

Hence, it is proved that the proposed formulation encompasses the one conventionally used.

A.3 Proof of the frequency transformations of the solutions with time-extended pulses

The proof of the equalities in (3.29) is provided. Let us first denote the energy emitted by the pulse in (3.27) in the closest notched band, $\mathcal{B}_n^+(k-i)$, as

$$\begin{aligned} E_k^{(i)} = \left(\mathbf{p}_k^{\text{t-e}} + \sum_{m=-M_\mathrm{a}}^{M_\mathrm{d}} \mathbf{C}_{k-i,m}^{+\,\text{t-e}}\boldsymbol{\alpha}_{k,m}^{(i)} + \sum_{m=-M_\mathrm{a}}^{M_\mathrm{d}+1} \mathbf{t}_{k,m}^{(i)}\right)^\mathrm{H} \boldsymbol{\Phi}_{\mathcal{B}_\mathrm{n}^+(k-i)}^{\text{t-e}} \\ \left(\mathbf{p}_k^{\text{t-e}} + \sum_{m=-M_\mathrm{a}}^{M_\mathrm{d}} \mathbf{C}_{k-i,m}^{+\,\text{t-e}}\boldsymbol{\alpha}_{k,m}^{(i)} + \sum_{m=-M_\mathrm{a}}^{M_\mathrm{d}+1} \mathbf{t}_{k,m}^{(i)}\right), \end{aligned} \tag{A.3.1}$$

where

$$\boldsymbol{\Phi}_{\mathcal{B}_\mathrm{n}^+(l)}^{\text{t-e}} = \int_{\mathcal{B}_\mathrm{n}^+(l)} \mathbf{f}_{\widetilde{L}}(f)\mathbf{f}_{\widetilde{L}}^\mathrm{H}(f)df = \int_{\frac{l}{N}-B_\mathrm{n}}^{\frac{l}{N}} \mathbf{f}_{\widetilde{L}}(f)\mathbf{f}_{\widetilde{L}}^\mathrm{H}(f)df, \tag{A.3.2}$$

where $\mathbf{f}_{\widetilde{L}}(f) = \left[e^{-j2\pi f(M_\mathrm{a}N_\mathrm{s})}, \ldots, e^{j2\pi f(M_\mathrm{d}N_\mathrm{s}+L-1)}\right]^\mathrm{T}$.

For the time-shifted pulse, the energy emitted in the corresponding notched band is

$$E_{k+\Delta k}^{(i)} = \left(\mathbf{p}_{k+\Delta k}^{\text{t-e}} + \sum_{m=-M_{\text{a}}}^{M_{\text{d}}} \mathbf{C}_{k+\Delta k-i,m}^{+\,\text{t-e}} \boldsymbol{\alpha}_{k+\Delta k,m}^{(i)} + \sum_{m=-M_{\text{a}}}^{M_{\text{d}}+1} \mathbf{t}_{k+\Delta k,m}^{(i)}\right)^{\text{H}} \boldsymbol{\Phi}_{\mathcal{B}_{\text{n}}^{+}(k+\Delta k-i)}^{\text{t-e}} \left(\mathbf{p}_{k+\Delta k}^{\text{t-e}} + \sum_{m=-M_{\text{a}}}^{M_{\text{d}}} \mathbf{C}_{k+\Delta k-i,m}^{+\,\text{t-e}} \boldsymbol{\alpha}_{k+\Delta k,m}^{(i)} + \sum_{m=-M_{\text{a}}}^{M_{\text{d}}+1} \mathbf{t}_{k+\Delta k,m}^{(i)}\right), \tag{A.3.3}$$

where it can be proved that

$$\begin{aligned} \mathbf{p}_{k+\Delta k}^{\text{t-e}} &= \boldsymbol{\Omega}_{\Delta k}^{\text{t-e}} \mathbf{p}_{k}^{\text{t-e}} \\ \mathbf{C}_{k+\Delta k-i}^{+\,\text{t-e}} &= \boldsymbol{\Omega}_{\Delta k}^{\text{t-e}} \mathbf{C}_{k-i}^{+\,\text{t-e}} \\ \boldsymbol{\Phi}_{\mathcal{B}_{\text{n}}^{+}(l+\Delta k)}^{\text{t-e}} &= \boldsymbol{\Omega}_{\Delta k}^{\text{t-e}} \boldsymbol{\Phi}_{\mathcal{B}_{\text{n}}^{+}(l)}^{\text{t-e}} (\boldsymbol{\Omega}_{\Delta k}^{\text{t-e}})^{\text{H}}, \end{aligned} \tag{A.3.4}$$

where it is recalled that $\boldsymbol{\Omega}_{\Delta k}^{\text{t-e}} = \text{diag}\left(\left[e^{-j\frac{2\pi}{N}\Delta k(M_{\text{a}}N_{\text{s}}+N_{\text{GI}})}, \ldots, e^{j\frac{2\pi}{N}\Delta k(M_{\text{d}}N_{\text{s}}+L-1-N_{\text{GI}})}\right]\right)$.

Then, expression (A.3.3) can be transformed into

$$E_{k+\Delta k}^{(i)} = \left(\mathbf{p}_{k}^{\text{t-e}} + \sum_{m=-M_{\text{a}}}^{M_{\text{d}}} \mathbf{C}_{k-i,m}^{+\,\text{t-e}} \boldsymbol{\alpha}_{k+\Delta k,m}^{(i)} + \sum_{m=-M_{\text{a}}}^{M_{\text{d}}+1} \left(\boldsymbol{\Omega}_{\Delta k}^{\text{t-e}}\right)^{\text{H}} \mathbf{t}_{k+\Delta k,m}^{(i)}\right)^{\text{H}} \boldsymbol{\Phi}_{\mathcal{B}_{\text{n}}^{+}(k-i)}^{\text{t-e}} \left(\mathbf{p}_{k}^{\text{t-e}} + \sum_{m=-M_{\text{a}}}^{M_{\text{d}}} \mathbf{C}_{k-i,m}^{+\,\text{t-e}} \boldsymbol{\alpha}_{k+\Delta k,m}^{(i)} + \sum_{m=-M_{\text{a}}}^{M_{\text{d}}+1} \left(\boldsymbol{\Omega}_{\Delta k}^{\text{t-e}}\right)^{\text{H}} \mathbf{t}_{k+\Delta k,m}^{(i)}\right). \tag{A.3.5}$$

Since the magnitude of (A.3.1) and (A.3.5) must be equal, the first row of relations in (3.29) are obtained,

$$\boldsymbol{\alpha}_{k+\Delta k,m}^{(i)} = \boldsymbol{\alpha}_{k,m}^{(i)}, \qquad \mathbf{t}_{k+\Delta k,m}^{(i)} = \boldsymbol{\Omega}_{\Delta k}^{\text{t-e}} \mathbf{t}_{k,m}^{(i)}. \tag{A.3.6}$$

For the second row of transformations, let use define a scenario with a single wide passband centered at the carrier index 0. It can be proved that the power emitted by both edges of the passband must be identical. Then, due to the properties of the Fourier transform, if $\mathbf{h}_{k}^{(i)\,\text{t-e}}$ is the optimal pulse for the k-th data carrier at the left edge of the passband, $\mathbf{h}_{N-k}^{(-i)\,\text{t-e}} = \left(\mathbf{h}_{k}^{(i)\,\text{t-e}}\right)^{*}$ is the optimal pulse for the $(N-k)$-th data carrier, located close to the right edge of the passband. Then, it is proved that

$$\boldsymbol{\alpha}_{k,m}^{(-i)} = \left(\boldsymbol{\alpha}_{k,m}^{(i)}\right)^{*}, \qquad \mathbf{t}_{k+\Delta k,m}^{(-i)} = \boldsymbol{\Omega}_{2k-N}^{\text{t-e}} \left(\mathbf{t}_{k,m}^{(i)}\right)^{*}. \tag{A.3.7}$$

Note that the proofs for these relations are an extension of those in [22] for the pulses without time-shifted terms.

Now, the proof of the first two equalities in (A.3.4) can be easily obtained by comparing the expressions of $p_{k+\Delta k}(n - mN_{\text{s}})$ and $p_{k}(n - mN_{\text{s}})$. For the last equality, let $\boldsymbol{\Phi}_{\mathcal{B}_{\text{n}}^{+}(l+\Delta k)}^{\text{t-e}}$ be

$$\boldsymbol{\Phi}_{\mathcal{B}_{\text{n}}^{+}(l+\Delta k)}^{\text{t-e}} = \int_{\mathcal{B}_{\text{n}}^{+}(l+\Delta k)} \mathbf{f}_{\widetilde{L}}(f) \mathbf{f}_{\widetilde{L}}^{\text{H}}(f) df = \int_{\frac{l+\Delta k}{N}-B_{\text{n}}}^{\frac{l+\Delta k}{N}} \mathbf{f}_{\widetilde{L}}(f) \mathbf{f}_{\widetilde{L}}^{\text{H}}(f) df, \tag{A.3.8}$$

where the change of integration variable $f^{'} = f - \frac{\Delta k}{N}$ yields

$$\mathbf{\Phi}^{\text{t-e}}_{\mathcal{B}^{+}_{\text{n}}(l+\Delta k)} = \int_{\frac{l}{N}-B_{\text{n}}}^{\frac{l}{N}} \mathbf{f}_{\widetilde{L}}(f^{'} + \frac{\Delta k}{N}) \mathbf{f}^{\text{H}}_{\widetilde{L}}(f^{'} + \frac{\Delta k}{N}) df^{'}. \tag{A.3.9}$$

Now,

$$\begin{aligned} \mathbf{f}_{\widetilde{L}}(f^{'} + \frac{\Delta k}{N}) &= \left[e^{-j2\pi(f^{'}+\frac{\Delta k}{N})(M_{\text{a}}N_{\text{s}})}, \ldots, e^{-j2\pi(f^{'}+\frac{\Delta k}{N})(M_{\text{d}}N_{\text{s}}+L-1)} \right]^{\text{T}} \\ &= e^{j2\pi\frac{\Delta k}{N}N_{\text{GI}}} \underbrace{\text{diag}\left(\left[e^{-j2\pi\frac{\Delta k}{N}(M_{\text{a}}N_{\text{s}}+N_{\text{GI}})}, \ldots, e^{j2\pi\frac{\Delta k}{N}(M_{\text{d}}N_{\text{s}}+L-1-N_{\text{GI}})} \right] \right)}_{\mathbf{\Omega}^{\text{t-e}}_{\Delta k}} \mathbf{f}_{\widetilde{L}}(f^{'}), \end{aligned} \tag{A.3.10}$$

which can be replaced in expression (A.3.9), yielding

$$\mathbf{\Phi}^{\text{t-e}}_{\mathcal{B}^{+}_{\text{n}}(l+\Delta k)} = \mathbf{\Omega}^{\text{t-e}}_{\Delta k} \int_{\frac{l}{N}-B_{\text{n}}}^{\frac{l}{N}} \mathbf{f}_{\widetilde{L}}(f^{'}) \mathbf{f}^{\text{H}}_{\widetilde{L}}(f^{'}) df^{'} \left(\mathbf{\Omega}^{\text{t-e}}_{\Delta k} \right)^{\text{H}} = \mathbf{\Omega}^{\text{t-e}}_{\Delta k} \mathbf{\Phi}^{\text{t-e}}_{\mathcal{B}^{+}_{\text{n}}(l)} \left(\mathbf{\Omega}^{\text{t-e}}_{\Delta k} \right)^{\text{H}}, \tag{A.3.11}$$

which equals the third equality in (A.3.4).

Appendix B

Publications

B.1 Publications

B.1.1 A modified pulse and design framework to halve the complexity of OFDM spectral shaping techniques

[21] J. Giménez, J. A. Cortés, F. Javier Cañete, E. Martos-Naya and L. Díez, "A Modified Pulse and Design Framework to Halve the Complexity of OFDM Spectral Shaping Techniques," in *IEEE Communications Letters*, vol. 28, no. 9, pp. 2146-2150, Sept. 2024, doi: 10.1109/LCOMM.2024.3432155.

Abstract Orthogonal frequency division multiplexing (OFDM) is a widespread modulation but suffers from high out-of-band emissions (OOBE). Spectral shaping strategies such as precoding, active interference cancellation (AIC) and time-domain methods are effective at reducing the OOBE but entail optimization procedures and real-time implementation costs which might be considerable. This letter proposes a modification of the conventional OFDM waveform aimed at reducing the cost associated to many of the state-of-the-art spectral shaping techniques and sets a framework for future works that want to benefit from the same reduction. This approach may reduce both the number of coefficients involved in the optimization and the number of products of its implementation by up to 50%.

B.1.2 Low-complexity spectral shaping method for OFDM signals with dynamic transmission band location

J. Giménez, J. A. Cortés, F. J. Cañete, E. Martos-Naya and L. Díez, "Low-complexity Spectral Shaping Method for OFDM Signals with Dynamic Transmission Band Location," *IEEE International Symposium on Power Line Communications and its Applications* (Presented in the *Recent Results* session), Oct. 2021.

Low-complexity spectral shaping method for OFDM signals with dynamic transmission band location

Javier Giménez, José A. Cortés, Francisco J. Cañete, Eduardo Martos-Naya, Luis Díez
Communications and Signal Processing Lab, Instituto Universitario de Investigación en Telecomunicación (TELMA)
Universidad de Málaga, CEI Andalucía TECH
ETSI Telecomunicación, Bulevar Louis Pasteur 35, 29010 Málaga (Spain).
email: {javierg, jaca, francis, eduardo, diez}@ic.uma.es

***Abstract*—Power line communications (PLC) systems that use orthogonal frequency division multiplexing (OFDM) modulation show low spectral confinement. The reduction of the out-of-band emissions (OOBE) required to comply with electromagnetic compatibility (EMC) regulations obliges to null a considerable number of data carriers, which penalizes the data rate. This work proposes a low-complexity spectral shaping method in which the location of the transmission band can be changed dynamically. The influence of some OFDM parameters on its performance is assessed.**

I. Introduction

Reducing the OOBE is of primary importance in in-home broadband PLC. In Europe, these systems are subject to the [1], which defines many permanent and dynamically excluded subbands. A considerable number of carriers have to be nulled at the edges of these subbands to comply with the power spectral density (PSD) limit, which lowers the data rate.

Several methods can be found in the literature to reduce the OOBE [2]. The active interference cancellation (AIC) and time-domain techniques are of particular interest because they can be applied transparently to the receiver [3] [4].

A spectral shaping method that unifies AIC and time-domain techniques is proposed in [5]. It defines a new pulse, referred to as generalized pulse, that can be designed off-line when the location of the transmission band is known in advance. This notably reduces the complexity with respect to previous proposals.

This work presents a low-complexity spectral shaping method for scenarios in which the transmission band changes dynamically. To this end, the solution of [5] for a generic transmission band is firstly obtained and then adapted to its actual location by means of simple transformations. It also examines the most appropriate location of the cancellation carriers (CC) for different guard intervals.

II. Background

The discrete-time lowpass-equivalent of an OFDM signal can be written as,

$$x(n) = \sum_{i=-\infty}^{\infty} x_i(n - iN_s), \tag{1}$$

where $N_s = N + N_{GI}$ is the symbol period, N represents the length of the OFDM symbol, N_{GI} is the number of samples in the guard interval. When the generalized pulses proposed in [5] are employed, the i-th OFDM symbol is given by

$$x_i(n) = \sum_{k\in\mathcal{D};k\notin\mathcal{D}^h} p_k(n)s_k(i) + \sum_{k\in\mathcal{D}^h} h_k(n)s_k(i), \tag{2}$$

where $p_k(n)$ is the pulse used by the data carriers that do not require OOBE suppression and $h_k(n)$ is the generalized pulse. $\mathcal{D}$ denotes the set of indexes of the data carriers and $\mathcal{D}^h$ the subset of data carriers using generalized pulses. The vector form of the generalized pulse used in the k-th carrier is written as

$$\boldsymbol{h}_k = \boldsymbol{p}_k + \boldsymbol{P}_{\mathcal{C}(k)}\boldsymbol{\alpha}_k + \boldsymbol{t}_k, \tag{3}$$

where the first term on the right hand side (RHS) is the vector form of the pulse $p_k(n)$, and the other two terms are used to cancel the OOBE of the first one. $\mathcal{C}(k)$ is the set of CC employed by the k-th data carrier, $\boldsymbol{P}_{\mathcal{C}(k)} = \left[\boldsymbol{p}_{c_1}, \cdots, \boldsymbol{p}_{c_{|\mathcal{C}(k)|}}\right]$ the pulses used by these carriers, $\boldsymbol{\alpha}_k$ the complex coefficients that weigh these pulses and $\boldsymbol{t}_k$ the transition pulses. Both $\boldsymbol{\alpha}_k$ and $\boldsymbol{t}_k$ are computed through an optimization procedure to minimize the energy emitted to the band $\mathcal{B}_n$ by the pulse $\boldsymbol{h}_k$. It can be analytically computed as

$$E_{k,\mathcal{B}_n} = \left(\boldsymbol{p}_k + \boldsymbol{P}_{\mathcal{C}(k)}\boldsymbol{\alpha}_k + \boldsymbol{t}_k\right)^H \boldsymbol{\Phi}_{\mathcal{B}_n} \left(\boldsymbol{p}_k + \boldsymbol{P}_{\mathcal{C}(k)}\boldsymbol{\alpha}_k + \boldsymbol{t}_k\right), \tag{4}$$

where $(\cdot)^H$ denotes the Hermitian operation, and

$$\boldsymbol{\Phi}_{\mathcal{B}_n} = \int_{\mathcal{B}_n} \boldsymbol{f}_L(f)\boldsymbol{f}_L^H(f)df \tag{5}$$

and $\boldsymbol{f}_L^H(f) = \left[1, e^{j2\pi f}, \ldots, e^{j2\pi f(L-1)}\right]$ performs the Fourier transform of the discrete-time signals.

III. Proposed method

A generalized pulse that has been optimized for a specific carrier can be easily adapted to be used by a different one, provided that the latter has the same position within the passband as the original data carrier.

Let $\boldsymbol{h}_k$ be a generalized pulse used by the k-th data carrier, designed to minimize OOBE in the band $\mathcal{B}_n = (f_s, f_e)$. Now, let $\boldsymbol{h}_{k+\Delta k}$ be the generalized pulse used by the $(k+\Delta k)$-th

data carrier, and designed to minimize the OOBE in the band $\widehat{\mathcal{B}}_n = (f_s + \Delta f, f_e + \Delta f)$, where $\Delta f = \frac{\Delta k}{N}$.

The energy emitted to the band $\widehat{\mathcal{B}}_n$ by the $\boldsymbol{h}_{k+\Delta k}$ pulse is computed like in (4). That is,

$$E_{k,\widehat{\mathcal{B}}_n} = \left(\boldsymbol{p}_{k+\Delta k} + \boldsymbol{P}_{\mathcal{C}(k+\Delta k)}\boldsymbol{\alpha}_{k+\Delta k} + \boldsymbol{t}_{k+\Delta k}\right)^H \boldsymbol{\Phi}_{\widehat{\mathcal{B}}_n} \left(\boldsymbol{p}_{k+\Delta k} + \boldsymbol{P}_{\mathcal{C}(k+\Delta k)}\boldsymbol{\alpha}_{k+\Delta k} + \boldsymbol{t}_{k+\Delta k}\right). \quad (6)$$

Expression (6) can be transformed into

$$E_{k,\widehat{\mathcal{B}}_n} = \left(\boldsymbol{p}_k + \boldsymbol{P}_{\mathcal{C}(k)}\boldsymbol{\alpha}_{k+\Delta k} + \boldsymbol{\Omega}_{\Delta k}^{-1}\boldsymbol{t}_{k+\Delta k}\right)^H \boldsymbol{\Omega}_{\Delta k}^H \boldsymbol{\Phi}_{\widehat{\mathcal{B}}_n} \boldsymbol{\Omega}_{\Delta k} \left(\boldsymbol{p}_k + \boldsymbol{P}_{\mathcal{C}(k)}\boldsymbol{\alpha}_{k+\Delta k} + \boldsymbol{\Omega}_{\Delta k}^{-1}\boldsymbol{t}_{k+\Delta k}\right), \quad (7)$$

provided that $\boldsymbol{\Omega}_{\Delta k} = diag\left\{1, e^{j\frac{2\pi}{N}\Delta k}, \ldots, e^{j\frac{2\pi}{N}\Delta k(L-1)}\right\}$ performs a displacement of Δk carriers when multiplied to $\boldsymbol{p}_k$, such that $\boldsymbol{p}_{k+\Delta k} = \boldsymbol{\Omega}_{\Delta k}\boldsymbol{p}_k$. It can be proved that $\boldsymbol{\Omega}_{\Delta k}^H \boldsymbol{\Phi}_{\widehat{\mathcal{B}}_n} \boldsymbol{\Omega}_{\Delta k} = \boldsymbol{\Phi}_{\mathcal{B}_n}$, and then terms in expression (7) can be identified with terms in expression (4). In the end, it results that to minimize the OOBE in band $\widehat{\mathcal{B}}_n$ the following coefficients can be used

$$\boldsymbol{\alpha}_{k+\Delta k} = \boldsymbol{\alpha}_k; \qquad \boldsymbol{t}_{k+\Delta k} = \boldsymbol{\Omega}_{\Delta k}\boldsymbol{t}_k \quad (8)$$

for the generalized pulse $\boldsymbol{h}_{k+\Delta k}$. These are transformations of the coefficients that had been computed for the original band, $\mathcal{B}_n$.

IV. Numerical results

The proposed spectral shaping method attains the same performance as the one in [5]. Hence, this section assesses the influence on the performance of some OFDM signal parameters that were not evaluated in [5]. To this end the maximum value of the normalized PSD in the band to be notched is used, denoted as PSD_{max}. The PSD can be analytically obtained from [5, Exp. (8)] by changing $\boldsymbol{p}_k$ to $\boldsymbol{h}_k$ where corresponds. The designed generalized pulses are applied to a passband with $N_D = 4$ data carriers (which is considered the worst-case scenario), besides the $N_{CC} = 2$ in-band CC at each end of the band.

A. Influence of the guard interval on the performance

Table I shows the PSD_{max} for several guard interval lengths, and for two different spectral shaping aproaches: one that only uses CC, denoted as AIC, and one that uses both CC and transtion pulses, denoted as AIC+tk. The PSD_{max} attained when no spectral shaping method is used is also shown. As seen, both AIC and AIC+tk methods generally achieve a notable OOBE reduction when compared to the case where no spectral shaping is performed. Results indicate that reducing the guard interval length increses the PSD in the notched band. However, the PSD does not grow monotonically as N_{GI} value decreases. When $N_{GI} = 512$ performance is worse than when $N_{GI} = 256$ for both methods, AIC and AIC+tk. The reason for this and a solution is given in the next subsection.

TABLE I: PSD_{max} obtained for different N_{GI} lengths in a $N_D = 4$ passband.

	AIC	AIC+tk	No shaping
$N_{GI} = 1024;\ \beta = 512$	-39.5	-48.0	-23.5
$N_{GI} = 512;\ \beta = 256$	-24.6	-28.8	-18.7
$N_{GI} = 256;\ \beta = 128$	-28.6	-31.6	-17.6
$N_{GI} = 128;\ \beta = 64$	-25.1	-25.6	-17.3

B. Influence of the CC position

In Table I the performance attained when $N_{GI} = 512$ was surprisingly low. This may be caused by how changing the spectrum of the cancellation elements affects its suitability for suppressing the OOBE. Consequently, changing the way CC are arranged relative to the notched band influences the performance of the spectral shaping method. Table II shows the gain attained when a data carrier is inserted between both in-band CC. Results show that this change in the CC configurations enhances the performance when $N_{GI} = 512$ and $\beta = 256$ by around 4 dB for both shaping methods, AIC and AIC+tk. It has to be emphasized that AIC+tk method has way more degrees of freedom than AIC method.

TABLE II: Gain, in terms of PSD_{max} reduction, obtained when a data carrier is inserted between the two in-band CC.

	Gain (dB)	
	AIC	AIC+tk
$N_{GI} = 512; \beta = 256$	3.8	4.3

V. Conclusion

This work has proposed a low-complexity spectral shaping method where the location of the transmission band can be dynamically changed. Also, the influence of guard interval and the position of the CC on its performance has been studied.

Acknowledgment

This work was supported in part by the Spanish Ministry of Ciencia e Innovación under Project PID2019-109842RB-I00.

References

[1] "Power line communication apparatus used in low-voltage installations - Radio disturbance characteristics - Limits and methods of measurement - Part 1: Apparatus for in-home use," European Standard, EN 50561-1, October 2013.

[2] Z. You and I.-T. Fang, J. Lu, "Out-of-band emission suppression techniques based on a generalized OFDM framework," *EURASIP Journal on Advances in Signal Processing*, vol. 2014:74, pp. 1–14, 2014.

[3] H. Mahmoud and H. Arslan, "Sidelobe suppression in OFDM-based spectrum sharing systems using adaptive symbol transition," *IEEE Communications Letters*, vol. 12, no. 2, pp. 133–135, 2008.

[4] J. F. Schmidt, S. Costas-Sanz, and R. López-Valcarce, "Choose Your Subcarriers Wisely: Active Interference Cancellation for Cognitive OFDM," *IEEE Jour. on Emerg. and Sel. Topics in Circuits and Syst.*, vol. 3, no. 4, pp. 615–625, Dec. 2013.

[5] L. Díez, J. A. Cortés, F. J. Cañete, E. Martos Naya, and S. Iranzo, "A generalized spectral shaping method for OFDM signals," *IEEE Trans. on Comm.*, 2019.

B.1.3 Low-complexity spectral shaping method for OFDM signals with dynamically adaptive emission mask

[22] J. Giménez, J. A. Cortés and L. Díez, "Low-Complexity Spectral Shaping Method for OFDM Signals With Dynamically Adaptive Emission Mask," in *IEEE Transactions on Communications*, vol. 71, no. 4, pp. 2351-2363, April 2023, doi: 10.1109/TCOMM.2023.3244937.

Abstract Orthogonal frequency division multiplexing (OFDM) signals with rectangular pulses exhibit low spectral confinement. Shaping their power spectral density (PSD) is imperative in the increasingly overcrowded spectrum to benefit from the cognitive radio (CR) paradigm. However, since the available spectrum is non-contiguous and its occupancy changes with time, the spectral shaping solution has to be dynamically adapted. This work proposes a framework that allows using a reduced set of preoptimized pulses to shape the spectrum of OFDM signals, irrespective of its spectral width and location, by means of simple transformations. The employed pulses combine active interference cancellation (AIC) and adaptive symbol transition (AST) terms in a transparent way to the receiver. They can be easily adapted online by the communication device to changes in the location or width of the transmission band, which contrasts with existing methods of the same type that require solving NP-hard optimization problems.

B.1.4 A low complexity spectral shaping method for OFDM signals with dynamically defined emission mask: optimization procedure

J. Giménez, J. A. Cortés and L. Díez, "A Low-Complexity Spectral Shaping Method for OFDM Signals with Dynamically Defined Emission Mask: Optimization Procedure," *14th Workshop for Power Line Communications*, Sept. 2023.

A Low-Complexity Spectral Shaping Method for OFDM Signals with Dynamically Defined Emission Mask: Optimization Procedure

Javier Giménez, José A. Cortés and Luis Díez
Communications and Signal Processing Lab, Telecommunication Research Institute (TELMA)
Universidad de Málaga
E.T.S.I. Telecomunicación, Bulevar Louis Pasteur 35, 29010 Málaga (Spain).
email: {javierg, jaca, diez}@ic.uma.es

***Abstract*—The low spectral confinement of orthogonal frequency division multiplexing (OFDM) signals obliges OFDM-based power line communications (PLC) systems to use out-of-band emissions (OOBE) reduction methods in order to comply with electromagnetic compatibility (EMC) regulations. This work proposes a computationally simple optimization procedure that yields a versatile set of solutions to shape the spectrum of OFDM signals regardless of the location and width of its passbands.**

I. Introduction

In-home broadband power line communications (PLC) systems in Europe have to comply with the EN 50561-1 [1], which defines multiple permanent and dynamically excluded subbands. Most PLC systems employ orthogonal frequency division multiplexing (OFDM) and need to null a significant number of data carriers by the edges of these subbands to comply with [1], which penalizes the data rate.

Among the pleiad of methods that have been proposed to reduce the out-of-band emissions (OOBE) of OFDM signals, pulse-shaping, active interference cancellation (AIC) and adaptive symbol transition (AST) are of particular interest as they do not require modifying the receiver's operation [2] [3].

In [4] the aforesaid techniques were combined yielding a pulse, referred to as generalized pulse, that is designed offline and that yields larger OOBE reductions than other methods of the same kind. The work in [5] proposed a modified version of the generalized pulses and an optimization strategy that allows computing a solution that can be adapted online, by means of computationally simple transformations, to comply with dynamic changes in the emission mask.

This work uses the modified version of the generalized pulses and the transformations in [5] and proposes an alternative optimization method for the calculation of its coefficients.

II. Background

The discrete-time low-pass expression of an OFDM signal can be expressed as

$$x(n) = \sum_{u=-\infty}^{\infty} \sum_{k \in \mathcal{D}} p_k(n - uN_\mathrm{s}) s_k(u) \qquad (1)$$

where $s_k(u)$ is the data symbol and $N_\mathrm{s} = N + N_\mathrm{GI}$ is the OFDM symbol period, being N the size of the discrete Fourier transform (DFT) and N_GI the number of samples in the guard interval. Using matrix notation, the basic pulse can be expressed as $\mathbf{p}_k = [p_k(0), \ldots, \ p_k(L-1)]^\mathrm{T}$, where $L = N_\mathrm{s} + \beta$, with β being the number of tapered samples at the beginning and at the end of $p_k(n)$.

To reduce the OOBE of (1), the basic pulse is replaced with the modified generalized pulse proposed in [5] in those data carriers located by the borders of the passbands. The indices of these data carriers are in the set $\mathcal{D}^\mathrm{h} \subset \mathcal{D}$. The expression of the modified generalized pulse is,

$$\mathbf{h}_k^{(i,j)} = \mathbf{p}_k + \underbrace{\mathbf{C}_{k-i}^{+}\boldsymbol{\alpha}_k^{(i)} + \mathbf{t}_k^{(i)}}_{\mathbf{r}_k^{(i)}} + \underbrace{\mathbf{C}_{k-j}^{-}\boldsymbol{\alpha}_k^{(j)} + \mathbf{t}_k^{(j)}}_{\mathbf{r}_k^{(j)}}, \begin{array}{l} i > 0, \\ j < 0 \end{array} \qquad (2)$$

where the superindex $i > 0$ denotes that carrier k is the i-th one above the left edge (located at $k-i$) of the passband and $j < 0$ that it is the j-th one below the right edge (located at $k-j$). The matrix $\mathbf{C}_l^{+} = [\mathbf{p}_{l-N_\mathrm{co}}, \ldots, \mathbf{p}_l, \ldots, \mathbf{p}_{l+N_\mathrm{ci}}]$ is an $L \times N_\mathrm{CC}$ matrix comprising the set of cancellation carriers (CC) placed around the left edge of the passband. The matrix $\mathbf{C}_l^{-}$ is the conterpart of $\mathbf{C}_l^{+}$ for the right edge of the passband. The AST terms $\mathbf{t}_k^{(i)}$ and $\mathbf{t}_k^{(j)}$, referred to as transition pulses, are vectors of L samples used to shape the initial and final time-domain samples of the pulse.

The values of the $N_\mathrm{CC} \times 1$ vectors $\boldsymbol{\alpha}_k^{(i)}$ and $\boldsymbol{\alpha}_k^{(j)}$ and of $\mathbf{t}_k^{(i)}$ and $\mathbf{t}_k^{(j)}$ are optimized to minimize the OOBE of the compound pulse. The optimization is accomplished offline to lower the OOBE in a predefined subband and can be adapted online to changes in the emission mask by means of the simple transformations in [5, Expr. (22) and (24)].

III. Proposed optimization

This section proposes an optimization procedure of the terms in (2), alternative to the one in [5]. The coefficients of the OOBE reduction terms $\mathbf{r}_k^{(i)}$ and $\mathbf{r}_k^{(j)}$ are independently optimized. Moreover, since the coefficients of both terms are related through [5, Expr. (22) and (24)], only one optimization process has to be performed. In the following, only the steps corresponding to the optimization of $\mathbf{r}_k^{(i)}$ are described.

Let us consider an OFDM signal with carriers indexed from $k \in \{-\frac{N}{2}, \ldots, \frac{N}{2}-1\}$. The number of active carriers is N_{D}, starting at index $k=1$. The OOBE is to be lowered in the two notched bands defined as *contiguous notched band*, denoted by $\mathcal{B}_{\mathrm{c}} = \left\{-\frac{N}{2}, \ldots, 0\right\}$, and *opposite notched band*, denoted by $\mathcal{B}_{\mathrm{o}} = \left\{N_{\mathrm{D}}+1, \ldots, \frac{N}{2}-1\right\}$. To this end, N_{h} consecutive carriers use the modified generalized pulse by each edge of the passband.

The proposed procedure starts by considering a passband with a minimum bandwidth of $N_{\mathrm{D\_min}}$ carriers and by determining the optimum coefficients of $\boldsymbol{\alpha}_k^{(i)}$ and $\mathbf{t}_k^{(i)}$ that minimize the OOBE of $\mathbf{p}_k + \mathbf{r}_k^{(i)}$ in $\mathcal{B}_{\mathrm{c}}$ and the one of $\mathbf{r}_k^{(i)}$ in $\mathcal{B}_{\mathrm{o}}$,

$$\begin{bmatrix} \widehat{\boldsymbol{\alpha}}_k^{(i)} \\ \widehat{\mathbf{t}}_k^{(i)} \end{bmatrix} = \arg \min_{\boldsymbol{\alpha}_k^{(i)}, \mathbf{t}_k^{(i)}} \left\{ (1-a) E_{k,\mathcal{B}_{\mathrm{c}}}^{(i)} + a E_{k,\mathcal{B}_{\mathrm{o}}}^{(i)} \right\}, \quad (3)$$

where a has to be tuned to attain the best performance, and

$$E_{k,\mathcal{B}_{\mathrm{c}}}^{(i)} = \int_{\mathcal{B}_{\mathrm{c}}} \left| P_k(f) + R_k^{(i)} \right|^2 df, \quad E_{k,\mathcal{B}_{\mathrm{o}}}^{(i)} = \int_{\mathcal{B}_{\mathrm{o}}} \left| R_k^{(i)}(f) \right|^2 df. \quad (4)$$

Hence, $\mathbf{r}_k^{(i)}$ is designed to reduce the OOBE of the basic pulse in $\mathcal{B}_{\mathrm{c}}$ while generating no additional emissions in $\mathcal{B}_{\mathrm{o}}$. Provided that there are N_{ci} CC inside the passband (in-band CC) by each end on the passband, $N_{\mathrm{h\_min}} = N_{\mathrm{D\_min}} - 2N_{\mathrm{ci}}$ modified generalized pulses are optimized in the first step and the resulting coefficients are stored. Then, the passband width is increased in one carrier (to the right) and the minimization in (3) is performed for the new data carrier. The process continues until the rightmost data carrier in the passband would yield an OOBE below the required level when using the basic pulse.

Finally, the coefficients $\boldsymbol{\alpha}_k^{(j)}$ and $\mathbf{t}_k^{(j)}$, $j<0$, are obtained from $\boldsymbol{\alpha}_k^{(i)}$ and $\mathbf{t}_k^{(i)}$, $i>0$, by means of [5, Expr. (24)].

IV. Numerical Results

In this section the influence of the parameter $N_{\mathrm{D\_min}}$ on this performance is evaluated. To that end, the optimization is performed with the parameters $N_{\mathrm{D\_min}} \in \{5, \ldots, 9\}$ and $N_{\mathrm{h\_max}} = 9$. An OFDM signal with $N = 4096$, $N_{\mathrm{GI}} = 1024$ and $\beta = 512$ is considered. The obtained coefficients are applied to two different scenarios: one consisting in a passband of width $N_{\mathrm{D\_min}}$ carriers (i.e., the narrowest one used in the optimization process) and a wider one of $N_{\mathrm{D}} = 13$ carriers. Two versions of the generalized pulse are also compared: one that only uses AIC tones and another that combines AIC and AST techniques. Three CC are used by each end of the passband: 2 inside the passband (in-band) and 1 in the notched band (out-of-band).

Fig. 1 shows the maximum value of the normalized power spectral density (PSD) attained by the proposed method in the aforementioned cases. First of all, it is clear that the combination of CC and transition pulses performs notably better than the CC alone, showing a difference that fluctuates between 6 and 12 dB.

Increasing the value of $N_{\mathrm{D\_min}}$ entails an enhancement in the obtained $\mathrm{PSD}_{\mathrm{max}}$. However, this reduces the range of passband widths where the computed pulses perform as expected, since using the pulses optimized for a range of passband widths starting at $N_{\mathrm{D\_min}}$ in narrower passbands yields larger values of $\mathrm{PSD}_{\mathrm{max}}$. Nonetheless, the solutions computed for $N_{\mathrm{D\_min}} = 7$ attain values of $\mathrm{PSD}_{\mathrm{max}}$ under -45 dB when applied to the same size of passband, which is lower than the limit of -43 dB specified for in-home broadband PLC systems in [1].

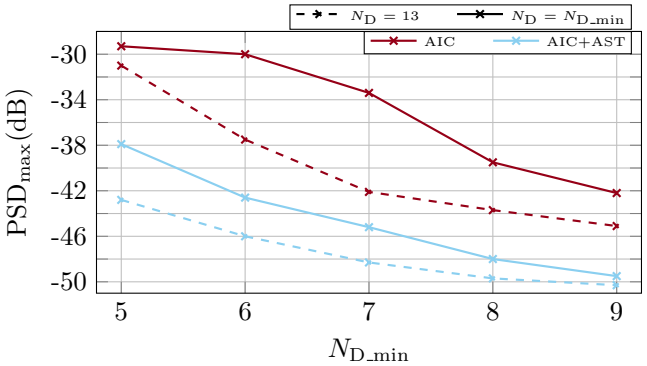

Fig. 1. $\mathrm{PSD}_{\mathrm{max}}$ in the notched band attained with the pulses in (2) when optimized with $N_{\mathrm{D\_min}} \in \{5, \ldots, 9\}$ and $N_{\mathrm{h\_max}} = 9$. Two passband widths are considered: $N_{\mathrm{D}} = N_{\mathrm{D\_min}}$ and a wider one with $N_{\mathrm{D}} = 13$. Two types of modified generalized pulses are considered: one which only employs AIC and another which also includes the AST terms.

The proposed optimization method is considerably simpler than the one in [5] at the expense of a more limited performance in specially stringent situations. Nevertheless, for many applications the OOBE reduction attained by the proposed strategy is enough.

V. Conclusion

This work has proposed a spectral shaping method for OFDM signals that is transparent for the receiver and that can be dynamically adapted to changes in the emission mask. It is grounded in the pulses proposed in [5], for which an alternative optimization procedure has been proposed.

Acknowledgment

This work is funded in part by the Spanish Government under FPU grant FPU20/03782 and project PID2019-109842RB-I00/AEI/10.13039/501100011033, by the European Fund for Regional Development (FEDER), Junta de Andalucía and the Universidad de Málaga under projects P18-TP-3587 and UMA20-FEDERJA-002.

References

[1] "Power Line Communication Apparatus Used in Low-Voltage Installations - Radio Disturbance Characteristics - Limits and Methods of Measurement - Part 1: Apparatus for in-Home Use," European Standard, EN 50561-1, Oct. 2013.

[2] K. Hussain and R. López-Valcarce, "Joint precoder and window design for OFDM sidelobe suppression," *IEEE Commun. Lett.*, vol. 26, no. 12, pp. 3044–3048, Dec. 2022.

[3] H. Mahmoud and H. Arslan, "Sidelobe suppression in OFDM-based spectrum sharing systems using adaptive symbol transition," *IEEE Commun. Lett.*, vol. 12, no. 2, pp. 133–135, 2008.

[4] L. Díez, J. A. Cortés, F. J. Cañete, E. Martos-Naya, and S. Iranzo, "A generalized spectral shaping method for OFDM signals," *IEEE Trans. Commun.*, vol. 67, no. 5, pp. 3540–3551, 2019.

[5] J. Giménez, J. A. Cortés, and L. Díez, "Low-complexity spectral shaping method for OFDM signals with dynamically adaptive emission mask," *IEEE Trans. Commun.*, vol. 71, no. 4, pp. 2351–2363, 2023.

B.1.5 Spectral shaping method for OFDM combining time-shifted active interference cancellation and adaptive symbol transition

[23] J. Giménez, J. A. Cortés, E. Martos-Naya and L. Díez, "Spectral Shaping Method for OFDM Combining Time-Shifted Active Interference Cancellation and Adaptive Symbol Transition," in *IEEE Open Journal of the Communications Society*, vol. 6, pp. 4476-4490, 2025, doi: 10.1109/OJCOMS.2025.3571196.

Abstract Out-of-band emission (OOBE) is a major concern in orthogonal frequency division multiplexing (OFDM) based systems, as it requires large guard bands to avoid interfering other channels or systems. Spectral shaping techniques combining active interference cancellation (AIC) and adaptive symbol transition (AST) strategies, herein shortened as C-AIC-AST, are effective to reduce it at the cost of a data rate penalty and a modest implementation complexity compared to precoding and filtering techniques. This paper presents a spectral shaping method that innovates previous C-AIC-AST proposals by expanding both the AIC and AST terms to preceding and subsequent OFDM symbols. The time-expanded terms are orthogonal to the current symbol, which makes them transparent to the receiver. The additional degrees of freedom given by these supplementary OOBE reduction terms can be exploited in different ways. In pulse-shaped OFDM systems, it allows attaining the same OOBE level than existing C-AIC-AST techniques but avoiding the data rate loss of the latter. In systems with rectangular OFDM signals, it can notably reduce the OOBE with a much smaller reduction in the effective cyclic prefix length compared to currently employed methods. The efficiency of the proposed method in achieving both goals with reduced implementation cost is demonstrated through results obtained in actual wired and wireless systems.

Apéndice C

Summary (Spanish)

De acuerdo con el Artículo 54 del Reglamento 4/2022 de la Universidad de Málaga, si la memoria de tesis se redacta al completo en inglés ha de incluir un resumen en español de las contribuciones principales de la misma. En este resumen, se presenta en primer lugar una introducción al tema de estudio, junto con las motivaciones de la tesis así como sus objetivos principales. A continuación, se resumen los resultados principales, junto a la discusión de los mismos. Finalmente, se incluyen las conclusiones más relevantes y líneas futuras.

C.1 Introducción

OFDM (orthogonal frequency division multiplexing) es una modulación ampliamente utilizada en sistemas de comunicaciones tanto inalámbricos como cableados. Entre sus ventajas están su robustez frente a canales selectivos en frecuencia, la simplicidad de los transmisores y receptores, la capacidad de realizar agregación de espectros (combinar múltiples bandas de frecuencia para mejorar el ancho de banda) y la facilidad para implementar técnicas MIMO (multiple-input multiple-output) [1]. Sin embargo, las señales OFDM convencionales tienen bajo confinamiento espectral, principalmente debido al uso de pulsos de transmisión rectangulares, cuyos espectros presentan lóbulos laterales de magnitud nada despreciable que se extienden a bandas adyacentes. Para mitigar esto último, tradicionalmente se han utilizado bandas de guarda, que son bandas en las que se deja de transmitir para evitar interferir con bandas vecinas. Sin embargo, esto último supone un uso ineficiente del espectro, puesto que se anula un gran número de potenciales portadoras de datos. Este problema tiene una especial relevancia en los sistemas de comunicaciones móviles, como LTE (long-term evolution) y 5G (fifth generation) NR (new radio), donde las bandas de guarda llegan a ocupar hasta un 10 % del ancho del canal. Siendo los recursos espectrales cada vez más escasos, es primordial aplicar técnicas que nos permitan resolver estas ineficiencias [2].

En la literatura se pueden encontrar un amplio abanico de técnicas para mejorar el confinamiento espectral de las señales OFDM [7]. Típicamente se clasifican según el dominio en el que se aplican: el de la frecuencia, o el del tiempo. En el primer grupo encontramos el precoding espectral y las técnicas AIC (active interference cancellation). En ambas técnicas se utilizan portadoras de datos para transmitir símbolos auxiliares con el objetivo de minimizar las emisiones fuera de banda (OOBE, out-of-band emission) de la señal. Esto provoca una penalización en la tasa de datos y un incremento de la complejidad del transmisor [8] [13]. Además, en el precoding espectral es frecuente que deban realizarse cambios también en el receptor, mientras que las técnicas AIC se pueden aplicar de forma transparente [42] [16]. En cualquier caso, ambas técnicas permiten obtener soluciones que son independientes de los datos transmitidos, por lo que se pueden obtener offline [34].

Entre las técnicas que se aplican en el dominio del tiempo, destacan el filtrado y el conformado de pulsos. La primera consiste en pasar la señal por un filtro antes de ser transmitida, a fin de reducir sus emisiones fuera de banda [17] [18]. Sin embargo, estas técnicas suelen presentar un elevado coste computacional, además de que distorsionan la señal, afectando la BER (bit error rate) [19]. En cuanto al conformado de pulso, consiste en modificar la forma del símbolo transmitido para mejorar su confinamiento espectral. Esto se puede hacer de varias formas: modificando los bordes el pulso de transmisión que emplean las portadoras, técnica conocida también como enventanado o WOLA-OFDM (weighted overlap and add based OFDM); o diseñando dichos bordes mediante un procedimiento de optimización [11]. También se puede hacer a través de un término aditivo que modifica los bordes del símbolo OFDM, término que se obtiene como una combinación lineal de los datos transmitidos. Esta técnica se conoce como AST (adaptive symbol transition) y hay varias formas de implementarlo [15] [16]. Una desventaja que tienen las técnicas de conformado de pulso es que acortan la duración efectiva del prefijo cíclico. Como ventaja, son técnicas que se pueden aplicar de forma transparente al receptor convencional de OFDM y existen implementaciones que no dependen de los datos [16].

Las técnicas AIC y AST tienen un gran interés por sus características: no complican el sistema, ya que son transparentes al receptor y requieren pocos cambios en el transmisor, y sus soluciones pueden ser independientes de los datos. Por eso muchos autores se han interesado en ellas [11] [16]. Si embargo, usar estas técnicas normalmente entraña dos problema: el régimen binario se ve penalizado por el uso de portadoras de datos como portadoras de cancelación (CC, cancellation carriers), y la duración efectiva del prefijo cíclico se ve acortada por culpa de las técnicas AST. Además, cualquiera de estas técnicas requiere recalcular las soluciones cuando la máscara de emisiones cambia. En ese sentido, esta tesis persigue un triple objetivo:

- Proponer una estrategia para reducir el coste computacional de las técnicas de conformación espectral.

- Proporcionar un esquema de diseño de soluciones que puedan ser recalculadas de forma sencilla cuando se producen cambios en la máscara de emisiones.
- Proponer una estrategia para mitigar la penalización de la tasa de datos de las técnicas AIC sin afectar negativamente a sus prestaciones.

C.2 Contextualización

En esta sección se establecen las bases sobre las cuales se construirán los desarrollos de los siguientes apartados.

C.2.1 Señales OFDM y conformación espectral

Una señal OFDM se compone de una sucesión de símbolos que se transmiten con periodicidad $N_\mathrm{s} = N + N_\mathrm{GI}$, donde N es el tamaño de la DFT (discrete Fourier transform) usada para generar los símbolos, y N_GI es el número de muestras que conforman la extensión cíclica del símbolo OFDM. Sea la expresión del equivalente paso bajo del símbolo u-ésimo en tiempo discreto para una señal OFDM convencional

$$x_u(n) = \sum_{k \in \mathcal{D}} p_k(n) s_k(u), \tag{C.2.1}$$

donde $\mathcal{D}$ es el conjunto de índices de las portadoras que se usan para transmitir datos, $p_k(n) = g(n) e^{j\frac{2\pi}{N}k(n-N_\mathrm{GI})}$ es el pulso usado en transmisión por la portadora k-ésima y $s_k(u)$ es el símbolo complejo que modula a éste último. Notar que $g(n)$ es un pulso conformador no nulo solo en $n \in [0, L-1]$ que limita la duración del pulso a $L = N_\mathrm{s} + \beta$ muestras. Las β muestras de ambos extremos del pulso conformador decaen de forma suave de 1 a 0 (por ejemplo, como un coseno alzado).

Debido al bajo confinamiento espectral que tienen estas señales, se han diseñado numerosas técnicas para conformar su espectro. En [16] se propone un pulso, llamado *pulso generalizado*, que contiene términos que se emplean para minimizar sus propias emisiones fuera de banda. De ese modo, será posible minimizar las emisiones producidas por la señal OFDM si para cada una de las portadoras que vayan a hacer uso del pulso se hace un diseño adecuado de sus términos de cancelación. Dicho pulso tiene la forma

$$h_k(n) = p_k(n) + \sum_{i \in \mathcal{C}} \alpha_{i,k} p_i(n) + t_k(n), \tag{C.2.2}$$

donde los dos términos que siguen a $p_k(n)$ en el miembro de la derecha reciben el nombre de *términos de cancelación* y se usan para minimizar las emisiones fuera de banda. El primero de los términos es el de *portadoras de cancelación* (CC en inglés), también conocido como término AIC. Este último consta de un conjunto de portadoras, $\mathcal{C}$, distinto del conjunto de

portadoras de datos, que se modulan con unos símbolos diseñados con el objetivo cancelar las emisiones fuera de banda de la señal. Los símbolos que cargan estas CC son el resultado de una combinación lineal de los símbolos de datos, que son pesados con los coeficientes $\alpha_{i,k}$ correspondientes. El otro término, $t_k(n)$, es el término AST, conocido también como *pulso de transición*. Es un término aditivo que modifica las β muestras a cada extremo del pulso, por lo que es no nulo solo para $n \in [0, \beta-1] \cup [L-\beta, L-1]$. Existe una implementación sencilla para el pulso de transición, a la que nos referimos como *desarrollo armónico* del pulso de transición, en la que éste se expresa como combinación lineal de exponenciales complejas (obtenidas mediante la DFT) [16].

Entonces, este pulso generalizado reemplaza a $p_k(n)$ en la expresión del símbolo OFDM (C.2.1) para minimizar las emisiones fuera de banda de la señal. Por comodidad, expresamos estos términos en forma matricial,

$$\mathbf{h}_k = [h_k(0), \ldots, h_k(L-1)]^{\mathrm{T}} = \mathbf{p}_k + \mathbf{P}_{\mathcal{C}}\boldsymbol{\alpha}_k + \mathbf{t}_k, \tag{C.2.3}$$

donde $\mathbf{p}_k = [p_k(0), \ldots, p_k(L-1)]^{\mathrm{T}}$, $\mathbf{P}_{\mathcal{C}} = \left[\mathbf{p}_{c_0}, \ldots, \mathbf{p}_{c_{|\mathcal{C}|-1}}\right]$, $\boldsymbol{\alpha}_k = \left[\alpha_{c_0,k}, \ldots, \alpha_{c_{|\mathcal{C}|-1},k}\right]^{\mathrm{T}}$ y $\mathbf{t}_k = [t_k(0), \ldots, t_k(L-1)]^{\mathrm{T}}$.

En [16] se demostró que no es necesario que todas las portadoras da datos hagan uso del pulso generalizado, pues solo las más próximas a los bordes de las bandas de paso contribuyen de manera importante a las emisiones en las bandas prohibidas. Es por eso que solo estas portadoras usan el pulso generalizado. Se define entonces $\mathcal{D}^{\mathrm{h}}$ como el subconjunto de portadoras de datos ($\mathcal{D}^{\mathrm{h}} \subseteq \mathcal{D}$) que usan este pulso.

C.3 Reducción del coste computacional usando nuevo pulso con simetría y un marco de diseño

En esta sección se resume la primera de las contribuciones de la tesis: la propuesta de un nuevo pulso que, por sus cualidades, permite reducir el coste computacional de un conjunto de técnicas de conformación espectral ampliamente usadas en señales OFDM. Las mencionadas técnicas son AIC, AST y precoding espectral. Para facilitar la generalidad de esta propuesta se propone unificar estas técnicas bajo una misma forma de pulso, que es

$$h_k(n) = p_k(n) + \sum_{i \in \mathcal{K}; i \neq k} \alpha_{i,k} p_i(n) + t_k(n), \quad k \in \mathcal{D}, \tag{C.3.1}$$

donde $\mathcal{K}$ es el conjunto de los índices de todas las portadoras activas del sistema. Este pulso, que llamamos *pulso supergeneralizado*, se puede particularizar en cada una de las mencionadas técnicas de conformación espectral (AIC, AST y precoding espectral) mediante la combinación u omisión de determinados términos:

- Precoding espectral: Omitiendo $t_k(n)$ y agrupando los términos del miembro derecho de la igualdad, notando que $\alpha_{k,k}$ es típicamente igual a 1.
- AIC: Omitiendo $t_k(n)$ y limitando el sumatorio de pulsos al conjunto de portadoras de cancelación, $\mathcal{C}$.
- AST: Se omite el segundo término del miembro de la derecha, siendo $t_k(n)$ el término del pulso de transición, que modifica los extremos del pulso.

La estrategia de reducción del coste computacional de estas técnicas consiste en sustituir el pulso $p_k(n)$ por una versión del mismo que tiene simetría Hermítica[1]. El pulso en cuestión es

$$\widetilde{p}_k(n) = g(n+\eta)e^{j2\pi kn}, \quad \forall k \in \mathcal{D}, \tag{C.3.2}$$

donde $\eta = (L-1)/2$. Notar que para que este pulso tenga simetría Hermítica es necesario que L sea impar. De ese modo, el pulso es distinto de 0 para $n \in [-(L-1)/2, (L-1)/2]$.

Cuando todas las portadoras activas en el transmisor utilizan este pulso, el pulso supergeneralizado de (C.3.1) toma la siguiente forma

$$\widetilde{h}_k(n) = \widetilde{p}_k(n) + \sum_{i\in\mathcal{K};i\neq k} \widetilde{\alpha}_{i,k}\widetilde{p}_i(n) + \widetilde{t}_k(n), \tag{C.3.3}$$

donde $\widetilde{\alpha}_{i,k}$ y $\widetilde{t}_k(n)$ son los coeficientes que deben ser obtenidos mediante optimización para minimizar la OOBE de la señal. Para tal fin, se propone utilizar un modelo de problema de optimización como el siguiente

$$\begin{aligned} &\widehat{\widetilde{\mathbf{H}}}_{\mathcal{D}} = \arg\min_{\widetilde{\mathbf{H}}_{\mathcal{D}}} \left\{ \sum_{k\in\mathcal{D}} \sigma_k^2 \int_{-1/2}^{1/2} M(f) \left|\widetilde{H}_k(f)\right|^2 df \right\} \\ &\text{sujeto a} \\ &\quad \sum_{k\in\mathcal{D}} \sigma_k^2 \int_{-1/2}^{1/2} M_j(f) \left|\widetilde{H}_k(f)\right|^2 df \leq \delta_j, \quad 1 \leq j \leq R, \end{aligned} \tag{C.3.4}$$

donde $\widetilde{\mathbf{H}}_{\mathcal{D}} = \left[\widetilde{\mathbf{h}}_{d_0}, \ldots, \widetilde{\mathbf{h}}_{d_{|\mathcal{D}|-1}}\right]$, y $\widetilde{\mathbf{h}}_{d_i}$ es un vector columna que contiene las muestras no nulas del pulso $\widetilde{h}_{d_i}(n)$, con $i \in \{0, \ldots, |\mathcal{D}|-1\}$. $\widetilde{H}_k(f)$ es la transformada de Fourier del pulso $\widetilde{h}_k(n)$, por lo que $|\widetilde{H}_k(f)|^2$ es su densidad espectral de energía. La varianza de la secuencia de datos transmitidos por al portadora k es σ_k^2, que suponemos son símbolos independientes entre sí, e independientes de las secuencias transmitidas por otras portadoras.

El problema de optimización consta de una función de coste a minimizar y un conjunto de R restricciones a satisfacer. La función de coste busca minimizar la suma de las energías emitidas por los pulso supergeneralizados en la región de frecuencias donde la función máscara $M_0(f)$ es distinta de 0. Típicamente, $M_0(f)$ será tal que vale 0 dentro de la banda de paso y

[1] Una señal $x(n)$ se dice que tiene simetría Hermítica si se cumple que $x(-n) = x(n)^*$

1 para cualquier otra frecuencia. Sin embargo, es posible que tome valores intermedios entre 0 y 1, a fin de pesar de distinta forma distintas regiones de frecuencia (p.ej. si queremos dar más peso a las regiones próximas a la banda de paso que a las lejanas). Del mismo modo, la restricción j-ésima busca mantener la energía emitida por los mismos pulsos en las frecuencias definidas por $M_j(f)$ por debajo de δ_j. Además, la función $M_j(f)$ también pueden tomar valores intermedios entre 0 y 1. Una restricción típica consiste en limitar la energía total transmitida por símbolo OFDM, para lo cual $M_j(f) = 1 \ \forall f \in (-\frac{1}{2}, \frac{1}{2}]$, entre otras.

Notamos que para resolver el problema de optimización es necesario minimizar la energía del pulso generalizado fuera de la banda de paso. La densidad espectral de energía de dicho pulso, la cual se integra en (C.3.4), puede expresarse como

$$\left|\widetilde{H}_k(f)\right|^2 = \left(\widetilde{H}_k^{\Re}(f)\right)^2 + \left(\widetilde{H}_k^{\Im}(f)\right)^2, \tag{C.3.5}$$

donde, puesto que $\widetilde{P}_k(f)$ es una función real[2]

$$\begin{aligned} \widetilde{H}_k^{\Re}(f) &= \widetilde{P}_k(f) + \sum_{i\in\mathcal{K};i\neq k} \widetilde{\alpha}_{i,k}^{\Re}\widetilde{P}_k(f) + \widetilde{T}_k^{\Re}(f), \\ \widetilde{H}_k^{\Im}(f) &= \sum_{i\in\mathcal{K};i\neq k} \widetilde{\alpha}_{i,k}^{\Im}\widetilde{P}_k(f) + \widetilde{T}_k^{\Im}(f). \end{aligned} \tag{C.3.6}$$

En ese caso, es importante señalar que encontrar el mínimo de la función de coste en (C.3.4) pasa por anular $\widetilde{H}_k^{\Im}(f)$, puesto que a este término sólo contribuyen los términos de cancelación. En ese caso, se comprueba que los coeficientes $\widetilde{\alpha}_{i,k}$ y $\widetilde{T}_k(f)$ son estrictamente reales y que, en consecuencia, el pulso de transición $\widetilde{t}_k(n)$ ha de tener simetría Hermítica. Esto implica que el número de coeficientes reales que se han de obtener en el problema de optimización (número de grados de libertad) se reduce a la mitad, simplificando notablemente el problema. En cuanto a la implementación de cada una de las técnicas de conformación espectral vistas, el número de productos con operandos reales[3] que requiere cada una de ellas se reduce también sustancialmente:

- Precoding espectral: El número de productos reales se reduce en un 50 %.
- AIC: El número de productos reales se reduce es un 50 %.
- AST: El número de productos reales se reduce en un 50 % con la implementación regular, y algo menos con la implementación sencilla (desarrollo armónico).

[2]En virtud de las propiedades de dualidad y de conjugación, la transformada de Fourier de una señal con simetría Hermítica es real $\Rightarrow x(-n) = x(n)^* \Leftrightarrow X(f) = \mathscr{F}\{x(n)\} \in \mathbb{R}$.

[3]Un producto donde ambos operandos son complejos equivale a 4 productos con operandos reales. Si uno de los operandos es real, el número de productos reales se reduce a la mitad. Por último, si un mismo número complejo se multiplica por otro complejo y por su conjugado, en dos operaciones independientes, los productos reales necesarios para una y otra operación son los mismos, cambiando únicamente cómo suman los resultados parciales: $ab = a^{\Re}b^{\Re} - a^{\Im}b^{\Im} + j(a^{\Re}b^{\Im} + a^{\Im}b^{\Re})$ mientras $ab^* = a^{\Re}b^{\Re} + a^{\Im}b^{\Im} - j(a^{\Re}b^{\Im} - a^{\Im}b^{\Re})$

La contribución de este primer trabajo es doble. En primer lugar, se ha demostrado que usando el pulso con simetría Hermítica propuesto en (C.3.3) y obteniendo sus términos de cancelación como solución de un problema de optimización como el que se modela en (C.3.4) es condición suficiente para beneficiarse de la notables reducciones en el coste computacional citadas anteriormente, tanto en la optimización como en la implementación. En segundo lugar, también se demuestra que para algunas técnicas de conformación espectral es posible conseguir los mismos beneficios simplemente con usar el pulso propuesto, y sin necesidad de usar el modelo de problema de optimización propuesto.

En la Tabla C.1 se recogen ejemplos de ambas situaciones: métodos de conformación espectral que utilizan el pulso con simetría Hermítica propuesto y resuelve un problema de optimización que encaja con (C.3.4); y métodos que simplemente usan el pulso $\widetilde{p}_k(n)$ en (C.3.2) y obtienen los mismos beneficios.

Finalmente, para aquellos métodos de conformación espectral que no pudieran beneficiarse de las reducciones en el coste de implementación por no poder usar el pulso con simetría Hermítica propuesto, demostramos cómo pueden obtener reducciones en el coste de la optimización. Esto ocurre solo si el problema de optimización que resuelven puede adaptarse al modelo propuesto en (C.3.4). En ese caso, los coeficientes del pulso sin simetría, (C.3.1), se pueden obtener a partir de los que resuelven el problema con simetría usando las siguientes relaciones,

$$\alpha_{i,k} = \widetilde{\alpha}_{i,k} e^{j\frac{2\pi}{N}(k-i)(\eta-N_{\mathrm{GI}})}, \qquad \mathbf{t}_k = \widetilde{\mathbf{t}}_k e^{j\frac{2\pi}{N}k(\eta-N_{\mathrm{GI}})}. \tag{C.3.7}$$

A continuación, se comprueba que usar el pulso con simetría Hermítica en (C.3.2) en lugar del convencional no afecta a las prestaciones. Para ello, se han seleccionado algunos métodos de conformación espectral de la Tabla C.1, para los cuales se ha obtenido la densidad espectral de potencia (DEP) en dos casos: usando el pulso de transmisión convencional $p_k(n)$, y usando el pulso con simetría Hermítica $\widetilde{p}_k(n)$ en (C.3.2). Los métodos seleccionados son los basados en técnicas AIC y AST propuestos por Díez *et al.* [16] y Hussain and López-Valcarce [11]; y los de precoding espectral propuestos por Zhou *et al.* [9] (particularizado a un único usuario), por van de Beek [8] y por Ma *et al.* [10]. La DEP obtenida queda representada en la Fig. C.1, donde se muestra que la capacidad de las mencionadas técnicas para reducir las emisiones fuera de banda no se ve afectada por el uso de un pulso con simetría. Se hace notar que la DEP obtenida por Zhou *et al.* y por van de Beek son idénticas, por eso se muestran en una misma curva. Sin embargo, sus precodificadores óptimos son diferentes, por lo que sus señales difieren en la BER que alcanzan. Además, también se ha comprobado que los valores de PAPR (peak-to-average power ratio) son los mismos con el pulso simétrico, $\widetilde{p}_k(n)$, y el convencional, $p_k(n)$. Estos resultados demuestran que la estrategia propuesta permite reducir el coste en la implementación de las 5 técnicas seleccionadas en un 50 % (se reduce en ese porcentaje el número de productos reales necesarios por símbolo OFDM).

Tabla C.1: Métodos de conformación espectral para señales OFDM que pueden beneficiarse del uso del pulsos con simetría Hermítica propuesto.

Referencia(s)	**Demostración**
[16, ecs. (18)-(20)] [28, ecs. (6)-(8)] [13, ec. (3)] [22, ecs. (12)-(13)]	Los problema de optimización propuestos en [16, ecs. (18)-(19)] y [22, ecs. (12)-(13) y (30)-(31)] son esencialmente idénticos al propuesto en (3.3). Por lo tanto, si se emplea en ellos el pulso $\widetilde{p}_k(n)$ de (3.1), los coeficientes óptimos de los términos AIC serán reales, y los términos AST tendrán simetría Hermítica. Finalmente, puesto que [16] es una generalización de [28] y [13], estos últimos también se benefician de la propuesta.
[32, ec. (9)] [33, ec. (10)] [34, ec. (27)]	Los problemas de optimización que resuelven son similares al propuesto en (3.3), y se imponen restricciones para asegurar la correcta recepción de los símbolos. Se utilizan algoritmos iterativos para resolver los problemas de optimización, en los cuales intervienen únicamente términos con valores reales (matrices de emisiones fuera de banda; matrices identidad, de selección y de permutación; etc.), lo que lleva a soluciones también reales.
[11, ecs. (17)-(18)]	Se proponen dos problema de conformación espectral: [11, ec. (17)] para precoding ortogonal y [11, ec. (18)] para una solución basada en técnicas AIC. Para el primer caso, la matriz de precoding que resulta toma valores reales cuando se utiliza el pulso $\widetilde{p}_k(n)$ de (3.1), ya que la conforman los autovectores de una matriz que es real y simétrica. Para el segundo caso, la matriz óptima resultante se calcula a partir de la misma matriz real, una matriz identidad y una matriz de selección, todas reales. En ambos casos, la ventana que se emplea para conformar el pulso en el tiempo se demuestra que tiene simetría Hermítica cuando se utiliza el pulso $\widetilde{p}_k(n)$ de (3.1).
[29, ec. (16)]	La matriz de precoding óptima se construye con los autovectores de la matriz en [29, ec. (16)], que se demuestra fácilmente que es real y simétrica, ya que resulta de sumar matrices que también lo son cuando se emplea el pulso $\widetilde{p}_k(n)$ de (3.1).
[35, ec. (12)]	La expresión cerrada que proponen para la matriz de precodificación óptima implica invertir una matriz que se demuestra fácilmente que es real, ya que resulta de sumar matrices que contienen la transformada de Fourier del pulso $\widetilde{p}_k(n)$ en (3.1).
[9, ec. (15)]	La expresión cerrada que proponen para la matriz de precodificación de cada usuario concatena vectores que resultan de la descomposición en valores singulares de una matriz real. Por lo tanto, la matriz óptima es también real.
[36, bajo ec. (7)] [8, ec. (12)]	La matriz óptima de precoding [36, bajo ec. (7)] toma valores reales, ya que se obtiene como el producto de otras matrices reales (una matriz identidad, una de pesos reales y una con la transformada de Fourier de los pulsos). En [8, ec. (12)] la matriz óptima se obtiene solo a partir de una matriz identidad y la que contiene las transformadas de Fourier de los pulsos, siendo ambas reales.
[10, ec. (12)]	La matriz de precoding óptima es real, ya que se obtiene a partir de la descomposición en valores singulares de una matriz real que contiene las transformadas de Fourier del pulso $\widetilde{p}_k(n)$ de (3.1), y a partir también de una matriz arbitraria que se puede escoger que sea real.

C.4 Esquema de conformación espectral para escenarios cambiantes de forma dinámica

Para los sistemas que aplican el paradigma de radio cognitiva (CR, cognitive radio), las subbandas de frecuencia donde tienen permitido transmitir pueden cambiar dinámicamente

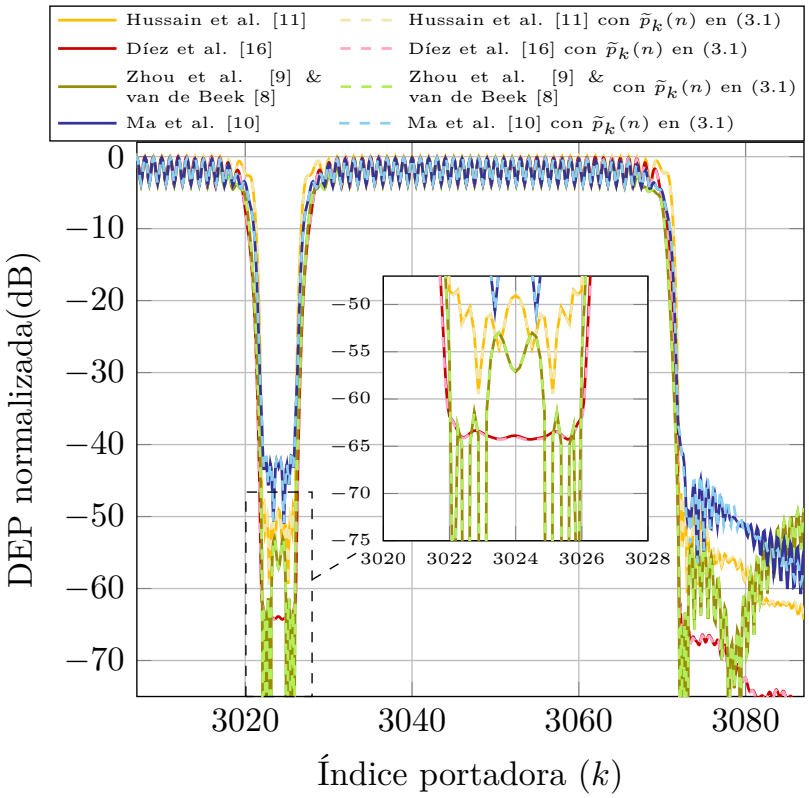

Figura C.1: DEP normalizada obtenida para varios métodos de conformación espectral de la Tabla C.1 usando el pulso convencional para OFDM, $p_k(n)$, y el pulso con simetría Hermítica propuesto, $\widetilde{p}_k(n)$ de (C.3.2). Notar que los métodos de [9] y de [8] generan señales con la misma DEP, por lo que se muestra una sola curva.

con el tiempo. Esto es porque su disponibilidad está sujeta a que el sistema primario, quien tiene asignados esos recursos, haga o no uso de ellos. Esto supone una dificultad añadida si estos sistemas aplican técnicas de conformación espectral sobre sus señales, puesto que las soluciones deberán ser recalculadas cada vez que el escenario cambie. La presente tesis propone una solución eficiente a esta problemática, que queda resumida en esta sección. En ese sentido, las contribución es triple:

- Se define una estrategia de conformación espectral que permite adaptar las soluciones de forma dinámica con cada cambio del escenario.
- Se demuestra la existencia de unas operaciones sencillas que permiten adaptar las soluciones al problema de conformación espectral.
- Se proponen dos procedimientos de optimización, con diferente complejidad y prestaciones, que permiten obtener un conjunto original de soluciones que podamos adaptar a cualquier escenario que se presente.

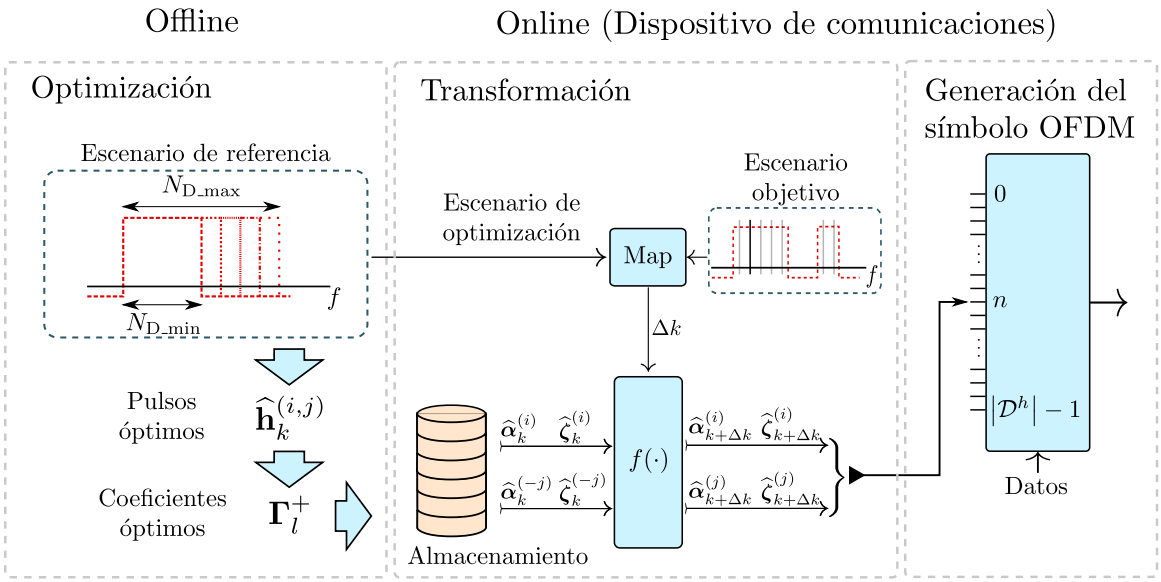

Figura C.2: Diagrama que describe la estrategia de conformación propuesta en esta sección, que consta de tres fases: 1) optimización del conjunto de coeficientes original; 2) transformación del conjunto original de soluciones; 3) generación del símbolo OFDM. La primera fase se realiza offline, mientras que los otros dos se realizan en el dispositivo de comunicaciones online.

La mencionada estrategia de conformación espectral consta de tres fases, representadas en la Fig. C.2:

1) Se obtiene un conjunto único de soluciones originales mediante uno de los procedimientos de optimización propuestos. Estas soluciones se calculan de manera *offline* y se almacenan en el dispositivo de transmisión.

2) Se calculan las soluciones al problema de conformación espectral adaptando el conjunto de soluciones precalculadas. Este proceso se hace de forma *online* en el propio dispositivo.

3) Se generan los símbolos OFDM usando las soluciones de conformación espectral calculadas para cada momento.

A fin de simplificar la exposición de la propuesta, primero explicamos cómo es su aplicación a una situación mas sencilla, en la que el escenario a conformar consta únicamente de una banda de paso aislada y con ancho arbitrariamente grande. Luego nos centramos en el problema general, con escenarios que cuentan con diversas bandas de paso con anchos cualesquiera que pueden ser arbitrariamente estrechos.

Esta propuesta emplea como base el pulso generalizado en (C.2.2), aprovechando sus prestaciones en términos de reducción de la OOBE a cambio de un limitado coste computacional

añadido. En consecuencia, la propuesta se limita a usar las técnicas AIC y AST ya mencionadas. Se recuerda que el pulso generalizado solo era necesario que lo emplearan un subconjunto de portadoras próximas a los bordes de las bandas de paso, ya que las más alejadas producen emisiones despreciables fuera de banda. Denotamos con N_{h} al número de portadoras de datos consecutivas que usan el pulso generalizado junto a cada borde de la banda de paso. De forma similar, los términos de cancelación que mayor capacidad tienen de controlar las emisiones en una región del espectro son los que se encuentran más próximos a la misma.

C.4.1 Soluciones adaptativas para bandas anchas

Consideramos un escenario como el representado en la Fig. C.3, donde una banda de paso de ancho arbitrariamente grande está flanqueado a izquierda y derecha por dos bandas prohibidas, $\mathcal{B}_{\mathrm{n}}^{+}(l_{\mathrm{l}})$ y $\mathcal{B}_{\mathrm{n}}^{-}(l_{\mathrm{r}})$, respectivamente. La banda primera comienza en el índice l_{l} y la segunda en l_{r}, y ambas tienen una extensión de B_{n}. En cuanto a la localización de la banda de paso, es arbitraria.

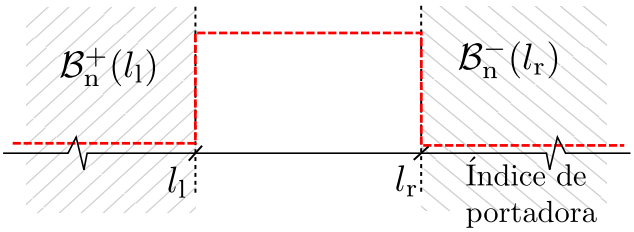

Figura C.3: Máscara de DEP para una banda de paso con bordes izquierdo y derecho en l_{l} y l_{r}, respectivamente. $\mathcal{B}_{\mathrm{n}}^{+}(l_{\mathrm{l}})$ y $\mathcal{B}_{\mathrm{n}}^{-}(l_{\mathrm{r}})$ son las bandas prohibidas a los respectivos lados de la banda de paso.

La estrategia de conformación espectral que proponemos pretende que las soluciones para un escenario se puedan transformar en las de otro escenario semejante de forma sencilla (otra banda ancha con distinta localización y distinto ancho). Hacemos notar que la magnitud de las emisiones fuera de banda de una portadora determinada depende de la distancia entre la portadora y el borde de la banda de paso. En particular, a menor distancia, mayor es la magnitud de las emisiones. Entonces, es necesario que las soluciones que definamos para esta estrategia de conformación espectral tengan una referencia explícita a dicha distancia. Se define el siguiente pulso, inspirado en el generalizado

$$\begin{aligned} \mathbf{h}_k^{(i)} &= \mathbf{p}_k + \mathbf{C}_{k-i}^{+}\boldsymbol{\alpha}_k^{(i)} + \mathbf{t}_k^{(i)}, \quad i > 0, \\ \mathbf{h}_k^{(i)} &= \mathbf{p}_k + \mathbf{C}_{k-i}^{-}\boldsymbol{\alpha}_k^{(i)} + \mathbf{t}_k^{(i)}, \quad i < 0, \end{aligned} \tag{C.4.1}$$

donde i es la distancia, dada en número de portadoras, entre el índice k de la portadora de datos y el borde más próximo de la banda de paso en la que se encuentra. Notar que cuando

$i > 0$ el borde más próximo es el izquierdo ($l_\mathrm{l} < k$), y cuando $i < 0$ el borde más próximo es el derecho ($l_\mathrm{r} > k$). La Fig. C.4 describe estas relaciones entre el índice i y la posición relativa de la portadora de datos, k, respecto al borde más cercano, $k-i$. Suponemos que las bandas de paso son lo bastante anchas como para poder despreciar las emisiones producidas más allá del borde más lejano de la banda de paso. Junto a cada borde, N_h portadoras de datos consecutivas usan el pulso modificado propuesto (en azul). Las portadoras en negro son aquellas que no están lo suficientemente cerca de ninguno de los dos bordes de la banda como para producir emisiones importantes fuera de ésta (usan el pulso convencional). El número de portadoras dentro de la banda de paso se denota con $N_\mathrm{D} = N_\mathrm{h} + 2N_\mathrm{ci}$.

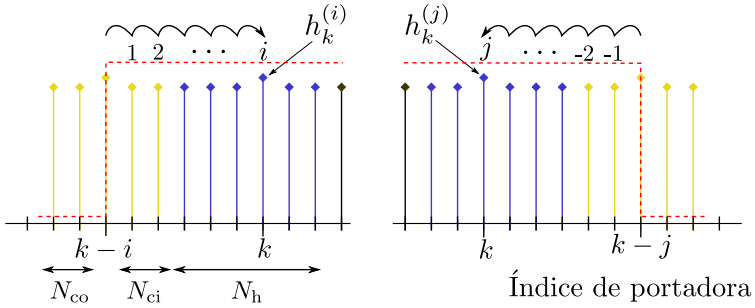

Figura C.4: Representación detallada de las portadoras situadas junto a los bordes izquierdo y derecho de una banda de paso.

En el miembro de la derecha de las ecuaciones en (C.4.1) aparecen el pulso base, $p_k(n)$, en forma vectorial, seguido de los términos de cancelación de las emisiones fuera de banda. Primero, las portadoras de cancelación, contenidas en las columnas de la matriz $\mathbf{C}_{k-i}^{+}$ ($\mathbf{C}_{k-i}^{-}$), pesados por los coeficientes $\boldsymbol{\alpha}_k^{(i)}$ para cancelar las emisiones en la banda prohibida situada a la izquierda (derecha) de la banda de paso. Estas portadoras de cancelación (en amarillo en la Fig. C.4) se situarán cerca del borde de la banda de paso donde deben actuar, N_ci dentro de la banda de paso, N_co fuera y una más justo en el borde, en el índice $k-i$ ($k-j$). En total se usan $N_\mathrm{CC} = N_\mathrm{ci} + N_\mathrm{co} + 1$ portadoras de cancelación en cada borde. El último término en (C.4.1), $\mathbf{t}_k(n)$, es el término AST.

Igual que con el pulso generalizado original, los coeficientes del pulso modificado propuesto pueden obtenerse portadora a portadora a través de una optimización

$$\widehat{\boldsymbol{\gamma}}_k^{(i)} = \begin{bmatrix} \widehat{\boldsymbol{\alpha}}_k^{(i)} \\ \widehat{\boldsymbol{\zeta}}_k^{(i)} \end{bmatrix} = \arg \min_{\boldsymbol{\alpha}_k^{(i)}, \boldsymbol{\zeta}_k^{(i)}} \left\{ E_k^{(i)} \right\}. \tag{C.4.2}$$

donde $\boldsymbol{\zeta}_k^{(i)} = \left[t_k^{(i)}(0), \ldots, t_k^{(i)}(\beta-1), t_k^{(i)}(L-\beta), \ldots, t_k^{(i)}(L-1) \right]^\mathrm{T}$ contiene las muestras no nulas del pulso de transición, y $E_k^{(i)}$ es la energía emitida por el pulso en la banda prohibida

más próxima,

$$E_k^{(i)} = \begin{cases} \int_{\mathcal{B}_{\mathrm{n}}^{+}(k-i)} \left| H_k^{(i)}(f) \right|^2 df, & i > 0, \\ \int_{\mathcal{B}_{\mathrm{n}}^{-}(k-i)} \left| H_k^{(i)}(f) \right|^2 df, & i < 0. \end{cases} \tag{C.4.3}$$

C.4.2 Transformación de las soluciones

En esta sección se presentan las operaciones que transforman los parámetros de un pulso que minimiza las emisiones en una determinada región al caso en que la región donde deben minimizarse las emisiones es una versión desplazada y/o girada espectralmente de la primera. Para ello, nos damos cuenta de que las emisiones producidas por una banda de paso, y una versión desplazada de la misma deben ser idénticas en magnitud. Por tanto, debe existir una relación entre las soluciones que resuelven un problema y una versión del mismo que desplazamos Δk portadoras a la derecha,

$$\boldsymbol{\alpha}_{k+\Delta k}^{(i)} = \boldsymbol{\alpha}_k^{(i)}, \qquad \mathbf{t}_{k+\Delta k}^{(i)} = \boldsymbol{\Omega}_{\Delta k} \mathbf{t}_k^{(i)}, \tag{C.4.4}$$

donde $\Omega_{\Delta k} = \mathrm{diag}\Big([e^{j\frac{2\pi}{N}\Delta k(0-N_{\mathrm{GI}})}, \ldots, e^{j\frac{2\pi}{N}\Delta k(L-1-N_{\mathrm{GI}})}] \Big)$.

De forma similar, nos damos cuenta de que las emisiones que produce una banda de paso más allá de su borde izquierdo son iguales a las que produce más allá del derecho. Por lo tanto, existirá también una relación entre las soluciones que resuelve uno y otro problema,

$$\boldsymbol{\alpha}_k^{(-i)} = (\boldsymbol{\alpha}_k^{(i)})^*, \qquad \mathbf{t}_k^{(-i)} = \boldsymbol{\Omega}_{2k-N} (\mathbf{t}_k^{(i)})^*. \tag{C.4.5}$$

Es importante notar que los superíndices presentes en uno y otro miembro de estas transformaciones son iguales en valor absoluto, con cambio de signo en (C.4.5). Esto implica que para resolver un problema de conformación espectral mediante transformaciones es necesario partir de un conjunto inicial de soluciones, el cual debe contener los coeficientes para las N_{h} portadoras que usan el pulso generalizado en cada borde de la banda. Por comodidad, se agrupan en una misma matriz los coeficientes óptimos para los pulsos de un mismo borde de la banda situado en el índice de portadora l,

$$\begin{aligned} \boldsymbol{\Gamma}_l^{+} &= \left[\boldsymbol{\gamma}_{l+N_{\mathrm{ci}}+1}^{(N_{\mathrm{ci}}+1)}, \ldots, \boldsymbol{\gamma}_{l+N_{\mathrm{ci}}+N_{\mathrm{h}}}^{(N_{\mathrm{ci}}+N_{\mathrm{h}})} \right], \\ \boldsymbol{\Gamma}_l^{-} &= \left[\boldsymbol{\gamma}_{l-N_{\mathrm{ci}}-1}^{(-N_{\mathrm{ci}}-1)}, \ldots, \boldsymbol{\gamma}_{l-N_{\mathrm{ci}}-N_{\mathrm{h}}}^{(-N_{\mathrm{ci}}-N_{\mathrm{h}})} \right], \end{aligned} \tag{C.4.6}$$

para los bordes izquierdo y derecho, respectivamente. Los coeficientes de una y otra matriz se relacionan a través de (C.4.5).

C.4.3 Soluciones adaptativas para bandas de ancho arbitrario

La sección anterior se ha centrado exclusivamente en bandas anchas. Por ello, los pulsos en (C.4.1) se han definido bajo el supuesto de que las bandas de paso son lo suficientemente anchas como para que una portadora de datos solo tenga emisiones apreciables en una de las bandas prohibidas que flanquean la banda de paso. Ahora, nos centramos en problemas más generales, con bandas de cualquier ancho. En ese caso, se debe contemplar la posibilidad de que una misma portadora produzca emisiones relevantes más allá de ambos bordes de la banda, para lo que proponemos un pulso más general

$$\mathbf{h}_k^{(i,j)} = \mathbf{p}_k + \underbrace{\mathbf{C}_{k-i}^{+}\boldsymbol{\alpha}_k^{(i)} + \mathbf{t}_k^{(i)}}_{\mathbf{r}_k^{(i)}} + \underbrace{\mathbf{C}_{k-j}^{-}\boldsymbol{\alpha}_k^{(j)} + \mathbf{t}_k^{(j)}}_{\mathbf{r}_k^{(j)}}, \quad \begin{matrix} i > 0 \\ j < 0, \end{matrix} \tag{C.4.7}$$

donde $i > 0$ denota que la portadora k es la i-ésima respecto del borde izquierdo de la banda de paso y $j < 0$ que es la j-ésima respecto del borde derecho. $\mathbf{r}_k^{(i)}$ y $\mathbf{r}_k^{(j)}$ denotan los términos de cancelación que usamos para minimizar las emisiones producidas junto a los bordes izquierdo y derecho de la banda, respectivamente.

Con el fin de poder aplicar la estrategia de conformación espectral propuesta a cualquier problema que se presente, con independencia de la localización y el ancho de las bandas de paso que haya en el escenario, es necesario un conjunto de soluciones original con determinadas características. No bastaría con resolver un problema como el de (C.4.2), puesto que está pensado para pulsos que producen emisiones relevantes en un único borde. En esta subsección se introducen dos procedimientos de optimización diferentes para realizar en la primera fase de la estrategia de conformación espectral propuesta. Ambos métodos tienen en común que, a fin de aportar un conjunto soluciones generales y aplicables a un amplio rango de escenarios, utilizan una escala de anchos de banda diferentes. Esta escala irá desde $N_{\mathrm{D\_min}} = N_{\mathrm{h\_min}} + 2N_{\mathrm{ci}}$, la más estrecha, hasta $N_{\mathrm{D\_max}} = N_{\mathrm{h\_max}} + 2N_{\mathrm{ci}}$, la más ancha. $N_{\mathrm{D\_min}}$ es un parámetro de diseño, que determina el mínimo ancho de banda que queremos contemplar en el diseño de las soluciones (en bandas de paso con $N_{\mathrm{D}} < N_{\mathrm{D\_min}}$ las estrategia propuesta producirá soluciones subóptimas). El valor de $N_{\mathrm{h\_max}}$ determina el número máximo de portadoras de datos consecutivas junto al borde de la banda de paso que requieren usar el pulso modificado propuesto. Es decir, si $N_{\mathrm{h\_max}}$ portadoras de datos utilizan el pulso propuesto, usarlo en $N_{\mathrm{h\_max}}+1$ implica una reducción adicional despreciable en las emisiones fuera de banda. Los procedimientos de optimización propuestos se describen a continuación:

Procedimiento incremental

La optimización de las soluciones se realiza de forma iterativa, obteniendo en cada iteración $\mathbf{r}_k^{(i)}$ $(i > 0)$ para un único pulso. Para ello, el foco se pone en el borde izquierdo de las bandas de paso consideradas, cuyo índice denotamos con l. Por comodidad, redefinimos las

bandas prohibidas a izquierda y derecha de la banda de paso como *banda prohibida contigua*, $\mathcal{B}_{\rm c} = \mathcal{B}_{\rm n}^{+}(l)$ y *banda prohibida opuesta*, $\mathcal{B}_{\rm o} = \mathcal{B}_{\rm n}^{-}(l + N_{\rm D} + 1)$.

Se define un doble objetivo para la optimización: se obtiene el $\mathbf{r}_k^{(i)}$ $(i > 0)$ que cancela las emisiones del pulso más allá del borde izquierdo, y que al mismo tiempo produce mínimas emisiones más allá del borde derecho. Esto se traduce en el siguiente problema de optimización

$$\widehat{\boldsymbol{\gamma}}_k^{(i)} = \begin{bmatrix} \widehat{\boldsymbol{\alpha}}_k^{(i)} \\ \widehat{\boldsymbol{\zeta}}_k^{(i)} \end{bmatrix} = \arg \min_{\boldsymbol{\alpha}_k^{(i)}, \boldsymbol{\zeta}_k^{(i)}} \left\{ (1-a) E_{k,\mathcal{B}_{\rm c}}^{(i)} + a E_{k,\mathcal{B}_{\rm o}}^{(i)} \right\}, \tag{C.4.8}$$

donde a determina cuánta importancia se da a cada objetivo, y donde

$$E_{k,\mathcal{B}_{\rm c}}^{(i)} = \int_{\mathcal{B}_{\rm c}} \left| P_k(f) + R_k^{(i)}(f) \right|^2 df; \qquad E_{k,\mathcal{B}_{\rm o}}^{(i)} = \int_{\mathcal{B}_{\rm o}} \left| R_k^{(i)}(f) \right|^2 df, \tag{C.4.9}$$

donde $R_k^{(i)}(f)$ es la transformada de Fourier del término $\mathbf{r}_k^{(i)}$.

El procedimiento iterativo que se propone está descrito en el Algoritmo C.4.1. Partimos de la banda más estrecha del conjunto, con $N_{\rm D} = N_{\rm D\_min}$ portadoras. Para ésta, se obtiene $\boldsymbol{\gamma}_k^{(i)}$ para las $N_{\rm h\_min}$ portadoras de datos en la banda, resolviendo el problema en (C.4.8), y se almacenan en la matriz $\boldsymbol{\Gamma}_l^{+}$. A continuación comenzamos a iterar, incrementando el ancho de banda en una portadora cada vez, y obteniendo $\boldsymbol{\gamma}_k^{(i)}$ solo para la portadora de datos más a la derecha, y almacenamos el resultado. El procedimiento termina cuando se alcanza el ancho de banda máximo, $N_{\rm D} = N_{\rm D\_max}$, en cuya iteración completamos la matriz de coeficientes óptimos $\boldsymbol{\Gamma}_l^{+}$.

Algorithm C.4.1 Procedimiento incremental

1: Partimos del ancho de banda $N_{\rm D} = N_{\rm D\_min}$
2: Obtenemos $\widehat{\boldsymbol{\gamma}}_k^{(i)}$ para las $N_{\rm h\_min}$ portadoras de datos resolviendo (C.4.8)
3: Almacenamos los coeficientes en $\boldsymbol{\Gamma}_l^{+}$
4: **while** $N_{\rm D} < N_{\rm D\_max}$ **do**
5: Incrementamos el ancho de banda en una portadora: $N_{\rm D} = N_{\rm D} + 1$
6: Obtenemos $\widehat{\boldsymbol{\gamma}}_k^{(i)}$ solo para la portadora de datos situada más a la derecha en la banda resolviendo (C.4.8)
7: Almacenamos los coeficientes en $\boldsymbol{\Gamma}_l^{+}$
8: **end while**

Procedimiento directo

La optimización de las soluciones se realiza de forma directa, teniendo en cuenta todos los anchos de banda de forma conjunta en un único problema de optimización. Con ese fin, denotamos como $E_k^{(i,j)}$, con $i > 0$ y $j < 0$, a la energía que emite el pulso $\mathbf{h}_k^{(i,j)}$ en las bandas

prohibidas a cada lado de la banda de paso. A partir de esto definimos la energía emitida fuera de banda por los pulsos usados por el conjunto de portadoras dentro de una banda de ancho N_{D} como

$$F_l^{(N_{\mathrm{D}})} = \sum_{m=1}^{N_{\mathrm{h}}} E_{l+N_{\mathrm{ci}}}^{(N_{\mathrm{ci}}+m,-N_{\mathrm{D}}-1+N_{\mathrm{ci}}+m)}. \tag{C.4.10}$$

Finalmente, sumamos la energía emitida en las bandas prohibidas por el conjunto de bandas de paso consideradas para la optimización

$$F_l(\mathbf{\Gamma}_l^+) = \sum_{n_{\mathrm{D}}=N_{\mathrm{D\_min}}}^{N_{\mathrm{D\_max}}} F_l^{(n_{\mathrm{D}})}, \tag{C.4.11}$$

que depende de todo el conjunto de coeficientes $\mathbf{\Gamma}_l^+$. El problema de optimización busca entonces el conjunto de coeficientes óptimos que minimiza $F_l(\mathbf{\Gamma}_l^+)$, es decir,

$$\widehat{\mathbf{\Gamma}}_l^+ = \arg\min_{\mathbf{\Gamma}_l^+} \left\{ F_l(\mathbf{\Gamma}_l^+) \right\}. \tag{C.4.12}$$

C.4.4 Resultados numéricos y discusión

En este apartado se valoran las prestaciones del esquema de conformación espectral propuesto y de los dos métodos que proponemos para obtener el conjunto único de soluciones. En particular, se va a evaluar la influencia que tiene el parámetro $N_{\mathrm{h\_min}}$ sobre la capacidad de las soluciones resultantes de obtener emisiones fuera de banda mínimas. La comprobación se hace para ambos procedimientos de optimización, y con dos tipos de pulso: uno con solo términos AIC, que llamamos $h_k(\mathrm{CC})$, y el pulso con términos AIC y AST, estos últimos desarrollados armónicamente[4], denotado como $h_k(\mathrm{CC}, t_k\text{-h})$. Los parámetros de diseño empleados para la obtención de estas soluciones han sido $N_{\mathrm{h\_min}} \in \{1, 2, \ldots, 5\}$, $N_{\mathrm{h\_max}} = 13$, $N_{\mathrm{ci}} = 2$, $N_{\mathrm{co}} = 0$. El pulso que emplea términos AST desarrollados armónicamente utiliza $N_{\mathrm{q}} = 2$.

Para la evaluación, se toma el valor máximo que alcanza la DEP normalizada dentro de la banda prohibida, que llamamos $\mathrm{DEP}_{\mathrm{max}}$. Los conjuntos de soluciones originales que se van a emplear se obtiene usando los dos procedimientos propuestos: incremental y directo. Estos se aplican a dos escenarios distintos y se grafican los valores de $\mathrm{DEP}_{\mathrm{max}}$ en función del $N_{\mathrm{h\_min}}$ empleado para su obtención. En la Fig. C.5(a) se refleja la $\mathrm{DEP}_{\mathrm{max}}$ obtenida cuando se aplican las soluciones en la banda más estrecha posible, con ancho $N_{\mathrm{D}} = N_{\mathrm{h\_min}} + 2N_{\mathrm{ci}}$, y en la Fig. C.5(b) la obtenida al aplicar las mismas soluciones en una banda ancha, con $N_{\mathrm{D}} = N_{\mathrm{h\_max}} + 2N_{\mathrm{ci}}$.

[4]Este resumen no incluye detalles sobre la implementación de los pulsos de transición desarrollados armónicamente. Estos se pueden encontrar en [22].

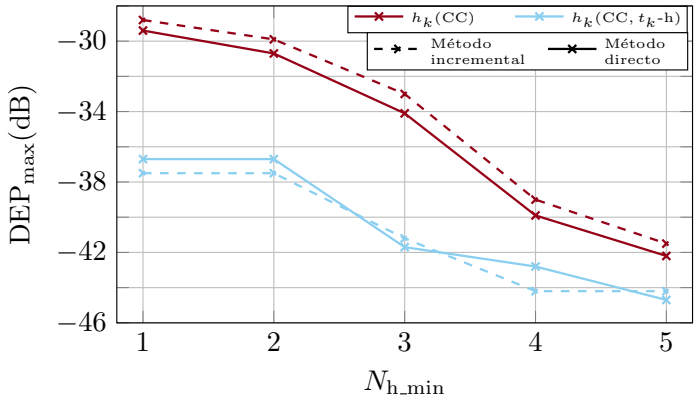

(a)

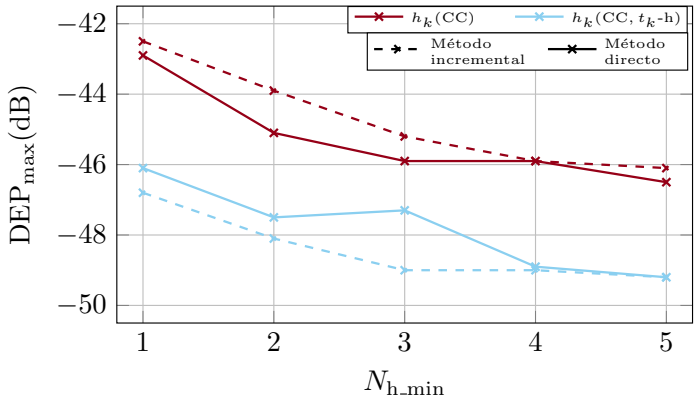

(b)

Figura C.5: $\text{DEP}_{\max}$ obtenida con $h_k(\text{CC})$ y $h_k(\text{CC}, t_k\text{-h})$ cuando se emplea la estrategia de conformación espectral propuesta para obtener el conjunto de soluciones original. Ambos procedimientos de optimización se han empleado: incremental y directo. Cada conjunto de soluciones se aplica a una banda de $N_{\text{D}} = N_{\text{h\_min}} + 2N_{\text{ci}}$ (a) y a otra de $N_{\text{D}} = N_{\text{h\_max}} + 2N_{\text{ci}}$ (b), donde $N_{\text{h\_max}} = 13$.

Se observa en primer lugar que $h_k(\text{CC}, t_k\text{-h})$ arroja mejores prestaciones que $h_k(\text{CC})$ debido al mayor número de grados de libertad con que cuenta el primero. También se ve que aumentar el valor de $N_{\text{h\_min}}$ reduce el valor de $\text{DEP}_{\max}$ para ambos tipos de pulso. Esto se debe a que a mayor ancho de banda, menores son las emisiones producidas por los pulsos en la banda prohibida que tenga más lejana. Esto ocurre tanto al evaluar en $N_{\text{D}} = N_{\text{h\_min}} + 2N_{\text{ci}}$ como en $N_{\text{D}} = N_{\text{h\_max}} + 2N_{\text{ci}}$. Sin embargo, notamos que en el primero la pendiente es más pronunciada. Esto se debe a que en el primero, al aumentar $N_{\text{h\_min}}$ también crece el ancho de la banda donde evaluamos los coeficientes, N_{D}, mientras que en el segundo el ancho de dicha banda permanece fijo.

Se observa también lo parecidas que son las curvas obtenidas con el procedimiento incremental y con el directo. Esto implica que ambos procedimientos dan lugar a soluciones similares en prestaciones, aunque existen algunas diferencias. En primer lugar, cuando se

usa el pulso $h_k(\mathrm{CC})$ el procedimiento directo supera en prestaciones al incremental casi para cada $N_{\mathrm{h\_min}}$. Esto se debe a que el primer procedimiento considera el rango completo de anchos de banda en la optimización. Por contra, cuando se usa el pulso $h_k(\mathrm{CC}, t_k\text{-h})$, en la banda estrecha (a) ninguno de los procedimientos refleja mejores prestaciones, mientras que en la ancha (b) es el procedimiento incremental el que supera en prestaciones al directo. Esto se puede atribuir al mayor número de grados de libertad que supone el uso de términos AIC y AST. Cuanto más complejo sea el problema, mayor probabilidad de que la solución encontrada sea subóptima (mínimo local).

Las Fig. C.5 (a) y (b) pueden ayudar a determinar qué valor de $N_{\mathrm{h\_min}}$ es necesario para un diseño concreto. Por ejemplo, si necesitamos mantener el valor de $\mathrm{DEP}_{\mathrm{max}}$ por debajo de -41 dB, con $h_k(\mathrm{CC})$ esto es posible con $N_{\mathrm{h\_min}} \geq 5$, mientras que para $h_k(\mathrm{CC}, t_k\text{-h})$ es necesario que $N_{\mathrm{h\_min}} \geq 3$.

C.5 Extensión temporal de términos AIC y AST para mejor cancelación de la OOBE

En esta sección se propone una forma de compensar dos problemas que se derivan normalmente de usar las técnicas de conformación espectral AIC y AST: la penalización del régimen binario por usar portadoras de datos como CC, y el acortamiento del prefijo cíclico efectivo a causa del solape de este último con los términos AST, respectivamente. La estrategia propuesta parte del pulso generalizado, y consiste en incrementar los grados de libertad del problema añadiendo versiones de los términos AIC y AST adelantados y atrasados en el tiempo. Estos grados de libertad adicionales permiten:

- Reducir el número de portadoras de datos que se usan como CC, y/o reducir el tamaño de los términos AST y de las transiciones suaves (determinado por β), mientras mantenemos el mismo nivel de emisiones fuera de banda que con el pulso generalizado.

- Reducir más aún las emisiones fuera de banda manteniendo la penalización del régimen binario y el acortamiento del prefijo cíclico que conlleva el uso del pulso generalizado.

La idea surge tras observar que los términos de cancelación del pulso generalizado pueden desplazarse un número entero de períodos de símbolo hacia adelante y atrás sin afectar la operación del receptor. Es decir, las versiones desplazadas de estos términos siguen siendo ortogonales a las portadoras de datos. El resultado es un pulso extendido en el tiempo com M_{a} términos de cancelación adelantados y M_{d} retrasados. El pulso tiene la siguiente

expresión,

$$\mathbf{h}_k^{\text{t-e}} = \underbrace{\begin{bmatrix} \mathbf{0}_{M_\text{a}N_\text{s},1} \\ \mathbf{p}_k \\ \mathbf{0}_{M_\text{d}N_\text{s},1} \end{bmatrix}}_{\stackrel{\text{def}}{=}\mathbf{p}_k^{\text{t-e}}} + \sum_{i=-M_\text{a}}^{M_\text{d}} \underbrace{\begin{bmatrix} \mathbf{0}_{(M_\text{a}+i)N_\text{s},|\mathcal{C}|} \\ \mathbf{P}_\mathcal{C} \\ \mathbf{0}_{(M_\text{d}-i)N_\text{s},|\mathcal{C}|} \end{bmatrix}}_{\stackrel{\text{def}}{=}\mathbf{P}_{\mathcal{C},i}^{\text{t-e}}} \boldsymbol{\alpha}_{k,i} + \sum_{i=-M_\text{a}}^{M_\text{d}+1} \underbrace{\begin{bmatrix} \mathbf{0}_{(M_\text{a}+i)N_\text{s},\beta} \\ \mathbf{I}_\beta \\ \mathbf{0}_{(M_\text{d}-i+1)N_\text{s},\beta} \end{bmatrix}}_{\stackrel{\text{def}}{=}\mathbf{T}_i^{\text{t-e}}} \boldsymbol{\zeta}_{k,i}, \quad k \in \mathcal{D}^\text{h}, \tag{C.5.1}$$

donde $\mathbf{p}_k^{\text{t-e}}$, $\mathbf{P}_{\mathcal{C},i}^{\text{t-e}}$ y $\mathbf{T}_i^{\text{t-e}}$ se definen para representar el pulso base y las versiones desplazadas de la matriz con las portadoras de cancelación y de la matriz de selección de los pulsos de transición, respectivamente. Cuando $M_\text{a} = M_\text{d} = 0$ el pulso $\mathbf{h}_k^{\text{t-e}}$ se convierte en el pulso generalizado de (C.2.3), quedándose únicamente con los términos AIC con $i = 0$ y los términos AST con $i = 0$ e $i = 1$, siendo estos últimos los segmentos inicial y final del pulso de transición ($\boldsymbol{\zeta}_k^\text{s}$ y $\boldsymbol{\zeta}_k^\text{e}$). Los términos restantes, esto es, los términos AIC con $i \in \{-M_\text{a} \ldots, -1, 1, \ldots, M_\text{d}\}$ y los AST con $i \in \{-M_\text{a} \ldots, -1, 2, \ldots, M_\text{d}+1\}$ son los términos nuevos.

A modo ilustrativo, la Fig. C.6 muestra la amplitud de un pulso base, $p_k(n)$, un pulso generalizado, $h_k(n)$, y un pulso extendido como el propuesto con $M_\text{a} = M_\text{d} = 1$, $h_k^{\text{t-e}}(n)$. Las zonas sombreadas delimitan la duración de los términos AIC (en color rosa) y AST (en color celeste). Los términos desplazados en el tiempo están etiquetados como AIC con $i \in \{-1, 1\}$ y AST con $i \in \{-1, 2\}$, y se extienden a símbolos anteriores y posteriores. El rizado que se observa en las regiones planas de $h_k(n)$ y $h_k^{\text{t-e}}(n)$ se debe a las portadoras de cancelación, y la forma que toman en los bordes se debe a los pulsos de transición.

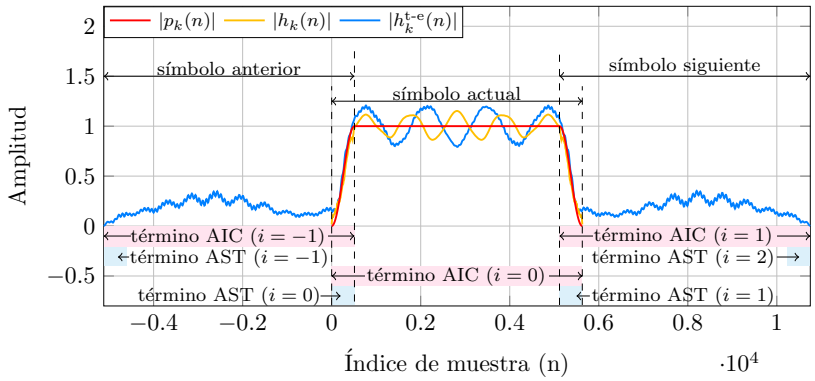

Figura C.6: Forma de onda del pulso propuesto, el pulso generalizado y el pulso base. Han sido generados con N=4096, N_GI=1024, β=512 y un pulso conformador $g(n)$ con transiciones en forma de coseno alzado. El pulso propuesto cuenta con $M_\text{a} = M_\text{d} = 1$. Las regiones sombreadas marcan la extensión de los términos AIC y AST.

Los coeficientes óptimos de los pulsos extendidos en el tiempo, al igual que los generalizados, se obtienen a través de un procedimiento de optimización.

C.5.1 Resultados numéricos y discusión

La estrategia de conformación espectral propuesta se ha evaluado en dos escenarios reales donde se hace uso de la modulación OFDM con características diferentes: el sistema 5G NR y el sistema cableado definido en la ITU-T Rec. G.9960 para comunicaciones por la red eléctrica (PLC, power line communications) que ya se ha empleado en secciones anteriores [38] [37]. En el primer escenario, estudiamos las prestaciones del método en canales desde los 3 MHz hasta los 50 MHz, usando un espaciado entre subportadoras (SCS, subcarrier spacing) de 15 kHz. En este resumen nos centramos en los de 5, 10 y 50 MHz por su representatividad. La figura de mérito que se emplea para medir las emisiones fuera de banda es el ACLR (adjacent channel leakage ratio), esto es, el cociente entre la potencia transmitida en la banda deseada y la potencia emitida en la banda adyacente. Este valor debe estar por debajo de los 45 dB [38]. El escenario de PLC destaca por la estricta máscara de emisiones que deben cumplir los sistemas para satisfacer la norma EN 50561-1 [6], en la que se definen 20 subbandas permanentes donde las emisiones están prohibidas, además de otras 14 donde la prohibición cambia de forma dinámica. Si bien no se definen en la norma los niveles de DEP admisibles para esas subbandas, los fabricantes típicamente buscan caídas de al menos 43 dB para las subbandas por debajo de los 5 MHz, y de al menos 39 dB entre los 5 y los 30 MHz. También se establece en la ITU-T Rec. G.9964 que por debajo de los 1.8 MHz y por encima de los 30 MHz la DEP debe caer por debajo de los 30 dB respecto del nivel máximo en la banda de paso [41].

Se ha estudiado la influencia que tiene el número de términos extendidos que forman el pulso y su posición dentro del mismo sobre las prestaciones (es decir, la influencia de los parámetros M_a y M_d sobre la $\mathrm{DEP}_\mathrm{max}$ alcanzada). Del estudio se concluye que la mayor ganancia se consigue cuando se usan términos extendidos a cada lado. Además, a partir de dos términos extendidos, idealmente uno a cada lado ($M_\mathrm{a} = M_\mathrm{d} = 1$), pero también pueden ser dos atrasados ($M_\mathrm{d} = 2$), la ganancia conseguida con cada término extendido comienza a ser marginal. Por eso, en adelante nos centramos en el caso con un único término adelantado y uno atrasado. En este resumen nos ahorramos los detalles sobre este estudio.

Es interesante mostrar directamente las prestaciones de la estrategia propuesta en ambos escenarios reales.

Sistema inalámbrico: 5G NR Nos centramos en los canales de 5, 10 y 50 MHz. En ellos, el porcentaje de ancho de banda dedicado a la banda de guarda va del 10 % para el de 5 MHz hasta el 2.8 % para el de 50 MHz. La Fig. C.7 muestra la DEP obtenida con el pulso con extensiones temporales propuesto ($M_\mathrm{a} = M_\mathrm{d} = 1$), y con el pulso convencionalmente

usado conformado con una ventana de coseno alzado (RC, raised cosine), ilustrados en el caso de un canal de 5 MHz. Este último pulso es utilizado por algunos fabricantes para satisfacer las restricciones de ACLR impuestas en el estándar de 5G NR. Para ambos pulsos, la figura muestra la dimensión a la que se puede reducir la banda de guarda garantizando un ACLR superior a 45 dB. En el caso del método propuesto, es posible reducirla a una sola subportadora (15 kHz). En el caso del pulso con conformación RC, aún es necesario una banda de guarda de 20 subportadoras. Aunque se observa que el pulso RC mejora al propuesto en valores de frecuencia muy distantes, esto no tiene efectos prácticos por ser el valor de las emisiones ya muy bajo.

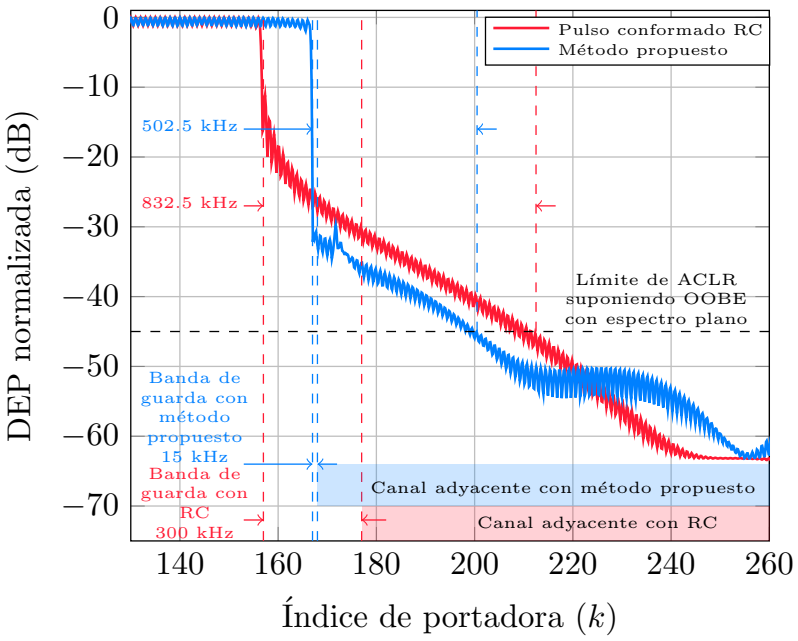

Figura C.7: DEP obtenida con el método propuesto y el pulso conformado RC en la banda de 5 MHz con un espaciado entre subportadoras de 15 kHz. La banda de guarda en cada caso se ha reducido al ancho mínimo que garantiza un ACLR $>$ 45 dB.

En la Tabla C.2 se detalla cuánto se puede reducir la banda de guarda usando el método propuesto y el pulso conformado RC satisfaciendo la restricción de ACLR y manteniendo el EVM (error vector magnitude) a 0 en los canales de 5, 10 y 50 MHz. Para cada uno de estos canales, el tamaño de la DFT (N) es 512, 1024 y 4096, respectivamente. De igual manera, el número de muestras del prefijo cíclico es 36, 72 y 288, respectivamente. Se indica también el coste computacional, que viene dado en términos del incremento porcentual del número de productos complejos necesarios por símbolo OFDM y en términos del incremento porcentual del número de productos reales cuando se usan pulsos con simetría Hermítica. En ambos casos se toma de referencia el coste por símbolo de implementar el pulso conformado RC, que se asume es $\frac{N}{2}\log_2(N) + 2\beta$.

Se observa que con $\beta = 3$ la condición de ACLR no se satisface para los canales de 5 y 10 MHz cuando se usa el pulso conformado RC, mientras que el método propuesto permite reducir la banda de guarda en más de la mitad para el primer caso, y en más de un tercio para el segundo. Para $\beta = 7$, las bandas de guarda se pueden reducir en más de un tercio con el pulso conformado RC, pero se suprimen casi por completo con el método propuesto. Las diferencias relativas entre la reducción de la banda de guarda que consiguen ambos pulsos disminuye cuando crece el ancho de banda, ya que aumentar el número de subportadoras (N) reduce el tamaño de los lóbulos laterales a frecuencias distantes. El coste relativo de usar el método propuesto decrece si el ancho de banda aumenta, pues la complejidad del sistema de referencia escala con N, mientras que la del pulso propuesto se ve dominada por β. En cualquier caso, cada punto porcentual que crece la complejidad aporta una reducción porcentual de la banda de guarda que va desde 0.5 puntos (para el canal de 5 MHz con $\beta = 3$), hasta los 8.5 puntos (para el canal de 50 MHz con $\beta = 1$). Para $\beta = 7$ las ganancias van desde los 1.9 puntos, para el canal de 5 MHz, hasta los 10.5 puntos, para el de 50 MHz. Estos valores son prácticamente el doble cuando se usan pulsos con simetría Hermítica.

Tabla C.2: Reducciones en el ancho de las bandas de guarda e incremento de la complejidad usando el pulso conformado RC y el método propuesto en señales 5G NR.

		Pulso RC	**Método propuesto**		
Ancho de banda del canal (MHz)	**Muestras conformadas (β)**	**Reducción de la banda de guarda[a]**	**Reducción de la banda de guarda[a]**	**Incremento de productos complejos/símbolo (%)**	**Incremento de productos reales/símbolo (%) (simetría Hermítica)**
5	3	-	-56.3 % (14/32)	+94 %	+47.1 %
	7	-37.5 % (20/32)	-96.9 % (1/32)	+51.7 %	+26.1 %
10	3	-	-35.7 % (27/42)	+34.2 %	+17.1 %
	7	-38.1 % (26/42)	-97.6 % (1/42)	+34.1 %	+17.1 %
50	1	-46.2 % (50/93)	-55.9 % (41/93)	+6.6 %	+3.3 %
	7	-87.1 % (12/93)	-98.9 % (1/93)	+9.4 %	+4.8 %

[a] Los valores entre paréntesis indican el número de subportadoras que hay en las bandas de guarda reducidas/número de subportadoras en la banda de guarda original.

Sistema cableado: PLC de banda ancha en interiores A fin de ilustrar las estrictas limitaciones impuestas por la norma EN 50561-1 y los niveles de DEP que usan los fabricantes, en la Fig. C.8 se muestra la máscara de DEP para la región correspondiente a los índices de portadora $500 \leq k \leq 630$, que se corresponde con el rango de frecuencias 12,21 MHz $\leq f \leq$ 15,38 MHz. Se muestra también la DEP obtenida con el pulso propuesto, $h_k^{\text{t-e}}(\mathcal{C}_5, M_\text{a} = M_\text{d} = 1)$, y por el pulso conformado RC. El primero emplea 6 CC dentro de las bandas de paso y 186 CC fuera de ellas, contenidos en $\mathcal{C}_5$. Se observa que el pulso conformado RC tiene que anular un gran número de portadoras de datos para satisfacer

la máscara, lo que da lugar a que subbandas completas, como las correspondientes a los índices $548 \leq k \leq 555$ y $570 \leq k \leq 573$ tengan que ser anuladas. Por el contrario, el pulso propuesto permite satisfacer la máscara sacrificando solo una portadora de datos dentro del rango de frecuencias mostrado.

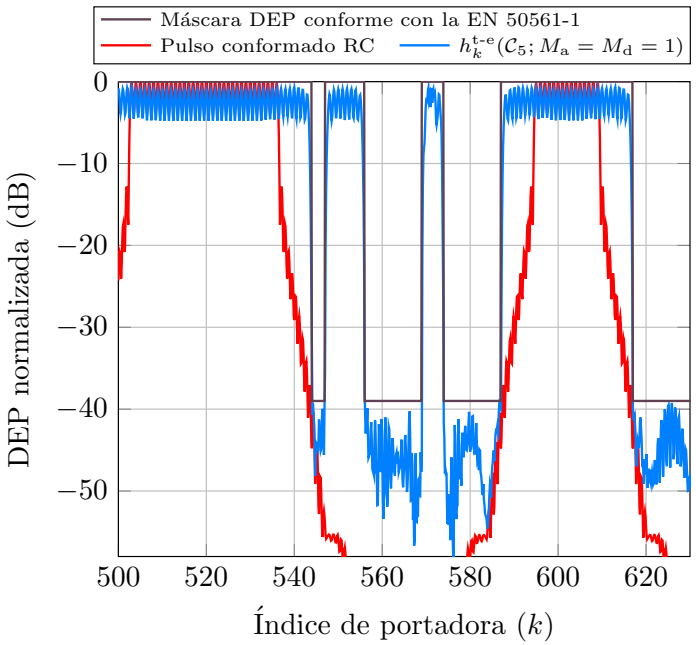

Figura C.8: Detalle de la DEP obtenida en la región $500 \leq k \leq 630$ con el pulso con extensiones temporales propuesto, $h_k^{\text{t-e}}(\mathcal{C}_5, M_\text{a} = M_\text{d} = 1)$, y con el pulso conformado RC cuando se usan para satisfacer las restricciones impuestas en la norma EN 50561-1 y los niveles de DEP definidos.

A continuación se compara la capacidad de diferentes métodos de conformación espectral para satisfacer las restricciones impuestas en la norma EN 50561-1 y los niveles definidos en la ITU-T Rec. G.9964. En particular, el método propuesto y el pulso generalizado de [16], $\mathbf{h}_k(\mathcal{C}_6)$, se incluyen en la comparación, junto con el pulso conformado definido en el estándar para este escenario (que, por elección nuestra, tiene transiciones tipo RC). El pulso generalizado emplea 54 CC dentro de las bandas de paso y 142 CC fuera de ellas, contenidas en el conjunto $\mathcal{C}_6$, mientras que el pulso propuesto emplea $\mathcal{C}_5$. En la Tabla C.3 se recoge el porcentaje de portadoras de datos perdidas por usarse como portadoras de cancelación y el incremento en el número de productos necesarios por símbolo OFDM para implementar cada método, tomado respecto del coste de implementación del pulso conformado RC de referencia. La comparación se centra en la banda por debajo de los 30 MHz. Notamos que la Tabla C.3 muestra también el incremento de complejidad cuando se usan pulsos con simetría Hermítica, dado como incremento porcentual del número de productos reales necesarios respecto al pulso conformado RC. Los valores muestran que con el pulso conformado es necesario anular un elevado número de portadoras de datos (más del 42 %), que se reduce a algo menos del 8 % cuando se usa el pulso generalizado en [16], $h_k(\mathcal{C}_6)$. Con el método

Tabla C.3: Portadoras de datos perdidas e incremento de la complejidad de diferentes métodos de conformación espectral usados para satisfacer las restricciones de las normas EN 50561-1 y la ITU-T Rec. G.9964.

Método	**Portadoras de datos perdidas (%)**	**Incremento de la complejidad por símbolo OFDM**	
		Productos complejos (%)	**Productos reales (%) (Simetría Hermítica)**
Pulso conformado RC	42.49	0	0
$h_k(\mathcal{C}_6)$[a]	7.73	19.56	14.28
$h_k^{\text{t-e}}(\mathcal{C}_5; M_\text{a} = M_\text{d} = 1)$[b]	0.86	39.79	24.4

[a] $\mathcal{C}_6$ contiene 54 CC dentro de las bandas de paso y 142 CC fuera de ellas.
[b] $\mathcal{C}_5$ contiene 6 CC dentro de las bandas de paso y 186 CC fuera de ellas.

propuesto, es posible satisfacer la máscara de emisiones mientras se mantiene este porcentaje por debajo del 1 %.

Estas ganancias en tasa de datos se consiguen a cambio de incrementar la complejidad de la implementación del sistema. Así, mientras el pulso generalizado requiere incrementar el número de productos complejos por símbolo en un 19.56 %, el pulso propuesto require incrementarlo en un 39.79 %. Sin embargo, usando pulsos Hermíticos, el número de productos reales necesarios crece en un 14.28 % para el pulso generalizado respecto del pulso conformado RC, y en un 24.4 % para el método propuesto. Conseguimos reducir las portadoras de datos perdidas en 7 puntos porcentuales a cambio de un incremento de 10 puntos en la complejidad.

C.6 Complementariedad de los métodos propuestos

Finalmente, en esta sección se enuncian las formas en que las estrategia de conformación espectral propuestas en esta tesis se complementan entre sí.

- La estrategia para reducir el coste computacional consistente en usar pulsos con simetría Hermítica puede aplicarse a las otras dos propuestas de esta tesis: a los pulsos con términos extendidos en el tiempo, como se ha demostrado, y a la estrategia de conformación espectral destinada a escenarios donde la máscara de emisiones cambian de forma dinámica.

- Los pulsos que se emplean en la estrategia de conformación espectral propuesta para escenarios donde la máscara de emisiones cambia con el tiempo pueden contar con

términos de cancelación extendidos en el tiempo, como los que se han propuesto en la última sección de este resumen.

C.7 Conclusiones y líneas futuras

Se resumen a continuación las conclusiones y líneas futuras de esta tesis.

C.7.1 Conclusiones

Como objetivos de esta tesis se proponían tres mejoras destinadas a las técnicas de conformación espectral para OFDM. El primero pretendía el diseño de una estrategia para reducir el coste de la optimización y de la implementación en tiempo real de técnicas de conformación espectral para señales OFDM. Este objetivo se ha traducido en una doble contribución:

- Nuevo pulso de transmisión con simetría Hermítica, del que pueden beneficiarse un importante número de técnicas de conformación espectral ya existentes en la literatura. En particular, permiten reducir el número de coeficientes a obtener en la optimización a la mitad, y el número de productos necesarios para la implementación se reduce en hasta un 50 %, en función de las técnicas involucradas.
- Un esquema de diseño para técnicas de conformación espectral que, si se aplica utilizando el pulso propuesto, garantiza reducciones en la complejidad semejantes a las enunciadas en el punto anterior.

Se ha indicado que utilizar el pulso propuesto y resolver un problema de optimización que se ajuste al esquema de diseño propuesto es una condición suficiente para las técnicas de conformación espectral se beneficien de las mencionadas reducciones en el coste computacional. Se ha demostrado también que existen técnicas ya propuestas en la literatura que pueden beneficiarse de las mismas reducciones si usan el pulso con simetría propuesto. Además, también se ha demostrado que su uso no influye en las prestaciones de las técnicas de conformación espectral ni en la PAPR de la señal OFDM resultante.

El segundo objetivo consistía en proponer una estrategia que redujera el elevado coste computacional que supone recalcular las soluciones de conformación espectral en escenarios donde las restricciones de las emisiones fuera de banda cambian de forma dinámica. Este objetivo se ha conseguido cumplir con la propuesta de un esquema de conformación espectral, el cual consta de tres fases:

- Una primera fase, realizada offline, en la que se calcula una única vez un conjunto original de soluciones para un escenario de referencia a través de uno de los procedimientos de optimización propuestos.

- Una segunda fase, que se lleva a cabo de manera online en el propio sistema de comunicaciones, en la que se transforman estas soluciones originales para obtener una solución adaptada a las condiciones de emisión impuestas.
- Una tercera fase en la que las soluciones transformadas se utilizan para generar los símbolos OFDM, también de manera online en el propio dispositivo.

Se ha mostrado en los resultados numéricos que con la estrategia propuesta se obtienen niveles de OOBE similares a los obtenidos con otras técnicas del estado del arte, y sin afectar a la PAPR de la señal OFDM resultante. Además, si bien algunas de estas últimas cuentan con costes de implementación menores que los de la propuesta, requieren que la fase de optimización se lleve a cabo con cada símbolo OFDM o, en el mejor de los casos, cada vez que la máscara de emisiones cambia. En cambio, en el esquema propuesto la fase de optimización se realiza una sola vez y de manera offline. Por ello, el coste global de la estrategia propuesta es notablemente menor que el de otras técnicas, puesto que la optimización es mucho más costosa que la implementación de los pulsos.

El tercer objetivo de esta tesis era reducir la penalización en la tasa de datos que presentan las técnicas AIC debido al uso de portadoras de datos (situadas dentro de las bandas de paso) como portadoras de cancelación, así como mitigar el acortamiento del prefijo cíclico efectivo a causa del solape con los términos AST. Para resolver esto, la propuesta ha consistido en usar términos de cancelación adelantados y atrasados en el tiempo que, siendo aún ortogonales a los datos, incrementan el número de grados de libertad con que contamos para reducir las emisiones fuera de banda. Esta propuesta ha resultado tener una doble aplicación:

- Permite conseguir los mismos niveles de emisión fuera de banda que otras técnicas similares de la literatura, pero reduciendo el número de portadoras de datos que se usan como portadoras de cancelación, y también permite disminuir la cantidad de muestras en que se reduce el prefijo cíclico efectivo.
- Los grados de libertad adicionales también se pueden emplear para conseguir mayores reducciones de las emisiones fuera de banda, manteniendo la misma penalización de la tasa de datos que convencionalmente afecta a las técnicas AIC y el acortamiento de prefijo cíclico efectivo.

La última propuesta se ha evaluado en escenarios reales: en 5G NR y en PLC de banda ancha en interiores. Se ha demostrado que, en el primer caso, permite reducir casi por completo las bandas de guarda que se han de dejar entre canales adyacentes. En el segundo escenario, el método propuesto permite satisfacer unas restricciones muy rigurosas (con hasta 34 subbandas eliminadas en una banda de 30 MHz) sacrificando un número muy reducido de portadoras de datos.

Por último, en esta tesis se han propuesto varios esquemas de diseño para soluciones a problemas de conformación espectral, que emplean técnicas ampliamente utilizadas como son

las AIC y AST. Dichas técnicas hacen uso de recursos (portadoras de cancelación, pulsos en las transiciones entre símbolos OFDM), que se definen de forma sistemática antes de la optimización. De igual manera se definen los límites que controlan que las soluciones al problema de optimización no produzcan sobrepicos de DEP dentro de las bandas de paso. Debido al amplio número de combinaciones posibles de recursos de cancelación y restricciones, parece imposible garantizar que una solución obtenida de esta forma sea la mejor posible para un escenario dado. Sin embargo, el procedimiento propuesto ha demostrado aportar soluciones satisfactorias para los distintos casos evaluados.

C.7.2 Líneas futuras

En el apartado de conclusiones se ha hecho mención al mecanismo sistemático que se ha empleado para definir los recursos que se emplean en la reducción de las emisiones fuera de banda, así como de las restricciones que se aplican al problema. En ese sentido, una posible línea de trabajo futura consiste en la definición de una herramienta integral que lleve a cabo todas las fases del diseño de las soluciones al problema de conformación espectral que queremos resolver:

- Determinar los recursos empleados por las técnicas de conformación espectral.
- Determinar las restricciones del problema de optimización.
- Optimización de las soluciones.

Para las dos primeras tareas se podría emplear un modelo de aprendizaje profundo debidamente entrenado. Así, la herramienta propuesta tomaría como entrada los parámetros de la señal OFDM, algunos parámetros de diseño de las técnicas de conformación espectral usadas en cada caso (p.ej., número de términos extendidos en el tiempo, existencia de portadoras de datos usadas como CC, etc.) y la máscara de DEP. Como respuesta, devolvería la solución al problema de conformación espectral propuesto.

Otra línea de estudio interesante consiste en emplear la estrategia de diseño de pulsos como el generalizado pero para utilizarse en recepción de señales OFDM. Conformar las señales que transmitimos puede permitirnos reducir el tamaño de las bandas de guarda, pero eso dependerá de la potencia de interferencia que captura el receptor empleado por los usuarios que operan en los canales adyacentes. Si las señales involucradas son ortogonales no hay problema, sin embargo la ortogonalidad puede romperse por varias causas: por efecto del Doppler, por la existencia de CFO (carrier frequency offset), el uso de un prefijo cíclico de tamaño insuficiente o el uso de numerologías diferentes, como en 5G. Para esos casos, diseñar pulsos de recepción de manera similar a como hacemos con el pulso generalizado puede resultar enormemente beneficioso.

Finalmente, también puede ser interesante analizar el efecto de la no-linealidad del amplificador de potencia sobre la señal conformada. Tradicionalmente, este efecto se ha compensado pre-distorsionando la señal transmitida, pero los modelos de amplificador empleados suelen ser muy simplistas. En ese sentido, puede ser interesante hacer un estudio más detallado.

References

[1] A. A. Zaidi, R. Baldemair, H. Tullberg, H. Björkegren, L. Sundström, J. Medbo, C. Kilinc, and I. Da Silva, "Waveform and numerology to support 5G services and requirements," *IEEE Communications Magazine*, vol. 54, no. 11, pp. 90–98, Nov. 2016.

[2] P. Guan, D. Wu, T. Tian, J. Zhou, X. Zhang, L. Gu, A. Benjebbour, M. Iwabuchi, and Y. Kishiyama, "5G field trials: OFDM-based waveforms and mixed numerologies," *IEEE Journal on Selected Areas in Communications*, vol. 35, no. 6, pp. 1234–1243, Jun. 2017.

[3] S. Haykin, "Cognitive radio: Brain-empowered wireless commnunications," *IEEE Journal on Selected Areas in Communications*, vol. 23, no. 201-220, February 2005.

[4] S. Galli, K. J. Kerpez, H. Mariotte, and F. Moulin, "PLC-to-DSL Interference: Statistical Model andImpact on VDSL2, Vectoring, and G.Fast," *IEEE Journal on Selected Areas in Communications*, vol. 34, no. 7, pp. 1992–2005, Jul. 2016.

[5] "Mitigation of interference between DSL and PLC," ITU-T Recommendation G.9977, Dec. 2016.

[6] "Power line communication apparatus used in low-voltage installations - Radio disturbance characteristics - Limits and methods of measurement - Part 1: Apparatus for in-home use," European Standard, EN 50561-1, October 2013.

[7] Z. You and I.-T. Fang, J. Lu, "Out-of-band emission suppression techniques based on a generalized OFDM framework," *EURASIP Journal on Advances in Signal Processing*, vol. 2014:74, pp. 1–14, 2014.

[8] J. Van de Beek, "Sculpting the Multicarrier Spectrum: A Novel Projection Precoder," *IEEE Communications Letters*, vol. 13, no. 12, pp. 881–883, 2009.

[9] X. Zhou, G. Y. Li, and G. Sun, "Multiuser spectral precoding for OFDM-based cognitive radio systems," *IEEE Journal on Selected Areas in Communications*, vol. 31, no. 3, pp. 345–352, Mar. 2013.

[10] M. Ma, X. Huang, G. Jiao, and Y. J. Guo, "Optimal Orthogonal Precoding for Power Leakage Suppression in DFT-Based Systems," *IEEE Transactions on Communications*, vol. 59, no. 3, pp. 844–853, March 2011.

[11] K. Hussain and R. López-Valcarce, "Joint precoder and window design for OFDM sidelobe suppression," *IEEE Communications Letters*, vol. 26, no. 12, pp. 3044–3048, December 2022.

[12] J. F. Schmidt, S. Costas-Sanz, and R. López-Valcarce, "Choose Your Subcarriers Wisely: Active Interference Cancellation for Cognitive OFDM," *IEEE Journal on Emerging and Selected Topics in Circuits and Systems*, vol. 3, no. 4, pp. 615–625, Dec. 2013.

[13] S. Brandes, I. Cosovic, and M. Schnell, "Reduction of out-of-band radiation in OFDM systems by insertion of cancellation carriers," *IEEE Communications Letters*, vol. 10, no. 6, pp. 420–422, 2006.

[14] R. Zayani, Y. Medjahdi, H. Shaïek, and D. Roviras, "WOLA-OFDM: a potential candidate for asynchronous 5G," in *IEEE Globecom Workshops*, Dec. 2016, pp. 1–5.

[15] H. Mahmoud and H. Arslan, "Sidelobe suppression in OFDM-based spectrum sharing systems using adaptive symbol transition," *IEEE Communications Letters*, vol. 12, no. 2, pp. 133–135, February 2008.

[16] L. Díez, J. A. Cortés, F. J. Cañete, E. Martos-Naya, and S. Iranzo, "A generalized spectral shaping method for OFDM signals," *IEEE Transactions on Communications*, vol. 67, no. 5, pp. 3540–3551, May 2019.

[17] J. Abdoli, M. Jia, and J. Ma, "Filtered OFDM: A New Waveform for Future Wireless Systems," in *Proceedings of the IEEE International Workshop on Signal Processing Advances in Wireless Communications (SPAWC)*, 2015.

[18] M. Faulkner, "The effect of filtering on the performance of OFDM systems," *IEEE Transactions on Vehicular Technology*, vol. 49, no. 5, pp. 1877–1884, September 2000.

[19] R.-A. Pitaval and B. M. Popovic, "Filtered-Prefix OFDM," *IEEE Communications Letters*, vol. 23, no. 1, pp. 28–31, 2019.

[20] S. Brandes, I. Cosovic, and M. Schnell, "Techniques for reducing out-of-band radiation in OFDM based transmission systems," *European Transactions on Telecommunications*, vol. 21, no. 2, pp. 142–153, January 2010.

[21] J. Giménez, J. A. Cortés, F. Javier Cañete, E. Martos-Naya, and L. Díez, "A modified pulse and design framework to halve the complexity of OFDM spectral shaping techniques," *IEEE Communications Letters*, vol. 28, no. 9, pp. 2146–2150, September 2024.

[22] J. Giménez, J. A. Cortés, and L. Díez, "Low-complexity spectral shaping method for OFDM signals with dynamically adaptive emission mask," *IEEE Transactions on Communications*, vol. 71, no. 4, pp. 2351–2363, April 2023.

[23] J. Giménez, J. A. Cortés, E. Martos-Naya, and L. Díez, "Spectral shaping method for OFDM combining time-shifted active interference cancellation and adaptive symbol transition," *IEEE Open Journal of the Communications Society*, vol. 6, pp. 4476–4490, may 2025.

[24] S. Boyd and L. Vandenberghe, *Convex Optimization*. Cambridge University Press, 2014.

[25] E. P. Simon, L. Ros, H. Hijazi, and M. Ghogho, "Joint carrier frequency offset and channel estimation for OFDM systems via the EM algorithm in the presence of very high mobility," *IEEE Transactions on Signal Processing*, vol. 60, no. 2, pp. 754–765, 2012.

[26] M. Morelli and M. Moretti, "Fine carrier and sampling frequency synchronization in OFDM systems," *IEEE Transactions on Wireless Communications*, vol. 9, no. 4, pp. 1514–1524, 2010.

[27] J. F. Schmidt, D. Romero, and R. López-Valcarce, "Active Interference Cancellation for OFDM Spectrum Sculpting: Linear Processing Is Optimal," *IEEE Communications Letters*, vol. 18, no. 9, pp. 1543–1546, Sep. 2014.

[28] H. Yamaguchi, "Active interference cancellation technique for MB-OFDM cognitive radio," in *Proceedings of the European Microwave Conference*, 2004, pp. 1105–1108.

[29] R. Kumar, K. Hussain, and R. López-Valcarce, "Mask-Compliant Orthogonal Precoding for Spectrally Efficient OFDM," *IEEE Transactions on Communications*, vol. 69, no. 3, pp. 1990–2001, March 2021.

[30] J. van de Beek and F. Berggren, "N-continuous OFDM," *IEEE Communications Letters*, vol. 13, no. 1, pp. 1–3, Jan. 2009.

[31] A. V. Oppenheim, A. S. Willsky, and S. H. Nawab, *Signals & Systems (2nd Ed.)*. USA: Prentice-Hall, Inc., 1996.

[32] K. Hussain, A. Lojo, and R. López-Valcarce, "Flexible spectral precoding for sidelobe suppression in OFDM systems," in *Proceedings of the IEEE International Conference on Acoustics, Speech and Signal Processing*, 2019, pp. 4789–4793.

[33] K. Hussain and R. López-Valcarce, "OFDM spectral precoding with per-subcarrier distortion constraints," in *Proceedings of the European Signal Processing Conference (EUSIPCO)*, 2019, pp. 1–5.

[34] K. Hussain, R. López-Valcarce, F. Rey, J. Sala-Alvarez, and J. Villares, "Sidelobe Suppression for Multicarrier Signals via Structured Spectral Precoding," *IEEE Transactions on Communications*, vol. 72, no. 6, pp. 3155–3168, Jun. 2024.

[35] R. Kumar and A. Tyagi, "Computationally efficient mask-compliant spectral precoder for OFDM cognitive radio," *IEEE Transactions on Cognitive Communications and Networking*, vol. 2, no. 1, pp. 15–23, 2016.

[36] ——, "Weighted least squares based spectral precoder for OFDM cognitive radio," *IEEE Wireless Communications Letters*, vol. 4, no. 6, pp. 641–644, 2015.

[37] "Unified high-speed wireline-based home networking transceivers - System architecture and physical layer specification," ITU-T Recommendation G.9960, July 2015.

[38] ETSI TS 138 104 V18.5.0 (2024-05), "5G; NR; Base Station (BS) radio transmission and reception," ETSI, Tech. Rep., 2024-05.

[39] ETSI TS 138 101-1 V17.8.0 (2023-01), "5G; NR; User Equipment (UE) radio transmission and reception; Part 1: Range 1 Standalone," ETSI, Tech. Rep., 2023-01.

[40] 3GPP TSG RAN4 #45, "LTE eNB Timing Definition," Qualcomm Europe, Tech. Rep., 2007.

[41] "Unified high-speed wireline-based home networking transceivers - Power spectral density specification," ITU-T Recommendation G.9964, December 2011.

[42] K. Hussain and R. López-Valcarce, "Memory Tricks: Improving Active Interference Cancellation for Out-of-Band Power Reduction in OFDM," in *Proceedings of the IEEE International Workshop on Signal Processing Advances in Wireless Communications*, Sep. 2021, pp. 86–90.